Fractionated crystallization in semicrystalline polymers

Leire Sangroniz[1], Bao Wang[2], Yunlan Su[3], Guoming Liu[3,4]*, Dario Cavallo[2]*, Dujin Wang[3,4], Alejandro J. Müller[1,5]*

[1]POLYMAT and Department of Polymers and Advanced Materials: Physics, Chemistry and Technology, Faculty of Chemistry, University of the Basque Country UPV/EHU, Paseo Manuel de Lardizábal, 3, 20018 Donostia-San Sebastián, Spain.

[2]Department of Chemistry and Industrial Chemistry, University of Genova, via Dodecaneso, 31 - 16146 Genova, Italy

[3]Beijing National Laboratory for Molecular Sciences, CAS Research/Education Center for Excellence in Molecular Sciences, CAS Key Laboratory of Engineering Plastics, Institute of Chemistry, Chinese Academy of Sciences, Beijing, 100190 China.

[4] University of Chinese Academy of Sciences, Beijing 100049, China.

[5]IKERBASQUE, Basque Foundation for Science, Bilbao, Spain.

*Corresponding authors: gmliu@iccas.ac.cn, dario.cavallo@unige.it, alejandrojesus.muller@ehu.es

Abstract

The crystallization of heterogeneously nucleated bulk polymers typically occurs in a single exothermic process, within a narrow temperature range, i.e., a single exothermic peak is detected by Differential Scanning Calorimetry when the material is cooled from the melt. However, when a bulk semicrystalline polymer is subdivided or dispersed into a multitude of totally (or partially) isolated microdomains (e.g., droplets or cylinders), in number comparable to that of commonly available nucleating heterogeneities, several separated crystallization events are typically observed, i.e., fractionated crystallization. This situation is often found for the minor crystallizable component in immiscible blends.

When the bulk polymer is dispersed into a number of microdomains that is several orders of magnitude higher than the available number of heterogeneities within it, most microdomains will be heterogeneity-free. In these clean microdomains the nucleation can occur by contact with the interfaces (i.e., surface nucleation) or by homogeneous nucleation inside the microdomain volume. These cases can be easily encountered in cylinders or spheres within strongly segregated block copolymers, or in infiltrated polymers within nanopores of alumina templates.

In this work, a comprehensive review of the known cases of fractionated crystallization is provided. The changes upon decreasing microdomain sizes from a dominant single heterogeneous nucleation, through fractionated crystallization, to surface or homogeneous nucleation are critically reviewed. Emphasis is placed on the common features of the phenomenon across the different systems, and thus on the general conclusions that can be drawn from the analysis of representative semicrystalline polymers. The origin of the fractionated crystallization effects and their dramatic consequences on the nucleation and crystallization kinetics of semicrystalline polymers are also discussed.

Keywords: *Fractionated crystallization; Heterogeneous nucleation; Surface nucleation; Homogeneous nucleation; Self-nucleation; Crystallization kinetics.*

Abbreviations

2-D, two dimensional; 3-D, three dimensional; A, droplet surface area; AAO, Anodic Aluminum Oxide Templates; aPP, atactic poly(propylene); CNT, Carbon nanotube; *DI, Domain I* or *isotropic melt Domain; DII, Domain II or self-nucleation Domain; DIII, Domain III* or *self-nucleation and annealing Domain; $DIII_A$, Domain III_A* or *Domain* in which annealing is observed without self-nucleation; $DIII_{SA}$, *Domain* III_{SA} or *self-nucleation and annealing Domain*, equivalent to *Domain III*; DMBS, 1,3:2,4-bis(3,4-dimethyl-benzylidene sorbitol); DSC, differential scanning calorimetry; E-*b*-MB, ethylene-*b*-(3-methyl-1-butene); E-*b*-VCH, polyethylene-*b*-poly(vinylcyclohexane); E-*b*-SEB, polyethylene-b-poly(styrene-r-ethylene-r-butene); E-GMA, copolymer of ethylene and glycidyl methacrylate; EPDM, ethylene propylene diene methylene; EPDM-g-MA, ethylene propylene diene methylene grafted maleic anhydride; *f*, temperature correction term; f_Z^A, fraction of droplets with exactly z impurities;*G*, growth rate; HDPE, high density poly(ethylene); hPN, hydrogenated polynorbornene; I_V, volume dependent nucleation rate; I_A, area dependent nucleation rate; iPP, isotactic poly(propylene); *k*, the overall crystallization rate constant; K_g^τ, the energy barrier associated with the overall crystallization; LDPE, low density poly(ethylene); LLDPE, linear low density poly(ethylene); LPE, linear poly(ethylene); M^A, concentration of heterogeneities of type A in the bulk polymer; $M^A V_D$, average number of type A seeds per droplet with volume V_D; MA, Maleated PP; MA, Blend 30 cPA6 (NH_2 terminated PA)/70 PE-1 MAH(maleic anhydride):NH_2 ratio 4:1; MC, Blend 20 PA6/80 PE-3 MAH:NH_2 ratio 3:1; MDs, microdomains; M_n, number average molecular weight; *n*, Avrami index; n_{gd}, Avrami term related to growth dimensionality; n_n, Avrami term associated to nucleation; *N*, polymerization degree; N/N_0, is the fraction of droplets not yet crystallized at time *t*; N_0, is the total number of droplets that undergo nucleation; Na^+-MMT, layered sodium montmorillonite; NAs, nucleating agents; NA11, (4,6-di-tert-butylphenyl)phosphate; nm, nanometer; NMR, nuclear magnetic resonance; OBC, olefin block copolymer; P2VP, poly(2-vinylpyridine); P3HT, poly(3-hexylthiophene); P4tBS, poly(4-tert-butyl styrene); PA6, poly(amide 6); PB, poly(butadiene); PBA, poly(butylene adipate); PBS, poly(butylene succinate); PC, poly(carbonate); PCL, poly(caprolactone); PDI, polydispersity index; PE, poly(ethylene); PEG, poly(ethylene glycol); PEO, poly(ethylene oxide); PEP, poly(ethylene-*alt*-propylene); PES, poly(ethylene suberate); PET, poly(ethylene terephthalate); PHB, poly(3-hydroxybutyrate); PI, poly(isoprene); PLLA, poly(L-lactide); PLOM, Polarized Light Optical Microscopy; PMMA, poly(methyl methacrylate); POB, poly(oxybutylene); POE, poly(oxyethylene); POM, poly(oxymethylene); PPDX, poly(dioxanone); PPE, poly(phenylene-ether); PPP, poly(2,5-dihexyloxy-*p*-phenylene); PNCs, polymer nanocomposites; aPS, atactic poly(styrene); PS, poly(styrene); P(S-ODMA), poly(styrene-block-octadecylmethacrylate); PVDF, poly(vinylidene fluoride); P(VDF70-TrFE30), poly(vinylidene $fluoride_{70}$-$trifluorethyline_{30}$); PVSt, poly(4-(vinylpheneyl)-1-butene)); QQ, quinacridone quinone; *R*, gas constant; RT, room temperature; SAXS, small angle X-ray scattering; SB, sodium benzoate; SBS, poly(styrene-butadiene-styrene); SEBS, styrene ethylene butylene styrene; SEM, scanning electron microscopy; SEP, styrene-*block*-ethylene-*ran*-propylene; SiO_2, silica; SMA2, styrene-maleic anhydride copolymers; SSA, successive self-nucleation and annealing; SCB, short chain branches; *t*, time; t_0, the induction time; *T*, temperature; T_A, crystallization temperatures after nucleation from type A heterogeneity; $T_{annealing}$, temperature at which annealing occurs; T_B, crystallization temperatures after nucleation from type B heterogeneity; T_c, crystallization temperature; $T_C{}^B$, crystallization temperature of the B peak; T_{iso}, temperature of the isothermal experiment; T_g, glass transition temperature; T_m, melting temperature; $T_m{}^0$, equilibirum melting temperature; T_{ODT}, order disorder transition temperature; T_s, self-nucleation temperature; T_{SN}, highest temperature at which self-nucleation temperature is observed temperature; T_∞, temperature where chain mobility ceases; TEM, transmission electron microscopy; *U**, the activation energy for chain diffusion; ULDPE, ultra low density poly(ethylene); UV, ultraviolet; *V*, droplet volume; V_c, being the relative volumetric transformed fraction; V_D, average droplet volume; VLDPE, very low density poly(ethylene); X_c, crystallinity degree; X_t, crystallinity at different crystallization times; X_∞, final crystallinity; ZN-PP, Ziegler-Natta PP; $\frac{1}{\tau_{50\%}}$, the inverse of the half-crystallization time; *ΔG**, free energy for the formation of a nucleus of critical size; *ΔH(t)*, crystallization enthalpy at time *t*;

ΔH_C^A, crystallization enthalpy of peak A; ΔH_C^B, crystallization enthalpy of peak B; ΔH_{TOT}, is the final crystallization enthalpy at the adopted crystallization temperature; $\Delta\sigma$, interfacial free energy difference parameter; $\Delta\sigma_A$, interfacial free energy difference parameter for A type heterogeneity; $\Delta\sigma_B$, interfacial free energy difference parameter for B type heterogeneity; ΔT, undercooling; ΔT_A, supercooling corresponding to the crystallization from A type heterogeneity; ΔT_B, supercooling corresponding to the crystallization from B type heterogeneity; σ_{mc}, interfacial free energy between the polymer melt and the crystal; σ_{ms}, interfacial free energy between the polymer melt and the solid substrate; σ_{cs}, interfacial free energy between the crystal and the solid substrate; φ_{SiO2}, silica content; φ_{filler}, filler content; μm, micrometer; v_d,volume of the phase; χ, Flory Huggins interaction parameter between the blocks forming the copolymer.

Contents

1. Introduction

The phenomenon of fractionated crystallization in immiscible polymer blends, strongly segregated block copolymer or polymers infiltrated within AAO templates, or any situation where a bulk polymer is subdivided into many microdomains (MDs) can be conveniently illustrated with the aid of the scheme in Figure 1.

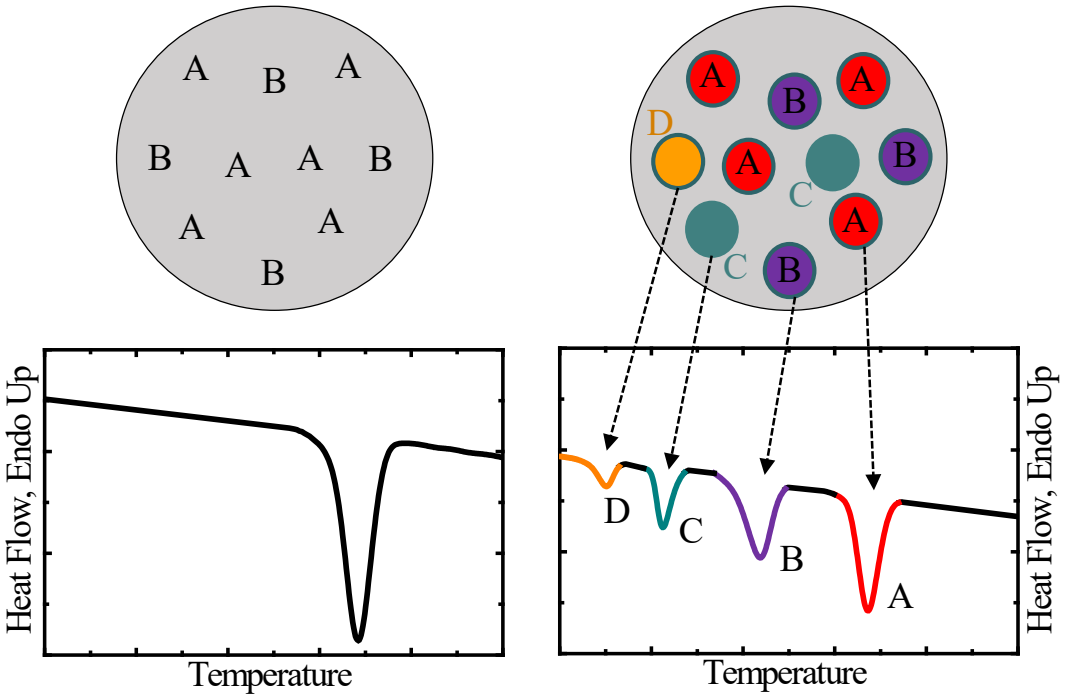

Figure 1. Schematic illustration of the fractionated crystallization concept. A bulk polymer containing different nucleating impurities (A, B) is shown on top, left. The related DSC cooling curve is reported below. The same polymer is divided into many different microdomains (top, right) with each color representing a possible nucleation modality: red, impurity A; violet, impurity B; green, matrix interface (impurity-free droplets); yellow, homogeneous nucleation (impurity-free droplets). The corresponding DSC trace exhibiting multiple crystallization exotherms on cooling is shown below the system scheme (bottom, right).

Let us consider a bulk polymer (Figure 1, top left), containing different nucleating heterogeneities (A, B), with the impurity A being much more efficient than impurity B, i.e., possessing a lower heterogeneous nucleation free energy barrier. Upon cooling from the melt, the type A heterogeneity will nucleate the polymer first and spherulites will start to grow from them. If such impurities are present in sufficient quantity, the undercooled melt will be consumed before leaving a chance to type B impurities to nucleate at lower temperatures. In this case, a single high temperature crystallization exotherm is commonly observed in non-isothermal DSC scans (Figure 1 bottom left).

When the crystallizing polymer is divided into numerous MDs, such as droplets dispersed in a liquid medium or in a matrix of an immiscible polymer, spheres or cylinders dispersed in a strongly segregated block copolymer or polymers infiltrated in AAO templates, fractionated crystallization can arise, if the number of the domains is of the same order of magnitude of the nucleating impurities contained in the bulk polymer (Figure 1, top right). It is intuitive to consider that, for statistical reasons, only some of the droplets will contain type A heterogeneity, while others will

enclose type B impurities or eventually be free of any nucleation-active particle (some of the original heterogeneities contained in the bulk polymer can also be wasted by migrating to the matrix during blending). Being the crystallization of each droplet independent from each other, several exotherms of crystallization can be observed, each attributed to a specific nucleation mechanism which is active in a certain droplets' population (Figure 1, bottom right). More specifically, the most effective heterogeneities (A in the example of Figure 1) will give rise to a bulk-like crystallization peak, and the undercooling will increase for other impurities (e.g., B in Figure 1) inversely to the corresponding nucleation efficiency.

Eventually, two other nucleation possibilities exist for droplets that are free of any impurity. In particular, a nucleus can form at the interface with the second phase, i.e., dispersing medium or matrix material in immiscible blends, as indicated by the letter C and the corresponding exotherm at larger undercoolings in the scheme (Figure 1, right). If even lower crystallization temperatures are achieved without the occurrence of interface-assisted nucleation, for instance for the presence of a relatively inactive surface, nucleation will occur inside the volume of the dispersed phase in a homogeneous fashion (letter D in Figure 1). Note that homogeneous nucleation takes place at the maximum allowed undercooling, often close to the glass transition temperature of the polymer. Surface-induced and homogeneous nucleation mechanisms are typically very difficult to distinguish by a conventional DSC run, without further evidences (e.g., domain size dependence of the nucleation rate). As such, it is not common to observe both types of nucleation in the same sample, therefore the representation of Figure 1 scheme is just for the sake of concise explanation.

Classical examples of fractionated crystallization in semicrystalline polymers are those obtained in the pioneering work of Cormia, Price and Turnbull, by using droplets experiments. [1] Adapting the experimental method of Vonnegut, [2] who developed it for studying the crystallization of tin and water, they created a suspension of polyethylene droplets in an inert medium and monitored their solidification by means of polarized optical microscopy. The droplets were polydisperse in sizes, ranging from less than 3 to about 10 micrometers in diameter. During continuous cooling, only 5 % of the droplets solidified above 100 °C, with a minor fraction crystallizing at 122-123°C, which is the typical temperature range

where nucleation of spherulites in the bulk material become appreciable. About 40% of the droplets crystallize between 100 and 90 °C, while more than 50% of them solidified at around 85-87 °C. Typically, larger droplets solidified at higher temperature since they are more likely to contain nucleating heterogeneities, and droplets smaller than 3 micrometer solidified at the critical temperature of 85 °C, which was tentatively attributed to the homogeneous nucleation regime. Analogous observations were later gathered by droplets experiments with different polymers, i.e., i-PP [3], PEO, PA6 and i-PS [4].

In this paper, we review the fractionated crystallization phenomena reported for semi-crystalline polymers. The review is mostly focused, but not strictly limited to, the past 25 years, with the hindsight of the recently published literature (last 10 years). We perform quantitative comparison of selected data obtained by many different authors to present unifying trends and thus be able to explain the origin of the observed effects. Rather than taking a chronological approach, we decided to divide the text by the different systems in which fractionated crystallization has been reported and analyzed: Polymer blends and binary systems (i.e., break up of multi-layered films and nanofibers); Block copolymers; Polymers infiltrated within AAO templates (i.e., nanoporous alumina templates) and nanocomposites. Finally, we devote the final section to the understanding of fractionated crystallization by closely examining the nucleation process with different ways to inject nuclei into the material MDs.

2. Fractionated crystallization in different polymeric systems

2.1. Polymer blends and two-phase systems

Polymer blends and two-phase systems are excellent models to study fractionated crystallization of semicrystalline polymers. The problem of fractionated crystallization and heterogeneous nucleation of an ensemble of crystallizing droplets has been formulated mathematically by Pound and La Mer for the case of tin. [5] Moreover, the attribution of the different crystallization exotherms to the presence of impurities with different nucleating efficiency derives from the interpretation of Frensch and Jungnickel [6] for semicrystalline polymers. Given the large number of droplets, the probability of finding heterogeneities of type A follows a Poisson

distribution. Considering the average droplet volume V_D, the fraction of droplets with exactly z impurities is given by:

$$f_z^A = \left[\frac{(M^A V_D)^z}{z!}\right] \exp(-M^A V_D) \quad (1)$$

where M^A is the concentration of heterogeneities of type A in the bulk polymer, while $M^A V_D$ is the average number of type A seeds per droplet with volume V_D.

Therefore, the fraction of droplets that will crystallize at the same undercooling of the bulk polymer is the one that contains at least one A impurity, hence:

$$f_{z>0}^A = 1 - f_0^A = 1 - \exp(-M^A V_D) \quad (2)$$

The rest of the droplets will thus solidify at larger undercooling, induced by heterogeneity of a different kind (e.g., B, etc.). The concentration of the respective heterogeneities can be somehow deduced by the relative area of the fractionated DSC peaks (see Figure 1, right), neglecting to a first approximation any issue with droplet size polydispersity.

The link between the undercooling at which a certain ensemble of droplets solidifies and the impurity that they contain is provided by Frensch and Jungnickel [6] with some considerations on heterogeneous nucleation theory for polymeric materials. The free energy for the formation of a nucleus of critical size (ΔG^*) on the surface of a given substrate, at a certain undercooling (ΔT), is approximately given by:

$$\Delta G^* \approx \frac{\Delta\sigma}{(\Delta T)^2} \quad (3)$$

where $\Delta\sigma$ is the interfacial free energy difference parameter which accounts for the energy penalty in substituting one substrate-melt interface with a crystal-substrate and crystal-melt interface. Thus $\Delta\sigma$ is defined as the difference in the interfacial free energies:

$$\Delta\sigma = \sigma_{mc} - \sigma_{ms} + \sigma_{cs} \quad (4)$$

with the subscript m, c and s representing the polymer melt, crystal and the solid substrate, respectively.

Under the assumption that the onset of nucleation at a given temperature occurs when $\Delta G^*/T$ is lower than a certain critical value, Frensch and Jungnickel

derived the following expression relating $\Delta\sigma$ and the undercooling at which the two different heterogeneities of type A and B give rise to crystallization:

$$\frac{\Delta\sigma_A}{\Delta\sigma_B} \approx \left(\frac{T_A}{T_B}\right)\left(\frac{\Delta T_A}{\Delta T_B}\right)^2 \quad (5)$$

where T_A and T_B are the crystallization temperatures after nucleation from type A and type B heterogeneities respectively, and ΔT_A and ΔT_B are the corresponding supercoolings.

This relation holds for different kind of heterogeneities, but it can be convenient to consider the comparison between the undercooling at which a certain seed can nucleate and homogeneous nucleation. This can be done by remembering that the ΔG^* for homogeneous nucleation is proportional to $2\sigma_{mc}$ and the homogeneous nucleation temperature is the highest achievable undercooling. In Figure 2, a derivation of equation (5) [6] is applied to real data obtained in iPP/PS blends in which different nucleating heterogeneities could be identified, either because purposely added (NA-11, sodium benzoate [7]) or from comparison of literature values of T_c (Irganox additive) or $\Delta\sigma$ (PS surface) [8, 9]. It can be seen that the highest is the nucleating efficiency, corresponding to a lower $\Delta\sigma/\sigma_{mc}$, the lower is the relative undercooling that is achieved by the nucleated droplet ensemble.

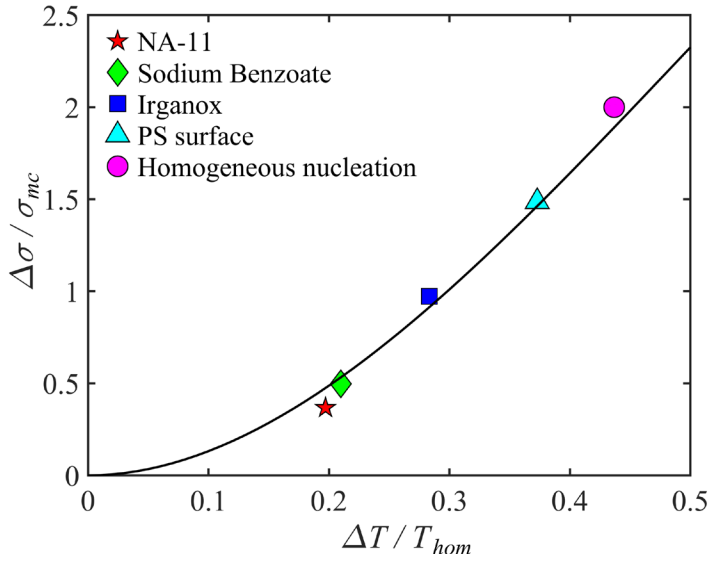

Figure 2. Relation between relative interfacial free energy difference of a given nucleating interface and relative undercooling with respect to homogeneous nucleation temperature for polystyrene/polypropylene blends (see text and equation 5). The line represents a fit of the experimental data with equation 5. A homogeneous nucleation temperature of 40 °C has been employed. Data are taken from refs. [7-9].

2.1.1. Immiscible blends

Extensive literature exists for the case of immiscible blends. Some of the works reporting fractionated crystallization are summarized in Table 1, along with information on the obtained morphology, composition and crystallization peak temperatures, when available. For a comprehensive discussion of all the literature, the reader is referred to the recent chapter from Groeninckx et al. [10], while hereby we will mainly highlight the most important observations for these systems, discussing them in the light of the general concepts outlined above.

Table 1. Collection of literature data for fractionated crystallization in immiscible blends. Whenever available, composition, domain size and fractionated crystallization temperatures are reported.

System	Component (weight)	Domain size (μm)	T_c (°C)	Reference
iPP/EPDM	21/79 (volume)	< 5	51/80	[11]
	10/90 (volume)	< 5	50	
	5/95 (volume)	< 5	48	
iPP/SBS	25/75	< 0.2	43/71	[12]
	50/50	< 0.7	46/74	
iPP/PS	10/90	0.6	75	[13]
	20/80	0.6	75/95	
iPP/PS/SBS	10/90	1.0	64	
	20/80	1.0	64	
iPP/aPP	70/30	-	65-80	[14]
iPP/LLDPE	10-20	-	83	[15]
iPP/PA6	20/80	2-4	76-87	[16]
iPP/LLDPE	20/80	< 1	89	[17]
	35/65	< 1	91	
iPP/LLDPE	20/80	1-3	86	
iPP/LLDPE	20/80	< 2	82/90	[18, 19]
iPP/VLDPE	20/80	< 2	70/85	
iPP/ULDPE	20/80	< 1	65/95	
iPP/PS	20/80	0.29 um^3	44/74/109	[20]
iPP/PS/SEP	20/80	0.1-0.33 um^3	44-47/74/101	
iPP/PA6/MA	30/70	< 1 um	110/123	[21]
	40/60	< 1 um	120/125	
iPP/PC	10/90	1-3	94.3/98.2/112.1	[22]
	20/80	3-5	96/112.7	
iPP/PCL	3/97	< 3	49.8/71.6/95.7	[23]
	5/95	< 3	51.1/72.3/95.3	
	10/90	2.8	51.6/72.4/96.9	
	30/70	12.8	52.3/71.6/114.5	
iPP/PS	10/90	1.46	43.7	[24]
	20/80	-	45.6/62.8/67.2/103.8	
iPP/PS/SEP	20/80/4	1.50	46.3/62.3	
LDPE/PS	20/80	-	53.5/61.5/70/100	[25]

LLDPE/PS	10/90	0.04 um^3	73/105	[19]
	20/80	0.06 um^3	74/105	
	30/70	0.18 um^3	72/102	
	40/60	0.38 um^3	74/104	
LLDPE/PS/SEBS	10/90/1	0.01 um^3	72/103	
	20/80/2	0.06 um^3	73/103	
	30/70/3	0.29 um^3	72/103	
	40/60/4	0.14 um^3	74/104	
HDPE/PS	10/90	mix morphology	77.2/100/115.7	[26]
	20/80	mix morphology	68.5/76.8/108.5/115.2	
	30/70	0.14	66.6/77.5/115.7	
LLDPE/PS	10/90	0.17	67.3	
	30/70	0.23	51.2/70.1/102.9	
ULDPE/PS	20/80	0.87	40/70.3/74.7	
HDPE/PA6/EPDM-g-MA	10/70/20	< 1	98/115	[27]
	15/70/15	< 2	100/115	
	20/70/10	< 1	102/115	
HDPE/PET	15/75	1.4-2.2	106/115	[28]
HDPE/E-GMA/PET	12.5/2.5/75	0.6	75/98	
HDPE/PMMA	9/91	0.2-2	70	[29]
PEO/iPP	50/50	3-5	12/38	[30]
	25/75	1-3	-18	
PCL/PEO	20/80	< 5	25	[31]

Two paradigmatic examples of fractionated crystallization encountered in immiscible blends by varying concentration are shown in Figure 3 for polystyrene/polypropylene (PS/iPP) and polystyrene/linear low-density polyethylene (PS/LLDPE) blends. Figure 3A presents the DSC cooling curves of PS/iPP blends at three different compositions. At an iPP content of 30 % two crystallization exotherms are already observed, with the main peak at the highest temperature, attributed to type A heterogeneities, being dominant. In fact, given the coarse morphology at this composition, with droplet size in the range of 7 - 9 μm, the presence of such impurities in the largest part of the droplets ensembles is very likely. With the reduction of iPP concentration to 20 and finally 10 %, the droplet size decreases to 2 μm and below 1 μm, respectively [20]. Correspondingly, the fraction of droplets containing highly active impurity A becomes much lower and finally disappears.

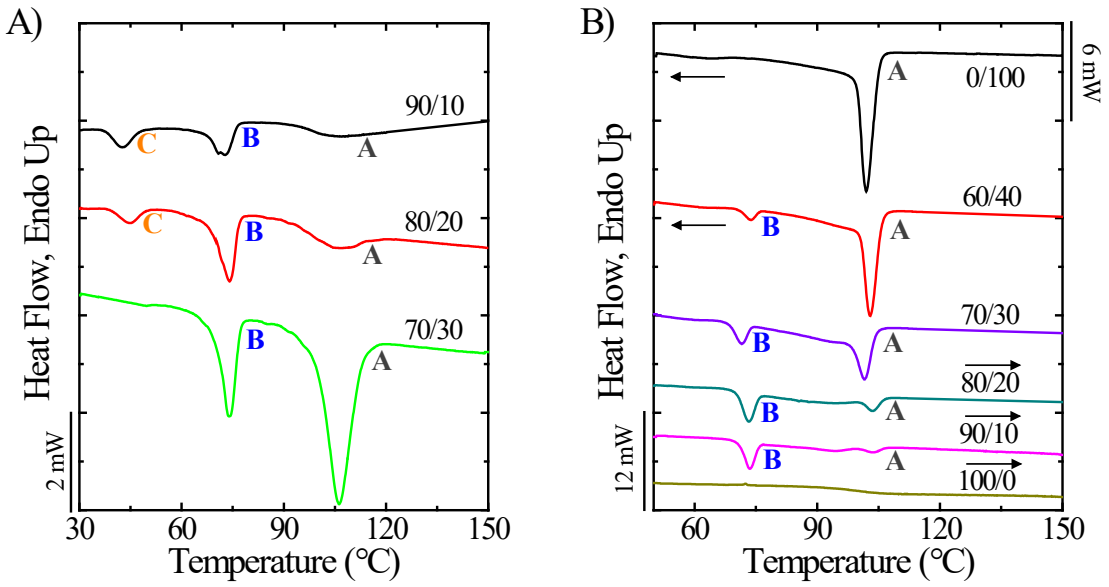

Figure 3. Selected examples of DSC cooling curves for immiscible blends at different indicated compositions for (A) PS/iPP and (B) PS/LLDPE. [20], Copyright 1998. Adapted with permission from John Wiley & Sons Inc.

We note that in the blend with 20 % iPP three fractionated crystallization peaks are observed, attributed to impurity A, B and homogeneous nucleation at the lowest temperature (peak C). The sub-micron droplets of PS/iPP 90/10, instead, only exhibit nucleation by the less active heterogeneity B and via surface/homogeneous modality at around 45 °C (peak C).

Similar considerations also hold for PS/LLDPE blends in Figure 3B. In this case, the blends feature two main crystallization peaks, the one at high temperature being coincident with the one which characterizes bulk crystallization via heterogeneous nucleation (type A impurity). With the progressive decrease of the LLDPE content in the blend, from 40 to 10 %, the area of such peaks decreases, at the expense of the low temperature fractionated crystallization peak which grows in intensity and becomes the dominant crystallization event. Such peak at around 75 °C could be tentatively attributed to a different kind of heterogeneity (type B) or to surface-induced nucleation by the PS matrix. It is interesting to note that under these conditions, despite the submicron droplet size, exotherm A does not totally disappear, indicating the presence of a small droplet population is still very efficiently nucleated.

To clarify the effect of blend composition on fractionated crystallization, we have collected data from several systems in the literature in Figure 4. In particular, we considered the extent of fractionated crystallization, as represented by the fractional area of the lowest temperature crystallization peak. Figure 4A shows the trends of this

quantity as a function of the concentration of the crystallizable blend component.

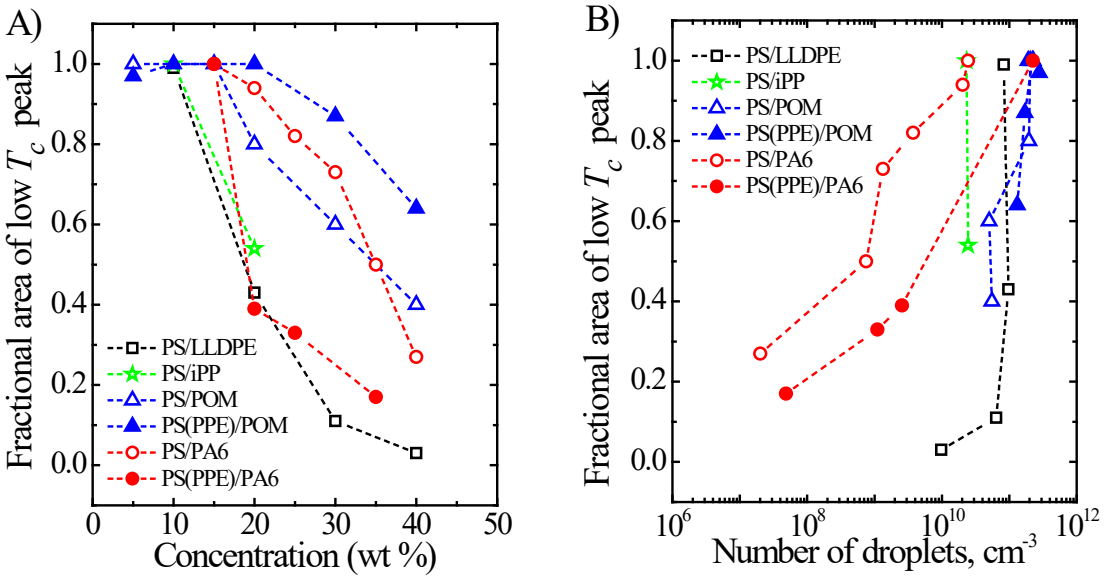

Figure 4. Fractional area of the low temperature fractionated crystallization exotherms for different immiscible blends systems as a function of (A) concentration of the semicrystalline component, (B) number of droplets of the dispersed phase per unit volume.

A gradual increase of fractionated crystallization with decreasing content of semicrystalline polymer can be noticed for all different blends, i.e., notwithstanding the specific polymer considered. Typically, saturation in the fractional area of low temperature crystallization peak is reached for concentration in the range 10 - 20 % of crystallizable component, depending on the specific polymer pair taken into account. The lack of a common trend among the different blends indicates that fractionated crystallization is not controlled by the overall concentration of the crystallizing component, but rather depends on the specific morphology that is generated during mixing, the latter being a function of composition, viscosity ratio, interfacial tensions, etc.

A more instructive way of looking at fractionated crystallization is reported in Figure 4B. Here, the extent of fractionated crystallization is shown as a function of the number of droplets per unit volume. The rationale for interpreting Figure 4B is that the low temperature crystallization peak would increase once the concentration of isolated microdomains overcomes that of active heterogeneous nuclei in the bulk material. It can be seen that the droplet concentration for the maximum of fractional area of the low T_c peak is different for each system, as expected given the specific content of impurities in each material. For most of the blends the transition from bulk

to fractionated crystallization is very sharp, as the fractional area of the low crystallization temperature peak saturates in an interval of droplet concentration smaller than one order of magnitude. This is also in agreement with the expectation, given the precise number of original nuclei. In this respect, the blends with PA6 are an exception. For those systems the extent of fractionated crystallization increases more gradually, over a larger range of droplet concentration. The possible reason could be related to the existence of different type of nucleating impurities with relatively high efficiency, or to polydispersity in the microdomain sizes.

To further strengthen the link between immiscible blends morphology and fractionated crystallization, it is of interest to consider compatibilized systems [20, 32]. In fact, besides tuning the composition, adding a compatibilizer is known as an effective way to tailor the dispersed phase size. Some clear examples showing the variation of fractionated crystallization behavior upon increasing the compatibilizing agent content in the blend are displayed in Figure 5.

Figure 5A presents the DSC cooling curves of an 80/20 PS/iPP blend containing increasing content of styrene-*block*-ethylene-*ran*-propylene (SEP) diblock copolymer as compatibilizer [20]. The non-compatibilized blend shows a distinct fractionated crystallization behavior, with the peaks at around 70 °C being the dominant. Peaks at higher temperature (ca. 115 °C) characterizing type A heterogeneities are also present, together with a small fraction of clean droplet nucleating at the homogeneous nucleation temperature, around 45 °C. Upon addition of the SEP compatibilizers, all the high temperature exotherms (A, B, C) tend to disappear, while the homogeneous nucleation peak (peak D) becomes more and more important with increasing SEP concentration. Such change in the fractionated crystallization behavior is associated with a decrease of droplet size of about a factor 2, from 1.6 to 0.9 μm. As a result, the higher number of smaller droplets lowers the probability of finding highly active heterogeneities in a relevant ensemble of droplets, thus favoring homogeneous nucleation in the impurity-free domains.

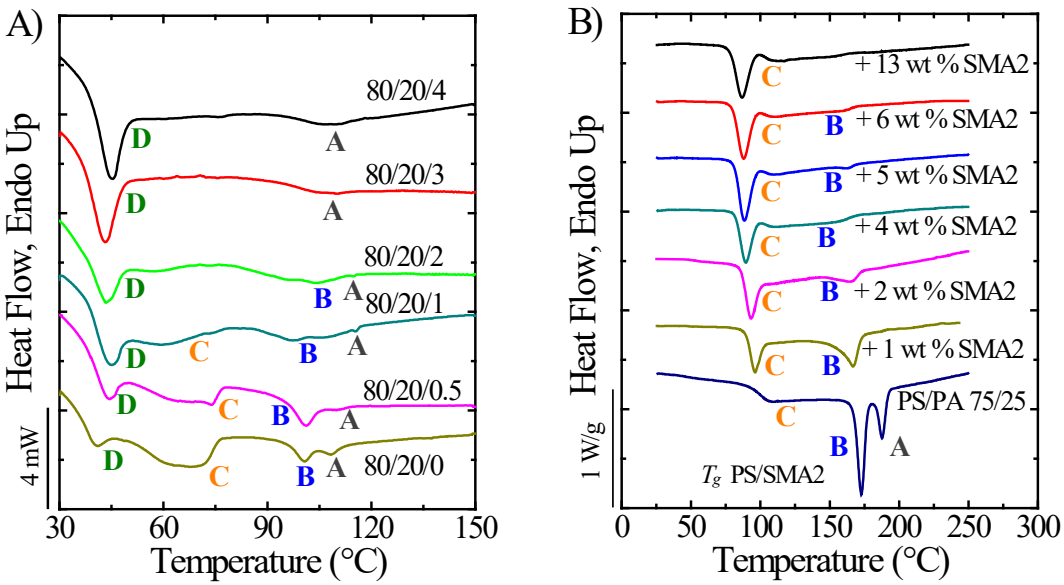

Figure 5. Selected examples of DSC cooling curves for immiscible blends including different indicated content of compatibilizers (A) PS/iPP/SEP and (B) PS/PA6/SMA2. [20], Copyright 1998. Adapted with permission from John Wiley & Sons Inc. [32], Copyright 2005. Adapted with permission from Elsevier Science Ltd.

Figure 5B displays the cooling curves of PS/PA6 75/25 blends reactively compatibilized upon extrusion, with the addition of different quantities of styrene-maleic anhydride copolymer (SMA2) [32]. PS/PA6 blend without compatibilizer exhibits fractionated crystallization with two main peaks: one at the bulk crystallization temperature (188 °C), and the second at around 170 °C. This fractionated crystallization is the result of a droplet dispersion with an average size of around 2 μm. The addition of SMA2 has a noteworthy effect, causing the appearance of a low-temperature exotherm, located around 95 °C, and the simultaneous decrease in area of the high temperature fractionated crystallization peaks. Above about a level of 5 - 6 % of SMA2, the morphology, which has changed to an average droplet size below 0.2 μm, does not change anymore, and thus fractionated crystallization is correspondingly unaltered.

Other than non-isothermal, isothermal crystallization experiments for the dispersed phase of immiscible blends have been very informative for studying nucleation mechanism [7, 33-36]. In fact, given the typically large undercoolings, it can be assumed that nucleation is the rate-determining step of the overall crystallization process, i.e., once one droplet is nucleated, the crystallites grow very fast to occupy the whole droplet volume and growth time can be neglected with respect to nucleation time. Under such conditions, only one nucleation event per

droplet occurs, and each isolated microdomain nucleates independently from the others and randomly in time. Such a process is thus described by a first-order kinetics, according to:

$$\frac{N}{N_0} = e^{-kt} \tag{6}$$

where N/N_0 is the fraction of droplets not yet crystallized at time t, and N_0 is the total number of droplets that undergo nucleation. The rate constant, k, depends on the specific nucleation mechanism considered. In particular, for homogeneous (volume) and surface nucleation it is equal to $I_V \cdot V$ and $I_A \cdot A$, respectively. I_V and I_A are the volume-dependent and area dependent nucleation rates, while V and A are the corresponding droplet volume and surface area.

In the literature, Equation 6 has been applied to describe the crystallization kinetics of several immiscible blends with droplet morphology, namely PS/PA6 [34], compatibilized ethylene/1-octene copolymer/PA6 [35], and more recently neat and nucleated PS/iPP blends [7].

DSC data are commonly used, under the assumption that each droplet gives an identical contribution to the crystallization enthalpy, thus resulting in the equality between N/N_0 and $(1-\Delta H(t)/\Delta H_{TOT})$, where ΔH_{TOT} is the final crystallization enthalpy at the adopted crystallization temperature. Therefore, plotting the natural logarithm of $(1-\Delta H(t)/\Delta H_{TOT})$ versus time, a straight line is commonly obtained, the slope of which gives access to the constant k. In the case of particularly polydisperse systems, a certain curvature can be appreciated [36], since larger droplets will solidify before smaller ones, giving rise to a more complex and time-dependent kinetics. In the case of PA6 blends [34, 35], the first-order kinetics has been associated with the occurrence of homogeneous nucleation. For the case of waterborne iPP microemulsions, both surface and volume-based nucleation equations could fit the obtained kinetic data appropriately [36], however, in light of the explored crystallization temperature range, we can probably attribute the mechanism to homogeneous nucleation (see later section 3.2). More recently, Wang et al. demonstrated that a first-order kinetics can also be associated with heterogeneously nucleated droplets [7] (see section 3.1).

It is worth to discuss the effect of immiscible blend morphology on the overall crystallization kinetics. In general terms, the isothermal crystallization can be described by the Avrami equation:

$$1 - V_c(t) = e^{-k(t-t_0)^n} \quad (7)$$

with V_c being the relative volumetric transformed fraction, t_0 the induction time, n the Avrami index and k the overall crystallization rate constant, which contains contributions from both nucleation and growth [37]. Müller et al. [37-40] proposed that Avrami exponent depends on two terms, n_n, which is the term associated to nucleation, and n_{gd}, which is related to growth dimensionality as:

$$n = n_n + n_{gd} \quad (8)$$

Following the Avrami analysis, the nucleation can fluctuate between instantaneous (i.e., all nuclei appear at the same incubation time) or sporadic (i.e., the nuclei appear as a function of time depending on T_c). Two extreme cases can be thus considered, n_n will be respectively 0 (for instantaneous nucleation at the lowest T_c values) or 1 (for very slow sporadic nucleation at very high T_c). However, depending on the crystallization temperature, non-integer n_n values could be generated when the nucleation is in between these two extreme cases. The term n_{gd} takes values from 1 to 3 depending on the dimensionality of the crystals formed: 1, 2 or 3 dimensions respectively. For n equal to 1, the Avrami equation is equivalent to a first-order kinetics (Equation (6)). A typical case of n=1 can be obtained for isolated numerous clean droplets, when the nucleation is the slow step of the kinetics because the growth is so fast (due to the small size of the droplets) that n_{gd} can be approximated to 0. The kinetics in this case only depends on the possible values of n_n (0 for instantaneous nucleation and 1 for sporadic nucleation). The typical case of n = 1 (first-order kinetics) arises because nucleation is usually sporadic in confined microdomains and growth is too fast to influence the kinetics.

A clear difference in the Avrami kinetics between dispersed and co-continuous phases in immiscible blends, as a consequence of the distinct nucleation mechanism, was shown by Córdova et al. [33], and is displayed in Figure 6. The system studied is constituted by a reactively compatibilized PE/PA6 blends. Careful tuning of the functionalized polyethylene weight fraction and extrusion conditions allowed the production of samples with different morphology, despite the very close composition.

In particular, both sub-micron dispersion of polyamide droplets in the PE matrix and co-continuous morphology could be produced (see TEM images in the insets of Figure 6).

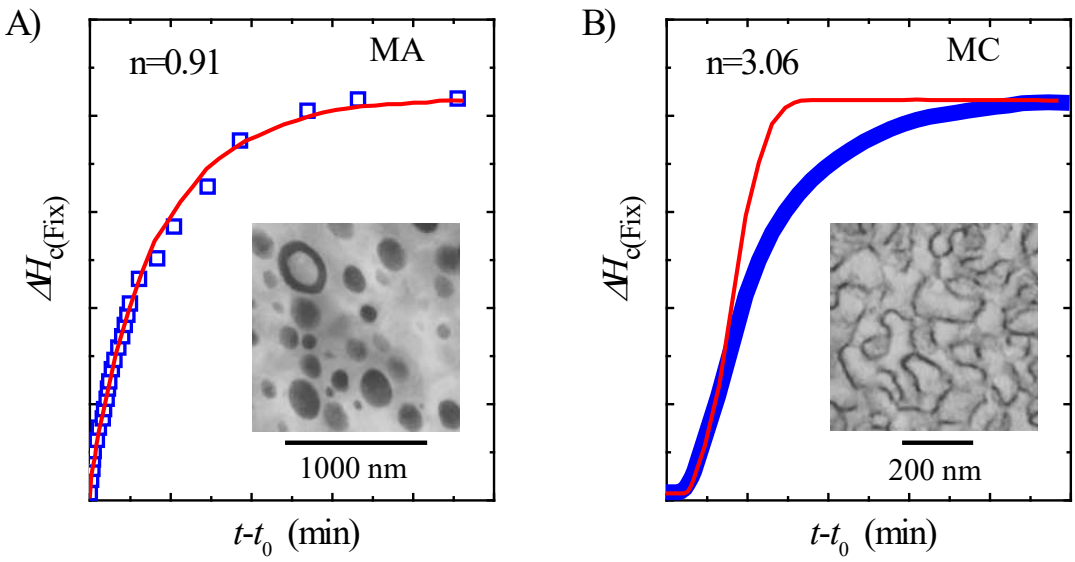

Figure 6. Selected examples of the evolution of the relative crystallization enthalpies as a function of time upon isothermal crystallization of the polyamide phase of immiscible PE/PA blends with either dispersed phase (left) or co-continuous (right) morphology. The induction time is subtracted. Red lines represent the fit to the Avrami equation (equation (6)). The insets are representative TEM images of the blend morphologies. [33], Copyright 2011. Adapted with permission from John Wiley & Sons Inc.

The evolution of the normalized crystallization enthalpy in the two cases, together with the corresponding fit to the Avrami equation, is shown in Figure 6. We note that the induction time is subtracted, and that the conversion range chosen for the fitting is between 3 and 20 %, as recommended for the correct application of the Avrami equation [37]. The obtained values of the Avrami index, *n*, are also reported in the Figure. For the dispersed phase morphology an exponent close to 1 is found, while the co-continuous blend presents a value of 3 [33]. The first-order kinetics in sub-micron droplets indicates sporadic nucleation, either surface-induced or homogeneous, and that each isolated microdomain crystallizes independently and randomly in time. On the contrary, the Avrami exponent equal to 3 in the case of co-continuous morphology can be understood as the result of the "spreading" of the nucleation events between the interconnected regions of the polyamide phase. In other words, once nucleation occurs at one point, crystal growth can proceed unimpededly within the percolated domains and the contribution of growth is now an important factor in the overall crystallization kinetics (that depends on both nucleation and

growth).

2.1.2. Breakup of multilayer films and nanofibers

Fractionated crystallization also occurs in multilayer films, after thermal breakup of nanolayered films in order to form polymer nanodroplets. The coextrusion process to fabricate multilayer films, combining two or more polymers as alternatively layered structures, was reviewed by Langhe and Ponting [41]. Since the multilayer films are constructed by a "forced" assembly process, the layered structures are intrinsically not stable. A schematic showing the mechanism of multilayer film breakup and droplet formation during thermal treatment is shown in Figure 7, including hole formation, hole growth, droplet formation and coalescence [42]. This approach has been applied by Hiltner and Baer [43] to investigate confined crystallization or fractionated crystallization of PP [8,44-49], PEO [50-54], PCL [55], HDPE [50,56], PC [57], PA6 [58], and PVDF [59], and the relevant references are summarized in Table 2.

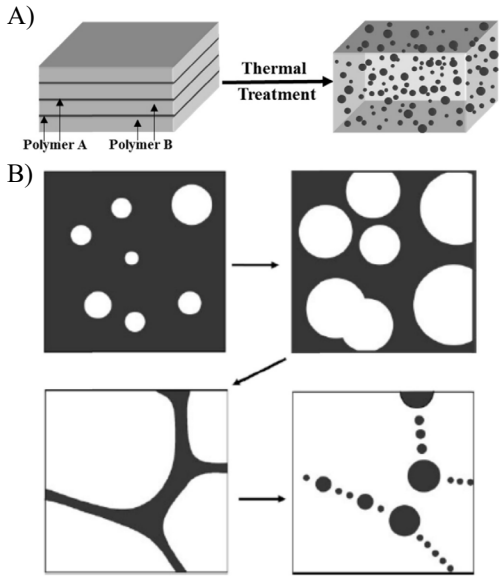

Figure 7. (A) Coextruded multilayer films including alternative layers of polymer A and B, where polymer A and B are the minor and major phases, respectively. During the heating process, polymer A breaks up by the effect of temperature and forms droplets dispersed in polymer B. (B) Schematic showing the mechanism of multilayer film breakup and droplet formation during thermal treatment. [42], Copyright 2018. Adapted with permission from Elsevier Science Ltd.

According to Bernal-Lara et al. [50], changing the number of alternated layers can vary the individual polymer layer thickness, which is directly related to the final droplet size distribution. As an example, HDPE/PS multilayer films with different

HDPE nanolayer thickness were prepared to study fractionated crystallization of HDPE droplets created through thermal breakup during heating. For HDPE nanolayers with thickness larger than 120 nm (droplet diameter about 2 μm), all the HDPE droplets heterogeneously nucleated at around 115 °C. Reducing the layer thickness to 20 nm resulted in fractionated crystallization of HDPE droplets where two clear exothermic peaks appeared at 115 (peak A) and 80 °C (peak B), respectively. However, all the HDPE droplets crystallized exclusively at 78 °C when the layer thickness was further reduced to 10 nm (droplet diameter about 140 nm).

Table 2. Examples of fractionated crystallization in multilayer films.

Composites	Component (Volume)	Single layer thickness (nm)	Domain size (break up, nm)	T_c (°C)	Reference
HDPE/PS 257 layers	10/90	120	-	81/116	[50]
	5/95	120	-	81/117	
	5/95	60	-	81/116	
	10/90	40	550	81/115	
	10/90	30	-	80/115	
	5/95	20	-	80/116	
	5/95	10	140	78/116	
HDPE/PS (high pressure)	10/90	120	6.4	81.5/118	[56]
	10/90	40	1.86	80.5/116	
	5/95	14	0.53	78/116	
iPP/PS 257 layers	10/90	12	30	40/60	[45]
iPP/PS/NAs (%)	10/90/0.1	12	200	40/60	[46]
	10/90/0.3	12	200	40/60	
	10/90/0.4	12	200	40/70	
	10/90/0.5	12	200	40/70	
	10/90/0.6	12	200	70/81.4	
	10/90/1.0	12	200	70/94.3	
	10/90/1.5	12	200	118.3	
	10/90/2.0	12	200	125.8	
iPP/PS 257 layers	10/90	12	500	44	[47]
iPP/PS 257 layers	10/90	12	100-1000	40	[8]
		20	8000-10000	40/64	
		40	8000-10000	40/64/90	
		200	8000-10000	64/90/103	
iPP/PC 257 layers	10/90	12	100-800	37/85	[8]
		20	6000-8000	37/85	
		40	6000-8000	85	
		200	6000-8000	107	
iPP/PS 257 layers	10/90	12	200	40/60	[48]
		20	2000	40/60/85	
		40	2000-8000	40/60/85	
		200	6000-8000	60/85/102	
iPP/PS (high pressure)	10/90	12 20	-	40 40/65/70	[60]

		40 100 200		40/65/70 65/70/91 91/105	
PEO/PS 9 layers	30/70	21000	-	44	[54]
257 layers	50/50	1000	-	44	[61]
257 layers	30/70	300	-	42	
1025 layers	30/70	75	-	40	
1025 layers	10/90	25	-	40	

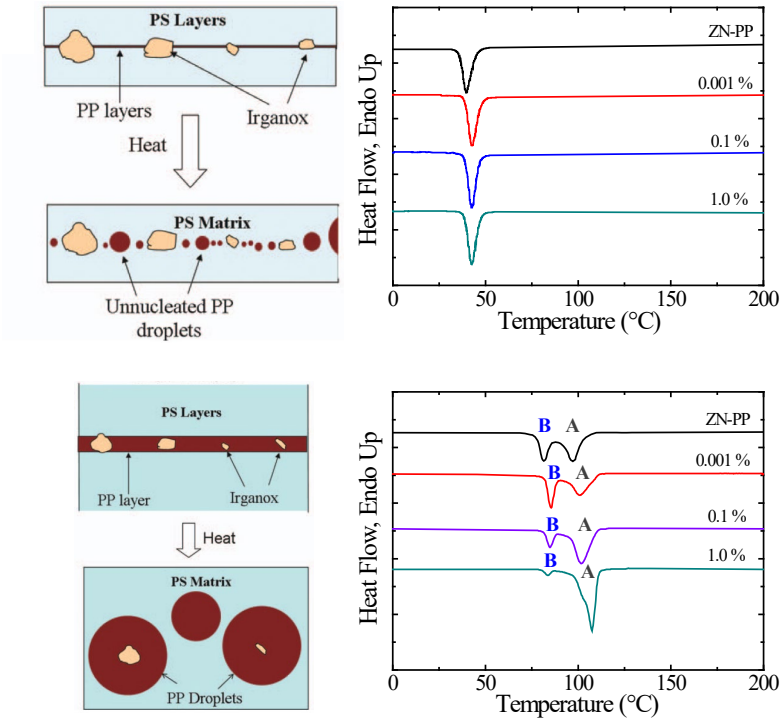

Figure 8 (A) Schematic (left) of the thermal breakup of 12 nm iPP nanolayers containing Irganox particles, which are excluded from the droplets during the process. DSC cooling scans (right) of iPP nanolayers with different concentrations of Irganox after thermal breakup at high temperatures. (B) Schematic (left) of the thermal breakup of 200 nm iPP nanolayers containing Irganox particles, which are encapsulated in the droplets. DSC cooling scans (right) of iPP nanolayers with different concentrations of Irganox after thermal breakup at high temperatures. In both cases, the cooling rate is 10 °C/min. [8], Copyright 2012. Adapted with permission from John Wiley & Sons Inc.

Fractionated crystallization in multilayer iPP/PS films with iPP layer thickness varying from 20-200 nm was also observed [8]. In order to elucidate the nature of heterogeneous nuclei associated to the various exothermic peaks, a commonly used antioxidant, Irganox, was added to iPP/PS multilayer films with compositions up to

1.0 % during the coextrusion process. For 12 nm iPP nanolayers containing Irganox (Figure 8A), the crystallization exotherms at large undercooling, ascribed to homogeneous nucleation, did not change significantly for all the samples, suggesting that Irganox particles were excluded from the iPP droplets due to the droplets size being smaller than the size of Irganox particles. However, iPP droplets obtained from 200 nm iPP nanolayers with relatively larger diameters showed fractionated crystallization with two exothermic peaks centered at 112 and 90 °C, as shown in Figure 8B. With increasing the Irganox concentration, the intensity of 112 °C peak (peak A) increased at the expense of the intensity of 90 °C peak (peak B). The results of these elegant experiments indicated that the high temperature fractionated crystallization peak of iPP droplets could be ascribed to Irganox or some other similar antioxidants. An analogous approach was applied to prove that catalyst residues were responsible for the fractionated crystallization peak at around 90 °C.

Immiscible polymer blends can be used to prepare nanofibers by electrospinning and a novel method to investigate fractionated crystallization in semicrystalline polymers is utilizing thermal breakup of electrospun fibers to obtain polymeric nanodroplets [62]. As-spun polymer blend fibers usually display co-continuous morphology and break into nanodroplets through thermal annealing at temperatures above the T_g of the matrix due to Plateau-Rayleigh instability.

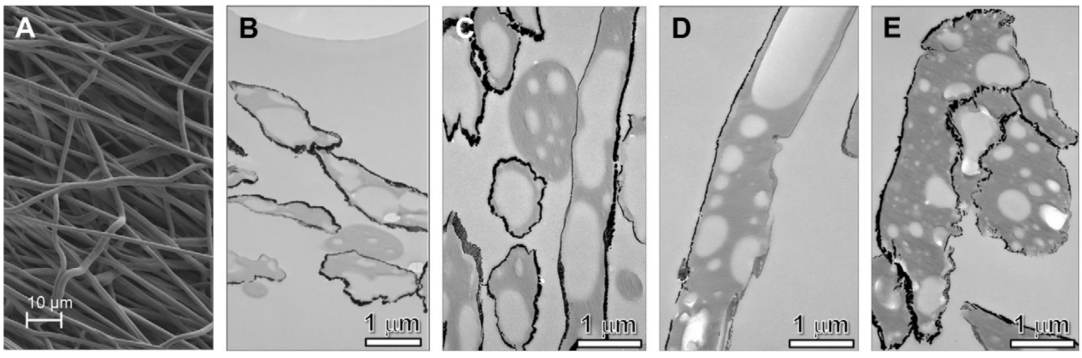

Figure 9 (A) SEM and (B) TEM of as-spun PEO/PS (30/70, wt %) blend fibers. TEM micrographs of P4tBS-coated PS/PEO blend fibers annealed at different temperatures for 15 min: (C) 85 °C, (D) 105 °C, and (E) 150 °C, respectively. For SEM and TEM observations, microtomed thin sections were sputter-coated with gold before being embedded into epoxy. [63], Copyright 2011. Adapted with permission from Elsevier Science Ltd.

As an example, fractionated crystallization in electrospun PEO/PS (30/70, wt. %) blend fibers was studied by Zhong [62,63] employing Rayleigh breakup at different annealing temperatures. In order to achieve a well-defined Rayleigh breakup, the polymer blends were coated with poly(4-tert-butyl styrene) (P4tBS) possessing a high T_g. As can be seen in Figure 9, raw PEO/PS blend fibers are co-continuous (A-B) and PEO nanodroplets (C-E) form through thermal breakup during heating. When the annealing temperature is below 95 °C, the temperature is not enough to break the largest part of the electrospun fibers, therefore, the majority of PEO/PS blend will crystallize heterogeneously at around 40 °C (Figure 10A). However, when the annealing temperature is above 125 °C, PEO/PS blend fibers break into numerous nanodroplets and homogeneous/surface-induced nucleation at large undercooling dominates the overall crystallization, due to the lack of heterogeneities.

To confirm the origin of fractionated crystallization peaks during cooling of PEO nanodroplets, Zhong [63] further investigated the isothermal crystallization kinetics of PEO/PS nanofibers by employing the Avrami equation. The results are shown in Figure 10B. The crystallinity of PEO was obtained as a function of crystallization time at different T_c. As a comparison, the crystallization kinetics of neat PEO was also studied, and the Avrami index around 3 at 53 °C indicates a 3-D unconfined crystal growth after instantaneous nucleation. When P4tBS coated PEO/PS fibers were annealed at 85 °C and then cooled down to crystallize at 48 °C (near the higher fractionated T_c), the Avrami index decreased to 2.1, revealing a 2-D confined crystal growth after instantaneous nucleation in electrospun nanofibers. With increasing the annealing temperature to 150 °C, numerous PEO droplets free of impurities are formed and the Avrami index is found to be around 1 at 0 or -10 °C, which confirms the homogeneous or surface-induced nucleation mechanism.

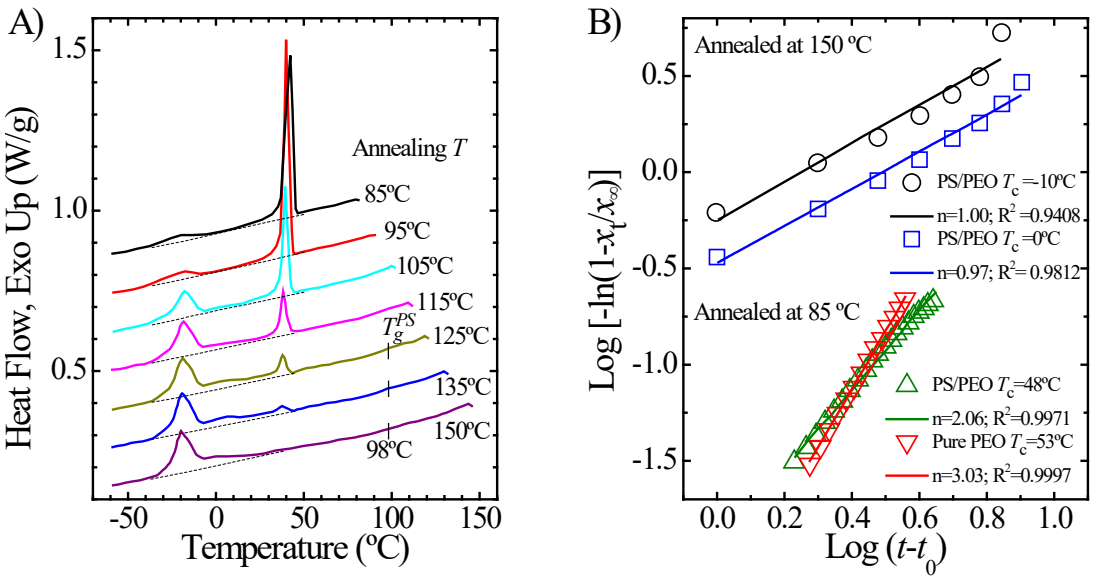

Figure 10 (A) DSC cooling curves at 5 °C/min of P4tBS-coated electrospun PS/PEO blend fibers after annealing at different temperatures for 15 min; (B) Avrami analysis of the isothermal crystallization data of P4tBS-coated PS/PEO blend fibers annealed at different temperatures. [63], Copyright 2011. Adapted with permission from Elsevier Science Ltd.

The above-described technique has been successfully employed for other polymeric materials, such as PEO [64,65], PVDF [66,67], PBA [68], in order to investigate homogeneous/surface nucleation or fractionated crystallization, even without the addition of compatibilizers.

2.1.3. Miscible blends

Fractionated crystallization not only appears in immiscible blends, but can also be present in miscible blends, where no phase separation occurs but a different kind of confinement of one crystallizable component can arise. In order to observe fractionated crystallization in miscible blends, both the two polymers should be semi-crystalline and have different ranges of crystallization temperatures (T_c). Moreover, the component that crystallizes at higher T_c must not nucleate the lower T_c component. Compared to immiscible blends, there are just few binary miscible blends showing fractionated crystallization, such as PEO/poly(butylene succinate) (PBS) [69-73], poly(butylene adipate) (PBA)/poly(vinylidene fluoride) (PVDF) [74,75], PBA/PBS [76], PEO/poly(3-hydroxybutyrate) (PHB) [77-80], PEO/ Poly(ethylene suberate) (PES) [81].

As an example, fractionated crystallization in PBS/PEO blends studied by He et al. [69,70] is discussed. The DSC cooling curves of PBS/PEO blends with the indicated compositions are shown in Figure 11A. Up to a 60/40 composition, only a high-temperature exotherm is observed for PEO crystallization. Three fractionated exothermic peaks appear for the blend with the weight composition of 70/30. In this case, when PBS crystallizes first, the amorphous PEO chains are isolated within PBS interfibrillar/interlamellar regions. As a consequence, PEO domains will crystallize at much larger undercooling upon cooling, not being interconnected with each other and having partially lost heterogeneities, segregated by the crystallization of PBS. With further decreasing the content of PEO the degree of confinement is stronger and a single crystallization peak at very low temperature is observed for this polymer.

Pan et al. [72] studied the effect of PBS crystallization temperature, $T_{c,\,PBS}$, on the fractionated crystallization of PEO. It should be noted from the comparison between Figure 11A and 11B that increasing $T_{c,\,PBS}$ has a similar effect of increasing the PBS component concentration on the fractionated crystallization behavior of PEO. As such peak A gradually disappears in favor of peak B by raising the isothermal crystallization temperature of PBS (Figure 11B). It is evident that a higher $T_{c,\,PBS}$ can facilitate the segregation of PEO chains within the interlamellar regions of PBS crystal.

A scheme drawn by Weng and Qui [81] is shown in Figure 12A, to illustrate the confinement environment responsible for fractionated crystallization in miscible blends. After the completion of high T_c component crystallization, if the majority of amorphous low T_c component is segregated within the interlamellar region of high T_c component, the low T_c component will crystallize at much larger undercooling compared to the bulk case, and only one exothermic peak appears. However, when the confined spaces are interconnected and most of low T_c polymer is located within the interfibrillar regions, two fractionated crystallization peaks are found.

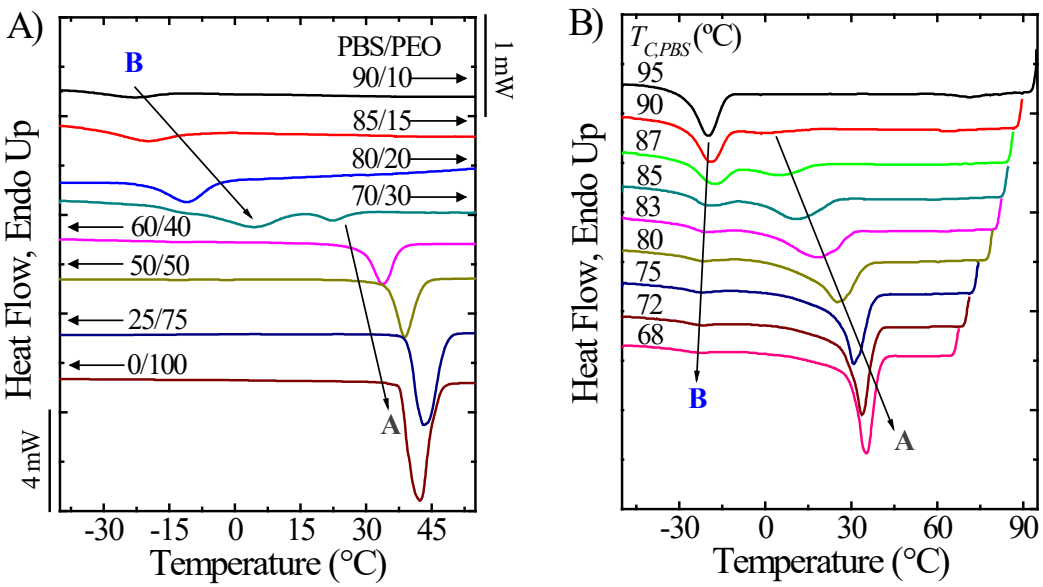

Figure 11 DSC cooling scans of (A) PBS/PEO blends with different compositions and (B) PBS/PEO blend (60/40, wt %) after the isothermal crystallization of PBS at different temperatures, $T_{c,\,PBS}$. Both the cooling rates are 10 °C/min. [70], Copyright 2004. Adapted with permission from American Chemical Society. [72], Copyright 2013. Adapted with permission from John Wiley & Sons Inc.

Furthermore, morphological evidence was provided by He et al. [71] to elucidate the origin of fractionated crystallization in miscible blends. PBS/PEO blend (50/50, wt %) was annealed at different $T_{c,\,PBS}$ first for the completion of PBS crystallization and then followed by standard cooling for the crystallization of PEO. Afterwards, PEO crystals were etched by alcohol and SEM observation was performed. With $T_{c,\,PBS}$ increasing from 80 °C to 100 °C, the PBS spherulitic "skeleton" changes from a highly branched and interconnected network to a predominantly cellular-like structure, where the confining geometry becomes more closed, regular and strict. Other morphological proofs were found by Wang et al. [82] in their study of PBS/PVDF blends. PBS crystallization within PVDF interfibrillar/interlamellar regions was directly visualized under PLOM.

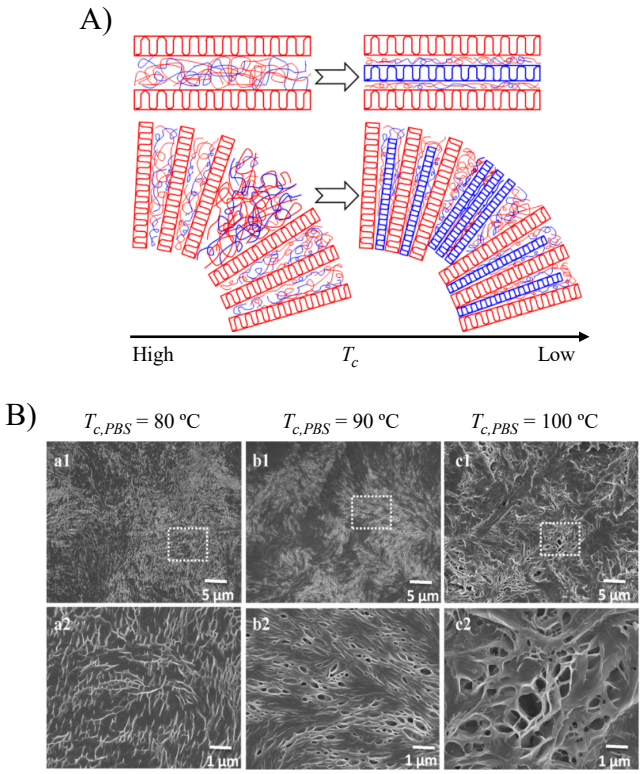

Figure 12 (A) Scheme showing fractionated crystallization within interlamellar (upper) or interfibrillar (bottom) regions, (red: high T_c component, blue: low T_c component); (B) SEM micrographs of PBS/PEO blends (50/50, wt %) after the crystallization of PBS at different $T_{c,PBS}$ and the extraction of PEO crystal. The dashed rectangular areas in a1 - c1 are enlarged and shown in the bottom a2 - c2. [71], Copyright 2013. Adapted with permission from American Chemical Society. [81], Copyright 2014. Adapted with permission from American Chemical Society.

For most of the binary crystalline miscible blends displaying fractionated crystallization, the two components usually possess very different T_c and only the low T_c component shows fractionated crystallization. An unusual fractionated crystallization behavior was observed by Weng and Qiu [81] in PES/PEO blends where both components showed fractionated crystallization at their lower content due to similar T_c.

2.2. Block Copolymers

Fractionated crystallization has also been observed in the crystallization of block copolymer microdomains. Diblock copolymers can exhibit a variety of morphologies depending on the segregation strength and on some key temperatures as will be explained in more detail in the next section. The crystallization of block copolymers has attracted much attention [39,83-96], and fractionated crystallization [39,85,86,91,93,97] has been reported for strongly segregated block copolymers, as

well as for weakly segregated or miscible block copolymers, some of the results reported in literature can be found in the following table (Table 3).

In the case of block copolymers in the strong segregation regime, the crystallization occurs in a confined fashion within the MDs originated by phase segregation in the melt, e.g., lamellae, cylinders or spheres. If the number of MDs is much higher than the number of heterogeneities present in the bulk crystallizable phase (i.e., like in the precursor or equivalent homopolymer synthesized by identical procedures), heterogeneity free microdomains could be obtained [39,85,86,91]. Regarding weakly segregated or miscible copolymers, if the block copolymer is formed by two crystalline blocks, the crystalline superstructure of the block that crystallizes first (e.g., axialites or spherulites) will confine the crystallization process of the second block, that has to crystallize within the interlamellar regions of the previously crystallized block [39,85,86,91]. The effect of the architecture of the polymer chain in confined crystallization has been also studied in the literature [39,87,91]. Different chain topology, such as miktoarm star copolymers, can result in higher confinement than analogous linear copolymers.

Table 3. Summary of the data reported in literature for block copolymers and terpolymers.

Block Copolymer	Composition (wt %)	M_n Kg/mol	Morphology (Domain size)	T_c (ºC)	Reference
PEG-*b*-PBS	72.5/27.5	PEG 6	Miscible	PEG -27.4 PBS 72.6	[98]
	64.1/35.9	PEG 6		PEG 17.8 PBS 69.5	
	51.96/48.04	PEG 6		PEG 17.9 PBS 71.1	
	38.58/61.42	PEG 6		PEG 19.2 PBS 57.8	
PEG-*b*-PBS	45/55	PEG 1	Miscible	(PEG)	[99]
	50/50	PEG 1		-26.3	
	57/43	PEG 1		-1.7	
	34/66	PEG 2		-34.7	
	39/61	PEG 2		-32.1	
	46/54	PEG 2		-7.2	
	26/74	PEG 6		-26.4	
	29/71	PEG 6		-26.2	

	35/65	PEG 6		17.9	
	18/82	PEG 10		-30.5	
	24/76	PEG 10		-26.0	
	32/68	PEG 10		13.3	
PES-*b*-PBS	0/100			77.7	[100]
	100/0			45.8	
	48.2/47.2	E 33 B 29	Miscible or partially miscible	PBS 59.1 PES 31.1	
	47.3/48.8	E 47 B 46		PBS 64.3 PES 30.5	
	48.9/47.7	E 54 B51		PBS 64.6 PES 37.7	
	49.6/47.6	E 59 B 56		PBS 66.1 PES 46.1	
	49.4/47.8	E 65 B 67		PBS 76.7 PES 51.7	
iPP-*b*-aPS	100/0			91.0	[101]
	43/57	10.4	Lamellae thickness 21.9 nm	23.9	
	34/66	11.6	iPP Cylinders radius 7.7 nm	15.4	
	23/77	17.8	iPP Spheres radius 10.3 nm	97.8	
E-*b*-MB	26/74	34.7 (Mw)	Weakly segregated	80	[102-104]
	26/74	44.3 (Mw)	Weakly segregated	71	
	27/73	62.7 (Mw)	Cylinders	62	
	27/73	87.9 (Mw)	Cylinders	62	
	100	19 (Mw)		95	
	E/VCH 29/71	35.8 (Mw)	Cylinders	62	
E-*b*-VCH	18/82	27.4	E spheres	58	[105]
	18/82	30.8	E cylinders	63	
	38/62	21.6	E channels, gyroid	76	
	43/57	42.9	E-poor lamellae	83	
	59/41	20	E-rich lamellae	84	
	100/0	41		87	
E-*b*-SEB	14/86	35.1	E spheres	57	[106]

	14/86	45	E spheres	60	
	14/86	63.7	E spheres	62	
	14/86	73.8	E spheres	63	
	25/75	69.8	E cylinders	63	
	100/0	41		84	
hPN-*b*-LPE	49/51 (volume)	hPN 9.3 LPE 8.6	Lamellae d 36 nm	105.4	[107]
	31/69 (volume)	hPN 6 LPE 11.6	d 30 nm	84.4	
	60/40 (volumen)	hPN 10.9 LPE 6.3	d 37 nm	112.6	
	47/53 (volumen)	hPN 26.3 LPE 25.8		-	
PE-*b*-PS	100/0	BD 24.4		85.1	[108]
	79/21	BD 31		77.3	
	53/47	BD 26.4	Lamellae (d 16 nm)	74.3	
	26/74	BD 26.4	PE cylinders (21 nm)	71.9 57.0	
	11/89	BD 27.6	PE spheres (12 nm)	68.7 55.3 46.7	
PE-*b*-PS PE-*b*-PEP	PE	PE 25		85.2	[109]
	E53S47	PE 27	Lamellae	74.4	
	E26S74	PE 27	PE Cylinders	71.8, 56.5	
	E11S89	PE 27	PE Spheres	68.7, 55.6, 46.6	
	E54EP46	PE 29	Lamellae	66.2	
	E29EP71	PE 29	Lamellae	65.7	
	E12EP88	PE 28		45.2, 35.1	
P3HT-b-PE	100/0			P3HT 196.0	[110]
	35/65		Alternating P3HT and PE rich domains	P3HT 194.4 PE 108.8	
	20/80			P3HT 174.5, 155.6, 133.6	

				PE 110.2	
	10/90			P3HT 151.6, 134.2 PE 111.8	
	5/95			P3HT 138.3 PE 109.7	
	0/100			PE 117.7	
PE-*b*-PEO	61/39	E 4.9 EO 4.0	Lamellae	PE 103.8 PEO 30.4	[111]
	78/22	E 5.1 EO 1.8	Lamellae	PE 103.8 PEO -7.0, -25.6	
PPL-*b*-PE	62/38	13.3	Lamellae	PPL 49.7 PE 83.9	[112]
PLLA-*b*-PE	PLLA	24.1		107.5	[113,114]
	L46E54	PLLA 23 PE 27	Lamellae	PE+ PLLA 88.7 PE 64.5	
	LD54E46	PLLA 32 PE 28	Lamellae	PE 88.3, 64.2	
PCL-*b*-PE	51/49	27.8	PCL layer thickness 16.5 nm	PCL 34.9 PE 86.6	[115]
PCL-*b*-PE	27/73 (volume)	16	PE Lamellae	PE 89.7 PCL 19.4	[116]
	51/49 (volume)	18	PE Lamellae	PE 88.1 PCL 36.4	
	75/25 (volume)	14	PE Lamellae	PE 87.6 PCL 36.3	
PCL-*b*-PS	PCL	29		31.5	[117,118]
	72/28 (Star)	31.6	Lamellae	29.9	
	39/61 (Star)	61.8	Cylinders	17.2	
	27/63 (Star)	109.1	Nanospheres	-	
	80/20 (Linear)	36	Cylinders	31.1	
	41/59 (Linear)	73	Lamellae	27.7	
	20/80 (Linear)	153		22.1	
PCL-*b*-PS	38/62	47	------	-45, -4, 27	[119]
	100/0			27	

PCL-*b*-PB	3/97 (volume)	100	Sphere radius 10.3 nm	-50.4	[120]
	8/92 (volume)	100	Sphere radius15.1 nm	-46.6	
	17/83 (volume)	100	Sphere radius 17.4 nm	-43.3	
	6/94 (volume)	62	Sphere radius 11.1 nm	-	
	100/0 (volume)	6.5		34.2	
PPDX-*b*-PCL	0/100	11.4		PCL 34.1	[121,122]
	100/0	15.2		PPDX 52.1	
	33/77	PCL 7.5 PPDX 27.1	Lamellae	PCL 31.3	
	40/60	PCL 7.1 PPDX 4.8		PCL 30.5	
	65/35	PCL 15.3 PPDX 26.2		PCL 29.1	
	77/23	PCL 10.3 PPDX 32.3		PCL 26.3	
PLLA-*b*-PCL	0/100	0.7		-	[123]
	0/100	2.5		21.4	
	0/100	4.1		23.7	
	100/0	4.4		98.5	
	100/0	7.7		108.0	
	100/0	8.9		105.3	
	100/0	11.2		113.0	
	PLLA3PCL2	29.6	Multiblock spherical or hexagonally packed cylinders	81.7	
	PLLA6PCL2	38.6		76.2	
	PLLA7PCL2	36.3		77.8	
	PLLA9PCL2	46.5		80.6	
	PLLA6PCL0.5	16.4		92	
	PLLA6PCL3	34.7		65.9	
	PLLA/PCL/PLLA	50.6	Lamellae	13/80	
	PLLA/PCL 5/5	30			
PEO-*b*-PCL	100/0	5		42.6	[124]

	84/16	6.65		35.3	
	82/18	7.24		36.4	
	77/23	7.48		35.9	
	71/29	8.07		PEO 33.9 PCL -1.3	
	64/36	8.54		PEO 33.0 PCL 13.4	
	57/43	8.92		32.9	
	50/50	9.81	Miscible in the melt	34.2	
	44/56	10.8		30.4	
	38/62	13.7		PEO 28.7 PCL 34.3	
	32/68	17.6		PEO 26.1 PCL 34.1	
	23/77	24.1		PEO 13.1 PCL 30.1	
	13/87	39.4		PEO -6.8 PCL 30.1	
	7/93	55.8		PCL 29.4	
	0/100	27.6		PCL 34.1	
PLLA-*b*-PCL	100/0	24	Partially miscible	LA 106.2	[125,126]
	93/7	18		LA 102.6	
	81/19	21		LA 102.8	
	60/40	21		LA 102.8 CL 0.5-11.3	
	55/45	18		LA 98.3 CL 20.8	
	44/56	25		LA 91.8 CL 23.2	
	32/68	22		LA 100.3 CL 28.1	
	10/90	24		LA 86.8 CL 32.5	
	0/100	29		CL 32.2	
PLLA-*b*-PEG	0/100	PEG5		PEG 40.2	[127]

	100/0	PLLA4.8		PLA 101.3	
	31.5/68.5	PLLA2.3 PEG5	Miscible in the melt	PLA 93.0 PEG 34.1	
	55.7/44.3	PLLA6.3 PEG5		PLA 105.2 PEG 34.6	
	70.6/29.4	PLLA12 PEG5		PLA 116.3 PEG 12.9	
PB-*b*-PEO PE-*b*-PEO	100/0	PB 25		87.1, 51.7	[128]
	0/100	PEO 1		21.0	
	0/100	PEO 2		29.8	
	B81EO19	PB 27.8 PEO 6.7	Sphere dn 13 nm	EO 46.1, -8.2, -27.1	
	E82EO18	PB 28.7 PEO 6.3	Sphere dn 21 nm	E 77.7, 75.0 EO 45.7, 20.2 -34.3	
	B89EO11	PB 90.2 PEO 11.5	Sphere dn 19 nm	EO -11.5, -26.8	
	E89EO11	PB 93.45 PEO 11.55	Sphere dn 31 nm	E 76.2, 53.1 EO 0.5, -24.3	
PS-*b*-PEO PS-*b*-PCL	EO100			21	[129-131]
	EO100	100		43	
	C100	32		33.5	
	S81EO19	18.5	PEO cylinders	-40	
	S39EO61	46	Phase segregated	39	
	S27C73	81	Phase segregated	PCL 36.5 -39.8	
PS-*b*-PEO-*b*-PCL	PEO1	1		21	[132]
	PEO2	100		43	
	PCL	37		35	
PCL-*b*-PEO-*b*-PS-*b*-PEO-*b*-	S81EO19	18.5	Phase segregated in all cases	-40	
	S63EO16C21	24		PEO -42	
	S46EO12C42	33		PEO -39	

PCL				PCL 27	
	S10EO4C86	150		PEO -38 PCL 33	
	S38EO10C52	39		PCL 26	
	S39EO61	46		PCL 40	
	S15EO37EO48	64		PEO -7 PCL 31	
	EO11S78EO11	71		PEO -38	
	C30EO4S32EO4C30	175		PEO -44 PCL -14, 32	
	C28EO5S34EO5C28	165		PEO -41 PCL -16, 30	
PB-*b*-PI-*b*-PEO	PEO1			21	[129-131]
	PEO100	100		43	
	PE19	19		73.4	
	B17I57EO26[130]	130	PEO cylinders	15, -21	
	B11I70EO19[120]	120	PEO spheres or cylinders	-23	
	B24I56EO20[67]	67	PEO spheres or cylinders	-25	
PE-*b*-PEP-*b*-PEO	E11EP71EO18[124] original	124	PEO cylinders	PE 52 PEO 22,-22	[129-131]
	E11EP71EO18[124] purified	123	PEO cylinders	PE 51 PEO -23	
	E24EP57EO19[69] original	69	PEO cylinders	PE 69 PEO 20, -22	
	E24EP57EO19[69] purified	69	PEO cylinders	PE 68 PEO,-27	
PS-*b*-PB-*b*-PCL	S57B27C16	137	Phase segregated in all cases	19.4, -55.4	[133]
	S27B37C36	132		22,8, -44.1	
	S35B15C50	150		20.7	
	S27B15C58	219		18.9	
	S33B06C61	207		23.1	
	S20B15C65	219		21.8	

	S09B14C77	181		21.8	
	PCL	83		23.8	
PS-*b*-PB-*b*-PCL	C100	32		33.5	[129-131]
	S62B27C11	62	Core-shell like cylinders with PCL cores	PCL 20.4 -45.1	
	S62E27C11	62		PE 71.5 PCL 10.1	
	S37B52C11	96	Core-shell like cylinders with PCL cores	PCL 6.4 -48.4	
	S37E52C11	96	PS cylinders	PE 75.2 PCL 18.4	
	S50B28C22	97	Core-shell cylinders with PCL cores	PCL 9.9, -45.9	
	S50E28C22	97	Undulated lamellae	PE 71.3 PCL 14.2	
	S26B36C38	110	Lamellar-lamellar	PCL 36.0 -40.8	
PS-*b*-PE-*b*-PCL	S26E36C38	110	Lemallar-lamellar	PE 72.1 PCL 25.8 14.2	
	S20B41C39	132	Lamellar-lamellar	PCL 16.7 -43.7	
	S20E41C39	132	PS cylinders	PE 79.8 PCL 8.8	
	S37B11C52	79	Lamellar-cylinders with PB cylinders	PCL 28.3	
	S37E11C52	79	PCL matrix, PE-rings and PS cylinders	PE 45.0 PCL 27.0 -5.0	
	S23B21C56	103	Lamellar-lamellar	PCL 31.2 -39.6	
	S23E21C56	103	Lamellar-lamellar	PE 53.3 PCL 24.1 -3.3	
PS-*b*-PE-*b*-	S35E15C50	150	PCL matrix	E 63.7	[38]

PCL				PCL 27.7	
	S57E27C16	137	PS matrix,	E 62.7 PCL 25.3	
	S36E35C29	81	PS, PE, PCL lamellae	E 69.9 PCL 13.4	
	S60E69C25	110	PE matrix, spherical PS and PCL microdomains	E 74.1 PCL 29.9	
	E29S50C21	34	Tetragonal cylinders of PCL and PE within PS matrix	E 72.5 56.0 PCL -	
PS-*b*-PEP-*b*-PE	S13EP76E11	121	PS cylinders and PE crystallites within PEP matrix	51.0	[134]
	S8EP71E21	121		56.8	
	S14EP64E22	122		57.6	
	S13EP57E30	112		59.8	
	S33EP37E30	115		65.2	
PS-*b*-PI-*b*-PCL	PCL 100	82.3		31.6	[135]
	PS18PI8PCL74	106	PCL Cylinders	26.2	
PPP-*b*-P3HT	16/84	28.4	Spinodal like morphology Domain size 10 nm-50 nm	T 201.4 B _	[136]
	34/66	29.7		T 224.8 B _	
	62/38	32.4		T 185.7 B 81.2	
	75/25	41.1		T 172.8 B 84.4	
OBC	Octene mol% (Hard block wt%) 17.87 (16)	7	-	87.8	[137]
	18.65 (17)	81	-	87.3	
	22.66 (15)	78	-	77.8	
	25.36 (18)	74	Phase separated spherical domains	76.7	
PLLA-*b*-PVDF-*b*-PLLA	0/100/0	18		146	[138]
	50/0/50	12		114	
	14/72/14	25	Miscible in the melt	LA 85 V 140	
	24/52/24	36		LA 125	

				V 141	
	29/42/29	43		LA 128 V 140	
P2VP-*b*-PVDF-*b*-P2VP	27/46/27	12.6	Spheres	-8.8	[139]
	30/40/30	30	Breakout crystallization	77.7	
	17/66/17	28	Lamellae	108.4	
	6/88/6	19.4	Crystallization driven self-assembly	114.1	
	0/100/0	14.3		115.0	
PS-*b*-P(VDF70-TrFE30)-*b*-PS	0/100/0	28.04	Lamellae 37 nm	119.5	[140]
	17.5/65/17.5	35.94	Nanospheres	80.0	
P2VP-*b*-P(VDF-TrFE)-*b*-P2VP	0/100/0 (volume)	10.5		105	[141]
	7.5/85/7.5 (volume)	11.6	Disordered melt	105	
	21.5/57/21.5 (volume)	15.3	Lamellae 21.5 nm	103	
	29/42/29 (volume)	19.1	Cylinders	103	
	31.5/27/31.5 (volume)	27.6	Nanospheres	71	
PVSt-*g*-(PS/PE)	42.7 % PS (volume)	221.6 (Mw)	Lamellae	PE 92.1	[142]
	55.4 % PS (volume)	269.9	Lamellae	91.6	
	76.9 % PS (volume)	368.1	Cylinders	60.1	
POE-*b*-POB	51/49 (volume)	6.1	Lamellae	34.0	[143]
POB-*b*-POE-*b*-POB	27/73	7.2	Hexagonal cylinders	15.3	
	21/79	7.4	Bcc	-19.3	
POE-*b*-POB-*b*-POE	63/37 B-E-B	12	Lamellae	36.3	
	36/64 B-E-B	11	Hexagonal cylinders	21.1	

	25/75 B-E-B	9.8	Bcc	-18.8	
	24/76 B-E-B	12.5	Bcc	-21.0	
	63/47 E-B-E	12	Lamellae	34.7	
	34/66 E-B-E	11.4	Hexagonal cylinders	17.8	
	24/76 E-B-E	11.3	Hexagonal cylinders	5.6 -28.2	
P(S-ODMA)	0/100 (vol ODMA)	9		25	[144]
	61/39 (vol)	24.4	Lamellae	22	
	82/18 (vol)	27.6	Cylinders	11	

In this section, the factors that affect the morphology of block copolymers will be briefly explained and the crystallization of several copolymers will be discussed.

2.2.1. Morphology

According to the Mean Field Theory, the morphology of diblock copolymers is determined by the segregation strength and the composition of the copolymer [39,83,85,145-149]. The segregation strength, χN, depends on the polymerization degree, *N*, and on the Flory Huggins interaction parameter between the blocks forming the copolymer, χ. Furthermore, there are three transition temperatures that have to be considered. In the case of A-B copolymers containing a crystalline and an amorphous block, these three important transition temperatures are: (a) the order disorder transition temperature, T_{ODT}, (b) the crystallization temperature of the crystalline block, T_c, and (c) the glass transition temperature of the amorphous block, T_g. Figure 13 displays the different morphologies that can be obtained for AB and ABA block copolymers considering the segregation strength and the aforementioned transition temperatures.

In the literature, the morphology of block copolymers has been extensively studied, according to these studies five different possible scenarios can be found, as shown in Figure 13.

1) Homogeneous melt, $T_{ODT} < T_c > T_g$. In diblock copolymers that form a homogeneous melt and in which the T_c of the crystalline block is higher than the T_g of the amorphous block, the microphase separation occurs by crystallization. In this case, usually a crystalline lamellar morphology is formed, in which layers of crystalline and amorphous block are alternated [99,100,102,107,126,150-153,154-159].

2) Weakly segregated systems (Low χN values), $T_{ODT} > T_c > T_g$. In this case, there is little morphological restriction for the crystallization process, which allows a break out from the ordered melt structure, therefore the crystallization determines the final structure, usually crystalline lamellae are formed, erasing the previous structure of the melt [102,103,109,121,125,150-153,160-171].

3) Medium segregated systems (medium χN values), $T_{ODT} > T_c > T_g$. For these block copolymers the final morphology (i.e., the morphology of the solidified sample) depends on the applied thermal procedure: if the sample is cooled from the melt very fast, i.e., quenching, the morphology of the melt is maintained. Otherwise, the final morphology will be governed by the crystallization process [102,103,150-153,160-164,172,173].

4) Strongly segregated systems (high χN values), $T_{ODT} > T_c > T_g$. When the segregation strength is strong, the phase segregated structure of the melt is preserved and the crystallization process is confined within the microdomains (MDs) formed in the melt, i.e., spheres, cylinders or lamellae. In this case, there is a soft confinement since the amorphous block is in the rubbery state (the same behaviour is observed for double crystalline diblock copolymers, when the first block crystallizes, while the second one is in the molten state) [102-104,114,115,128,164,165,174-184].

5) Strongly segregated systems (high χN values), $T_{ODT} > T_g > T_c$. The phase segregated structure of the melt is preserved, but in this case, the amorphous block is in the glassy state, therefore the crystallization process of the crystalline block occurs under hard confinement (the same behaviour is observed for double crystalline diblock copolymers, once the first block crystallizes, the second one crystallizes under hard confinement) [101,104,105,108,112,128,129,132,163,175,178-181,184-216].

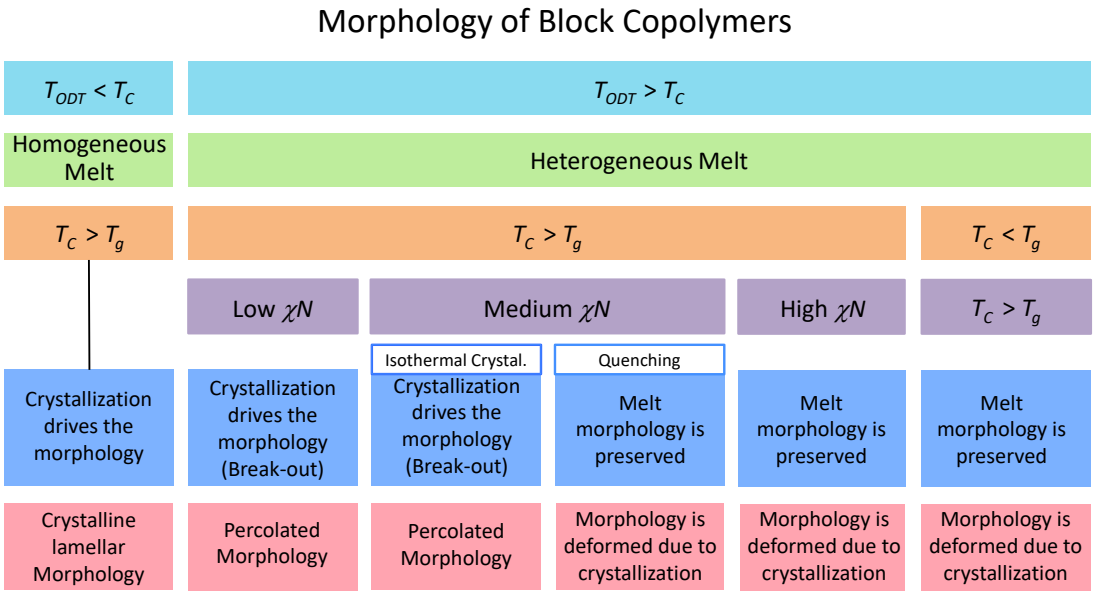

Figure 13. Morphology of AB and ABA block copolymers according to the segregation strength and the transition temperatures.

The morphology of AB double crystalline diblock copolymers and ABC triblock terpolymers with one or more crystallisable block is more complex. In the case of the double crystalline diblock copolymers, the crystallization temperature of each block will determine the final morphology, in addition to the melt segregation strength, composition of the blocks and order-disorder transition temperature. Regarding ABC triblocks, the composition of the terpolymer, the melt segregation strength, which is influenced by three interaction parameters, and the block sequence [38,217], i.e., ABC, BCA or ACB, will be important in addition to the previously mentioned transition temperatures.

2.2.2. Crystallization

Strongly Segregated Block Copolymers

Strongly segregated block copolymers are very interesting materials to study confined crystallization since in these copolymers the melt structure is preserved, and therefore the crystallization process is confined within the MDs formed in the melt. Depending on the composition of the copolymer, isolated MDs can be formed, and if the number of microdomains is much higher than the number of heterogeneities in the bulk polymer, heterogeneity free MDs can be obtained.

A-B amorphous-semicrystalline block copolymers have attracted large interest to study confined crystallization. The major advantages of those systems are the easiness to interpret the results since there is only one crystallisable block and the possibility to tune the degree of confinement by varying the length of the amorphous block (i.e., composition). Depending on the T_g of the amorphous block, in comparison with the crystallization temperature of the semicrystalline block, this block can be in the rubbery state or in the glassy state, and therefore crystallization will occur under a soft confinement or under a hard confinement. In the literature, a wide variety of block copolymers have been studied such as PE-*b*-PS [108], PB-*b*-PEO [128], PCL-*b*-PS [195,196] or PE-*b*-PVCH [105]. In the following paragraphs, some of the results reported in the literature are discussed.

Loo et al. studied polyethylene-*b*-poly(vinylcyclohexane) copolymers, in which PE crystallizes in a glassy matrix [105]. Varying the ethylene-vinylcyclohexane composition, they were able to obtain a wide range of morphologies: spheres, cylinders, gyroids or lamellae. The morphology of the copolymers was studied by SAXS experiments as well as TEM micrographs. In Figure 14, the SAXS data obtained at room temperature (RT) and at 160 ºC, at which the copolymer is in the molten state can be observed for a copolymer forming spheres (Figure 14A) and lamellae (Figure 14B). Analysing the data obtained at room temperature and at 160 ºC, the authors concluded that the melt morphology is preserved after the crystallization of PE block, since the data corresponding to room temperature show one peak at low q values that corresponds to the melt morphology and additional higher order peaks appear for the different copolymers studied.

In Figure 14C, the half-crystallization times obtained during isothermal crystallization at different temperatures are shown. E/VCH 5/22, in which the polyethylene block forms spheres, and E/VCH 6/25, in which the polyethylene forms cylinders, show a first order overall crystallization kinetics. The slope of this plot indicates the relationship between the overall crystallization rate and the temperature. In the case of E/VCH 5/22 and E/VCH 6/25, the growth of crystals is limited due to the size of the polyethylene domain, thus growth is instantaneous and the slope of the plot exclusively represents the dependence of the nucleation rate on temperature. Considering that the values of the slope of those copolymers (E/VCH 5/22 2.6/ºC and E/VC 6/25 2.2/ºC) are similar to values reported for supposedly homogeneously nucleated PE by droplet experiments (3.5/ºC), the authors conclude that the

polyethylene block nucleates homogeneously in these copolymers. However, this type of first order kinetics can also be observed in surface nucleated materials [39]. Therefore, as previously discussed, observing a first order overall kinetics is not a proof of homogeneous nucleation. In fact, several studies have shown that polyethylene homogeneous nucleation has not been obtained so far [218], since the polymer tends to nucleate at the interphase, in the case of block copolymers, or at the surface with the external medium, in the case of isolated droplets [219] or infiltrated materials within AAO templates [218].

Another strategy to check if clean MDs are obtained is to estimate the number of MDs per volume in the copolymer and compare this value with the number of heterogeneities in the bulk sample. According to the estimations of Loo et al., hydrogenated polybutadiene (precursor for the block copolymers) contains approximately 10^9 impurities per cm^3. The number of MDs in the E/VCH 5/22 sample, which forms spheres, is 9 x 10^{16} microdomains per cm^3 and 2 x 10^{15} microdomains per cm^3 in the case of E/VCH 6/25, in which cylinders are formed. The number of microdomains is 6-7 order of magnitude higher than the number of impurities, therefore there is a high number of microdomains that are statistically clean; in those microdomains the nucleation process can proceed only by surface nucleation or homogeneous nucleation.

On the other hand, E/VCH 8/13 copolymer which forms gyroids show a sigmoidal kinetics, which reflects the connectivity of ethylene block in this kind of morphology.

In the case of E/VCH 12/8, which has a lamellar morphology, a double exotherm is observed in the DSC when cooling from the melt, which indicates the presence of fractionated crystallization. The peak at high temperatures corresponds to the crystallization of connected lamellae, whereas the peak at low temperatures corresponds to isolated lamellae. Isothermal crystallization was performed considering each crystallization step. In the case of the isothermal crystallization corresponding to high crystallization temperature peak (low undercooling) a sigmoidal kinetic is obtained (see Figure 14C) which reflects the connectivity of the lamellae by grain boundaries or defects. However, when the isothermal crystallization of the low crystallization temperature peak is analysed a first order kinetics is obtained, this corresponds to the isolated lamellae. For this process, a slope of 2.9/ºC

is obtained which reflects a similar character as that obtained before and attributed by the authors to homogenous nucleation.

In Figure 14D, the Avrami exponent as a function of ethylene content is shown. Copolymers forming spheres and cylinders show an Avrami index equal to 1, indicating that nucleation determines the kinetics. For the lamellar morphology, in the case of the crystals formed at low crystallization temperature, the Avrami index is 1, this value corresponds to the isolated lamellae.

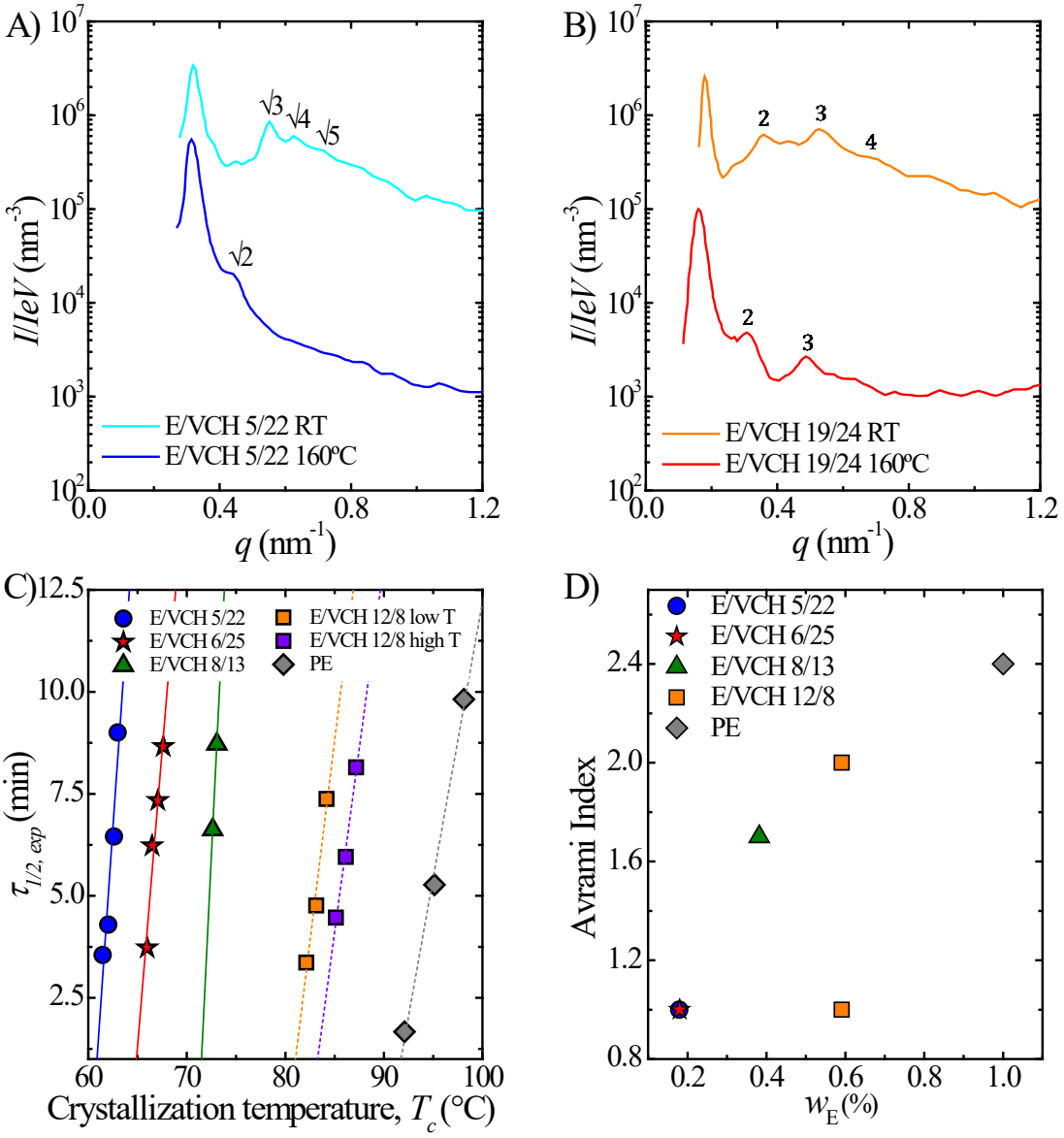

Figure 14. SAXS data obtained at room temperature and 160ºC for copolymers in the molten state: (A) E/VCH 5/22 (PE spheres) and (B) E/VCH 19/24 (lamellae). (C) Half-crystallization time of different copolymers as a function of crystallization temperature. (D) Avrami index of the different copolymers as a function of ethylene content. [105], Copyright 2001. Adapted with permission from American Chemical Society.

First order crystallization kinetics is obtained for different copolymer morphologies, according to the authors because the extent of crystal growth is governed by the size of the microdomain and crystal growth occurs instantaneously. Thus, the overall crystallization rate reflects only nucleation rate and this depends only on the microdomains´ volume or surface.

Lorenzo et al. have studied PE-*b*-PS copolymers, those copolymers were obtained by the hydrogenation of anionically polymerized polybutadiene-*b*-polystyrene copolymers [108,109]. In all cases, the molecular weight of hydrogenated high 1,4 polybutadiene (denoted PE, as it is a linear polyethylene with a small amount, i.e., 10% of ethyl branches coming from the residual 1,2 PB units), as well as 1,2 residual polybutadiene units within the PE block in the diblock copolymers were maintained constant. Varying the polystyrene content in the copolymer different morphologies were obtained: spheres, cylinders or lamellae.

In Figure 15A, the DSC curves obtained by cooling from the melt are shown for PE and a series of copolymers. In the case of neat PE, two exotherms are observed, one at 85 ºC that results from the crystallization of most of the material after being nucleated by type A heterogeneities (i.e., highly active heterogeneities present in bulk PE capable of nucleating the material at low undercoolings) and another small exotherm at 51ºC which results from the intramolecular fractionation of branches [108].

In the case of the $E_{79}S_{21}^{41}$ copolymer (where the subscripts indicate the NMR determined weight ratio and the superscript the M_n value of the copolymer in kg/mol), in which the PS block forms cylinders, and also in the case of the $E_{53}S_{47}^{51}$ copolymer, which has a lamellar morphology, two exotherms are observed in Figure 15A. The first one due to the crystallization after nucleation on type A heterogeneities and the second one at about 50 ºC that results from the crystallization of short sequences of the PE block produced by intramolecular fractionation. These copolymers show similar behaviour to neat PE because the PE block is forming either the matrix ($E_{79}S_{21}^{41}$) or percolated lamellae ($E_{53}S_{47}^{51}$). As can be seen in Figure 15B, the crystallization temperature, due to the crystallization after type A heterogeneities induced nucleation, is reduced when the PS block is incorporated in the diblock copolymer, even though the PE block is forming the matrix ($E_{79}S_{21}^{41}$). This reduction of T_c results from a limited confinement effect caused by the covalently bonded glassy PS block cylinders dispersed in the PE block matrix.

When the PE block is the minor component in the copolymer ($E_{26}S_{74}^{105}$ and $E_{11}S_{89}^{244}$), several endotherms are observed, i.e., fractionated crystallization occurs. This phenomenon could be caused by the presence of different types of heterogeneities in each microdomain, which are activated at different undercoolings, or by the presence of isolated and percolated MDs which have different nucleation processes. Lorenzo et al. discarded that fractionation occurs due to the presence of MDs of different sizes, since the copolymers were synthesized anionically, obtaining MDs with a narrow distribution in size. From the TEM images, the number of MDs were estimated, obtaining 10^{12} cm^{-3} for $E_{26}S_{74}^{105}$ copolymer in which the PE block is forming cylinders in a PS matrix and 10^{15} cm^{-3} for $E_{11}S_{89}^{244}$ copolymer, in which the PE block forms spheres. The number of microdomains is several orders of magnitude higher than the number of heterogeneities present in the bulk PE sample, i.e., approximately 10^{9} cm^{-3}.

The $E_{26}S_{74}^{105}$ copolymer (in which PE cylinders are formed in a PS matrix) shows two main exotherms, one originated by type A heterogeneities nucleation followed by crystallization at 72 ºC and the other at lower temperatures 56ºC, which is termed B. This B crystallization process probably occurs due to the presence of type B heterogeneities, that are less active than type A heterogeneities, since the undercooling needed to crystallize the sample is higher. According to Lorenzo et al., type B heterogeneities could be Wilkinson catalysts remaining particles that were used to hydrogenate the samples, even though the sample was purified.

Finally, the $E_{26}S_{74}^{105}$ copolymer (with PE spheres in a PS matrix) shows three exotherms. Exotherm A crystals were nucleated by the most active, type A heterogeneities, exotherm B by the less active type B heterogeneities, and exotherm C at about 47 ºC is probably due to the crystallization of a small sphere population being nucleated by a very weak heterogeneity or by surface nucleation. Considering that the T_c value is one of the lowest T_c reported in the literature for PE, but it is higher than the T_g of PE, the authors concluded that this nucleation process is due to surface (or interfacial) nucleation or a nucleation at the surface of the clean spheres, just at the border of the interphase between the PE block and the PS block.

In Figure 15C the Avrami index as a function of ethylene content is shown for PE-*b*-PS copolymers and ethylene-*b*-ethylene-*alt*-propylene (E-*b*-EP) copolymers. Considering that PE-*b*-PS copolymers are strongly segregated whereas PE-*b*-PEP are miscible [109]; in this figure, the effect of morphology and dilution can be compared.

The Avrami index reflects the nucleation process and the dimensions of the crystal growth. For neat PE, a value around 3 is obtained for the different isothermal crystallization temperatures employed, as could be expected for a polymer that forms instantaneously nucleated spherulites.

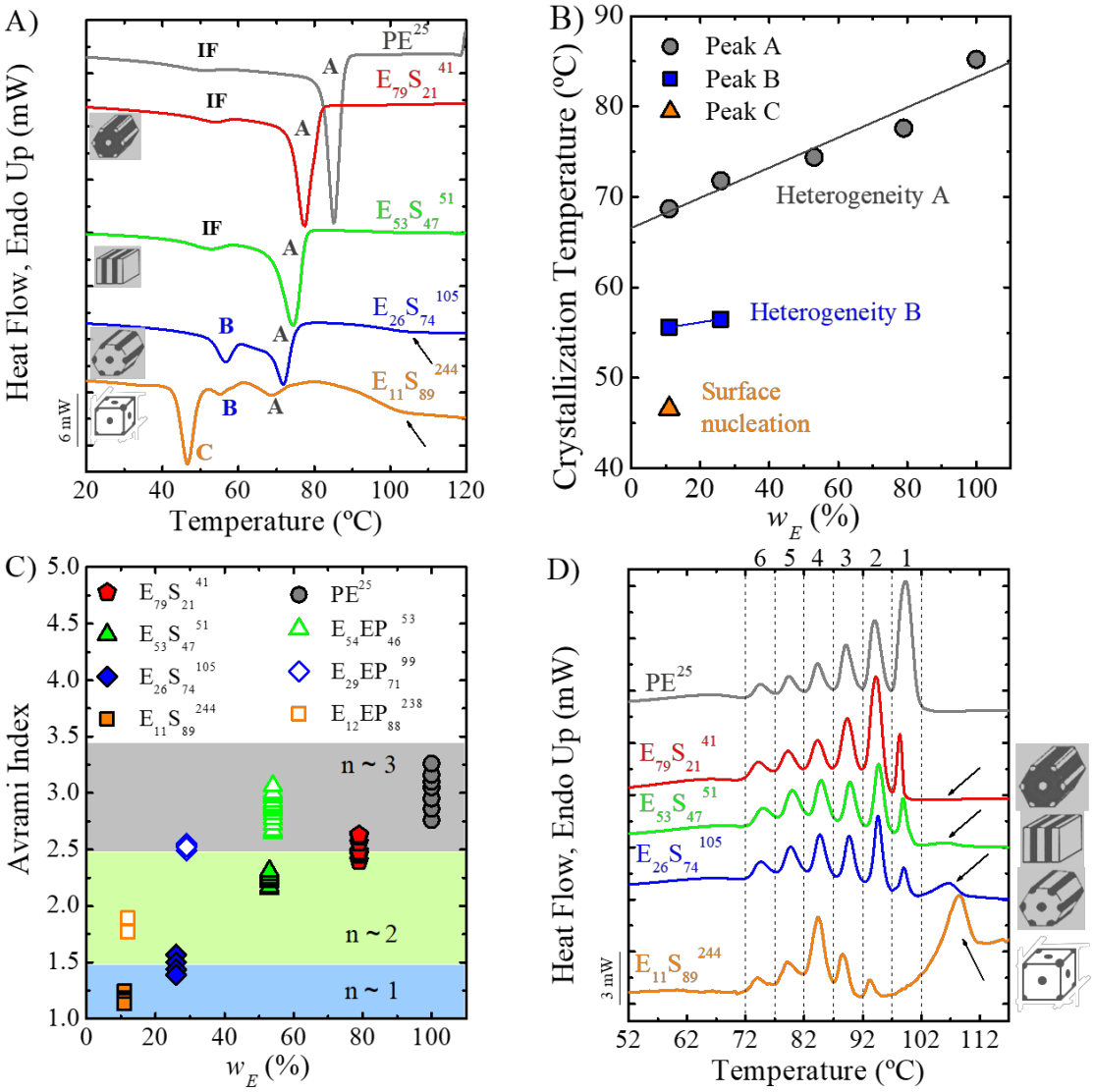

Figure 15. (A) DSC cooling scans from the melt for neat PE (hydrogenated high 1,4 polybutadiene) and a series of PE-*b*-PS copolymers. (B) Crystallization temperature of the different exotherms as a function of ethylene content and their interpretation. (C) Avrami index for PE, PE-*b*-PS and PE-*b*-PEP copolymers as a function of PE content. (D) Final DSC heating scans obtained after applying SSA thermal fractionation to PE and PE-*b*-PS copolymers. The arrows indicate the glass transition temperature of the PS block. [108], Copyright 2006. Adapted with permission from Elsevier Science Ltd. [109], Copyright 2007. Adapted with permission from American Chemical Society.

When the PE content is reduced, a decrease in the Avrami index is observed for both copolymer families due to topological restrictions. In the case of PE-*b*-PS copolymer, this restriction results from the confinement effect imposed by the morphology, whereas in the case of PE-*b*-PEP, the restrictions are caused by the dilution effect of the PEP block. The lowest Avrami index (i.e., very close to $n = 1$) is obtained for $E_{11}S_{89}^{244}$ copolymer, in which the PE block forms spheres. As discussed previously, this indicates that the rate-determining step is the nucleation process rather than crystal growth.

Lorenzo et al. applied the Successive Self-nucleation and Annealing (SSA) thermal fractionation technique to neat PE and PE-*b*-PS copolymers [108]. The SSA technique applies a well-designed thermal protocol consisting in heating and cooling cycles that produced thermal fractions by the differentiating the crystallizability of polymer chains possessing different crystallisable sequence lengths [220-223]. This technique is especially sensitive to short-chain branching in polyethylene chains, as branches do not enter the crystal lattice and represent defects that divide the chains into crystallisable methylene sequences. These crystallisable segments of different lengths undergo molecular segregation during crystallization and can form lamellar crystals of different thicknesses, which are stabilized by sequential annealing steps. As the neat PE is really a model hydrogenated polybutadiene, prepared by anionic PB polymerization followed by hydrogenation, this material is ideal for performing SSA studies [108].

In Figure 15D the final heating scans of SSA fractionated PE and PE-*b*-PS can be observed. Neat PE shows six melting peaks that correspond to six different lamellae populations, each one characterized by a distinct melting point. The highest melting temperature corresponds to the thickest lamellar population, that are formed by the longest methylene sequence length. In the case of copolymers, the melting trace changes significantly. Increasing the PS content, the melting peak corresponding to fraction 1 (the highest melting temperature fraction) is reduced and eventually disappears completely for the copolymer with the lowest PE content. For this copolymer, the most important melting peak corresponds to fraction 4. These results reflect the restriction of the diffusion of PE chains imposed by PS block and the confinement due to the morphology hindering the formation of thicker lamellae

during annealing. These restrictions are more severe as the PE content in the copolymer is reduced.

Nakagawa et al. analysed the effect of the junction between the blocks in poly(ε-caprolactone)-*b*-polystyrene, PCL-*b*-PS, that contain a photocleavable o-nitrobenzyl group in between the two block constituents [195]. This strongly segregated copolymer forms PCL nanocylinders at the studied compositions. The o-nitrobenzyl group can be cleaved by UV light irradiation. Once this occurs, no junctions will remain between PCL and PS blocks (PCL/PS) but the cylinder morphology will be preserved, see scheme in Figure 16.

In Figure 16A, the melting temperature as a function of cylinder diameter is shown. The blue arrow indicates the T_m of PCL homopolymer in bulk. The PCL confined inside the cylinders shows a lower T_m than bulk PCL; reducing the diameter of the cylinder a decrease of more than 10 ºC is observed in the melting temperature. The melting temperature is related to the thickness of the lamellae, so according to these results the thickness is limited by the diameter of the cylinder. Confinement induces this decrease in crystalline lamellar size (and T_m) in a similar way to the results shown in Figure 15D for PE MDs explained above. The PCL homopolymer confined in nanocylinders shows a slightly higher melting temperature than in the PCL-*b*-PS copolymer, which indicates that the block covalent junction also contributes to the confined crystallization.

In Figure 16B the crystallinity degree of PCL as a function of cylinder diameter is shown. The PCL/PS and PCL-*b*-PS show a lower crystallinity degree than PCL in bulk due to confinement. The crystallinity does not change significantly with the cylinder diameter, only for the smallest diameter a significant reduction of crystallinity can be found. According to Nakagawa et al. the crystallinity degree depends on the orientation of the crystals which is dominated by the crystallization mechanism [195].

The half-crystallization time is plotted versus the crystallization temperature in Figure 16C. It can be observed that the samples with the longest half-crystallization time are the ones with the smallest cylinder diameter. Increasing the size of the diameter a reduction of the half-crystallization time is observed. In the case of PCL/PS with diameters of 14.9 nm and 17.9 nm, very similar values are obtained. If the PCL/PS and the PCL-*b*-PS system are compared, at low cylinder diameters, the

crystallization is slower for PCL-*b*-PS, implying that the block junction restricts the mobility of the chains. However, for the sample with a cylinder diameter of 17.9 nm, the crystallization occurs faster for the block copolymer than for PCL/PS, which indicates that in this case, the junction accelerates the nucleation process.

A more detailed study has been performed with this kind of system analysing among others, the effect of chain tethering to nanolamellae interfaces in the crystallization process, as well as in the orientation of the crystals [196-199]. In addition, the effect of the chain mobility in the crystallization process has been investigated, studying PCL-*b*-PS copolymers with different bulky end groups as PCL chain ends [197]. The crystallinity degree, the melting temperature and crystallization rate were decreased when the molecular weight of the bulky group is increased due to the reduction of the mobility of the chain. However, comparing PCL chains with bulky groups with the standard PCL, the crystallization rate was higher for the PCL with bulky groups. This was explained by speculating that bulky end groups could enhance PCL nucleation by reducing chain mobility.

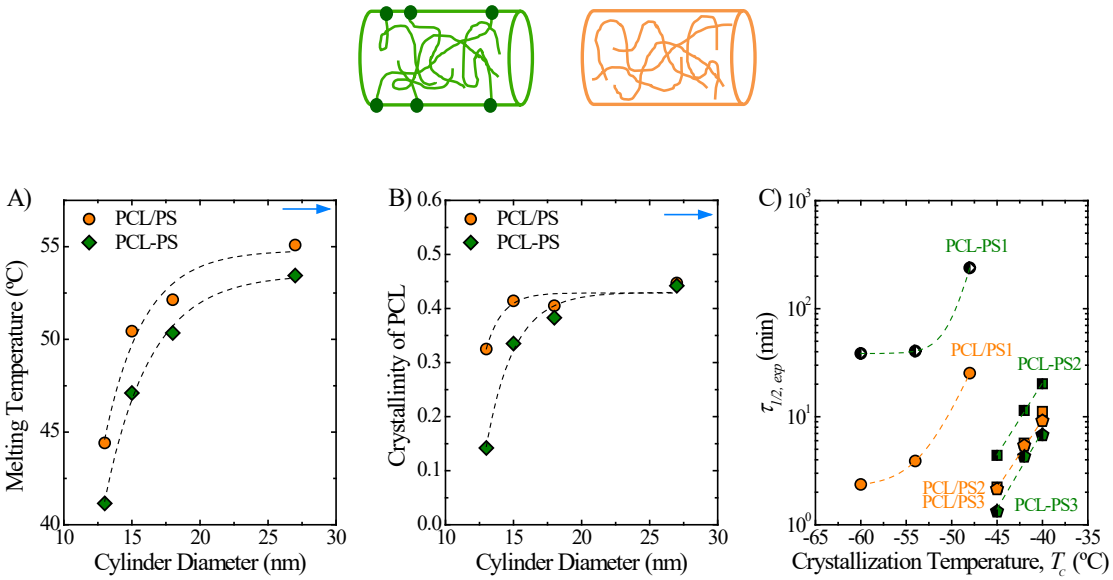

Figure 16. A scheme of PCL-PS copolymers and PCL/PS system is shown on the top. (A) Melting temperature as a function of cylinder diameter for PCL/PS and PCL-b-PS. The blue arrow indicates the T_m of PCL homopolymer in bulk. (B) Crystallinity degree as a function of cylinder diameter. The blue arrow indicates the crystallinity degree of PCL homopolymer in bulk. (C) Half-crystallization time as a function of crystallization temperature for PCL/PS 1 system (diameter of the cylinder 13.0 nm), PCL/PS 2 (14.9 nm) and PCL/PS 3 (17.9 nm). [195], Copyright 2012. Adapted with permission from American Chemical Society.

Several copolymers containing PEO as the crystallisable block have been studied in literature by Müller and coworkers [128,217,224,225]. Figure 17A presents a selection of DSC scans of different PEO containing copolymers and a similar molecular weight PEO homopolymer. The PEO homopolymer crystallizes around 43 ºC in an exotherm labelled A in Figure 17A. The crystallization occurs after the nucleation caused by type A heterogeneities, as usual in bulk homopolymers. In the case of PS-*b*-PEO copolymers, which are strongly segregated, the PEO block within the $S_{39}EO_{61}^{46}$ copolymer (with a lamellar morphology) crystallizes at 39 ºC, i.e., at a temperature similar to the T_c value for PEO homopolymer. The T_c is slightly lower for the copolymer in comparison with the homopolymer, this decrease could result from the lower molecular weight of the PEO block in the copolymer (M_n=28 kg/mol) in comparison with the molecular weight of the PEO homopolymer (M_n=100 kg/mol). In this copolymer PEO is the major component so heterogeneous nucleation similar to the bulk polymer is expected, as in copolymers with lamellar morphologies, the lamellae are typically percolated by defects.

In the case of the $S_{81}EO_{19}^{19}$ copolymer, in which PEO block form cylinders in a PS matrix, the crystallization peak is shifted to -40 ºC (peak D). It should be considered that in this case, the PEO block crystallizes at temperatures that are lower than the T_g of the PS block, therefore the PS matrix is glassy when the PEO cylinders crystallize upon cooling from the melt under hard confinement. The crystallization of PEO is quite close to its T_g, -58 ºC, therefore homogenous nucleation is probably occurring in this case. For this copolymer 10^{14} cylinders/cm^3 are estimated from TEM micrographs, whereas in a bulk PEO only 10^6 nuclei/cm^3 are present. The number of MDs is 8 orders of magnitude higher than the number of heterogeneities. All nanocylinders can be considered statistically clean, a fact that explains the crystallization of all PEO MDs at the lowest possible undercooling by homogeneous nucleation.

PEO-*b*-PB copolymers, which are strongly segregated, were also investigated by Castillo et al. [128], and in this case, the non-crystallisable block (PB) is in the rubbery state when PEO block crystallizes and PEO forms mostly spheres at the studied compositions, although some cylinders were also observed. The crystallization of the PEO block occurs under soft confinement. The $B_{81}EO_{19}^{34}$ copolymer shows an exotherm at 46 ºC which corresponds to crystallization after

nucleation by the most efficient type A heterogeneities. A second exotherm appears at 8.2 ºC which corresponds to the MDs that contain a less active type B heterogeneities or percolated spheres and/or cylinders. Finally, a third exotherm is observed at -27 ºC. Given the high supercooling at which the PEO block crystallization occurs, this could arise from surface or homogeneous nucleation. Considering that the T_g of PEO is between -50 and -60 ºC and that a lower T_c has been reported in the case of PS-*b*-PEO copolymers, as discussed above, it is possible that in this case, exotherm C corresponds to crystallization of a certain MDs population that nucleated at the surface (or interface with PB block matrix). In the case of $B_{89}EO_{11}$[102] copolymer, only nanospheres of PEO are formed inside a rubbery PB matrix. As expected by the increased confinement degree provoked by reducing the PEO content in the copolymer, exotherm A disappears and only a tiny B exotherm and a large C exotherm are detected.

In Figure 17B, the crystallization temperature of the PEO block as a function of composition has been plotted for the different copolymers considered. The homopolymer and some of the copolymers show a crystallization temperature at about 35-50 ºC due to the crystallization after nucleation by type A heterogeneities, and the differences are mainly due to molecular weight variations. The crystallization temperature at about -10 ºC occurs due to the presence of type B heterogeneities which are less active, this is the case of PB-*b*-PEO copolymers. Finally, at higher supercoolings, a crystallization exotherm peak at -27 ºC is observed (peak C) for PB-*b*-PEO which corresponds to surface nucleation, whereas for PS-*b*-PEO copolymers, the crystallization temperature is even lower, -40 ºC (peak D); in this case it corresponds to the formation of crystals that are homogeneously nucleated.

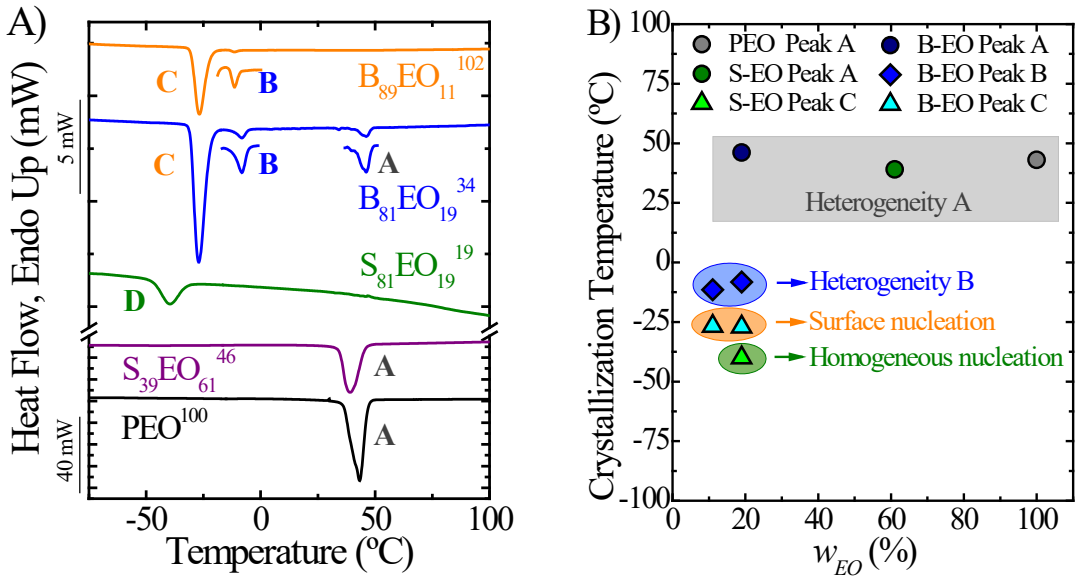

Figure 17. (A) DSC cooling scans from the melt for PEO homopolymer, PS-*b*-PEO copolymers, and PB-*b*-PEO copolymers. (B) Crystallization temperature of the different systems analysed as a function of PEO content in the copolymers. [128], Copyright 2008. Adapted with permission from American Chemical Society. [129], Copyright 2002. Adapted with permission from American Chemical Society.

The study of crystallization has been extended to more complex copolymers. ABA [138,139,141,185,193,199,226-235] as well as ABC [38,130,132,217,224,225,236-239] triblock terpolymers have been investigated with one or more crystalline blocks such as PB-*b*-PI-*b*-PEO [130,131], PE-*b*-PS-*b*-PEO [217], PS-*b*-PE-*b*-PCL [38, 236], PS-*b*-PEO-*b*-PCL [132,224] among others. The effect of the composition on the crystallization process, the appearance of fractionated crystallization and in some cases homogeneous nucleation, have been studied, as well as the effect of sequence order [38, 217] (ABC, BCA or ACB).

Miscible or Weakly Segregated Block Copolymers that exhibit fractionated crystallization

Miscible or weakly segregated block copolymers have also been studied. In this kind of system, if the crystallization processes of both blocks are separated, the block that crystallizes first when cooling from the melt templates the crystallization of the second block. Therefore, the crystallization of the second block can be confined to the interlamellar regions of the block that crystallizes first. Several copolymers have

been studied, among others, PLLA-*b*-PCL [125,155,169,240], PEG-*b*-PLLA [241], poly(ε-caprolactone-*b*-ε-caprolactam) [156] and hPN-*b*-LPE [107].

Castillo et al. studied PLLA-*b*-PCL double crystalline diblock copolymers [125]. These copolymers are partially miscible, when cooling from the melt the PLLA block crystallizes first, and at lower temperatures the PCL block crystallizes in the interlamellar regions of PLLA. In Figure 18 the crystallization and melting temperatures of the PCL block as a function of PLLA content are shown. For PLLA contents lower than 45% a linear reduction of T_m as well as T_c is observed with the increment in PLLA content. For L_{60}-*b*-CL_{40} copolymer, two PCL crystallization temperatures are observed, which indicates a fractionated crystallization process. This fractionation results from the confinement effect of PLLA lamellas; PCL chains confined in the interlamellar regions of PLLA contain less active heterogeneities than in bulk which results in lower T_c values. $L_{81}C_{19}$[21] copolymer shows a really low crystallization temperature, -45 ºC. This temperature is close to the glass transition temperature of PCL, about -60 ºC, therefore it can be considered that in this copolymer homogeneous nucleation occurs. It should be taken into account that the T_g of PLLA is reduced by decreasing PLLA content. For the copolymer rich in PCL, the crystallization of the PCL block occurs when PLLA is in the rubbery state, since the T_g of the PLLA block is below the crystallization of the PCL block. However, for copolymers rich in PLLA, the crystallization of PCL occurs at lower temperatures than the T_g of PLLA, in other words, when the PLLA block is in the glassy state. Therefore, for copolymers rich in PLLA, in addition to the confinement of the interlamellar region of previously crystallized PLLA, there is a restriction given by PLLA amorphous chains which are in the glassy state. For copolymers with a content of PCL lower than 7% by weight the PCL block was not able to crystallize.

In the case of the melting temperature of the PCL block a similar behaviour can be observed although in this case the reduction is much less significant in comparison with the decrease observed in the crystallization temperature (note the two different scales in Figure 18). For neat PCL a T_m around 58 ºC is observed and this T_m value is reduced with the decrease of PCL content obtaining a value of 44 ºC for the $L_{81}CL_{19}$ copolymer. The differences between T_c and T_m are expected, based on the metastability of polymeric crystals.

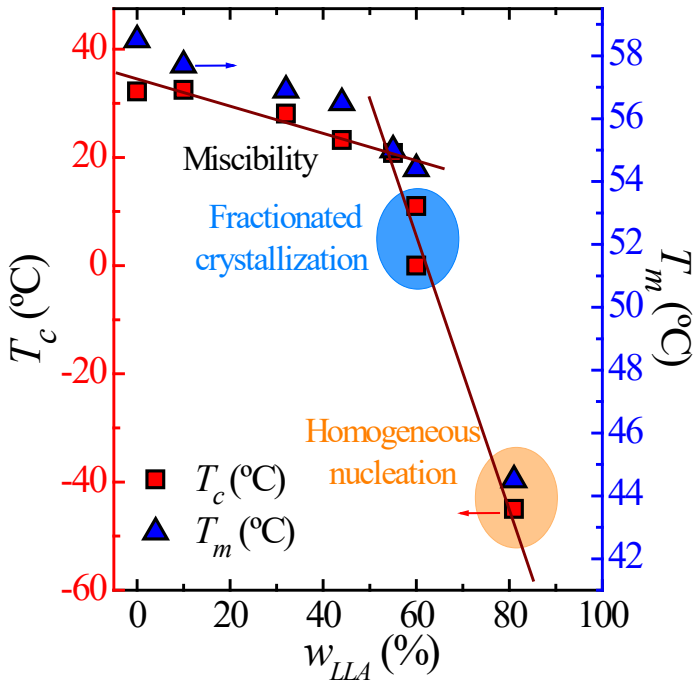

Figure 18. Crystallization and melting temperature of PCL block in PLLA-*b*-PCL partially miscible copolymers. [125], Copyright 2010. Adapted with permission from American Chemical Society.

More recently triblock terpolymers formed by PEO, PCL and PLLA have been studied in literature by several authors [242,243], although studies about triblock copolymers with three crystalline blocks are scarce. Palacios et al. studied PEO-*b*-PCL-*b*-PLLA copolymers [239,244,245], the absence of any SAXS reflection in the melt state as well as the estimation of the segregation strength lead to the conclusion that the terpolymers under study were miscible in the melt [239]. During cooling the first block that crystalizes is PLLA, and the crystalline structure formed by PLLA templates the crystallization of PEO and PCL blocks. However, fractionated crystallization is not easily detected in the studied compositions in view of the multiple crystallization of the constituent blocks.

Effect of Chain Architecture

The effect of chain architecture in the crystallization of copolymers has been studied employing star [117,118,246-249], graft [250-252], brush [253-255], dendritic [256], comb [142,257] or H shaped [258,259] copolymers. These kinds of systems are very interesting, since in those copolymers confinement can be induced by the composition of the block copolymer as well as by the chain topology, because both

parameters affect the final morphology of the copolymer. Different copolymers have been investigated, such as miktoarm star (PCL_2)-*b*-(PS_2) [117], star copolymers PS-*b*-PEO-*b*-PCL [247], star PDMS$(PCL)_2$ [246] and alternating polymer co-brushes of PEO and PCL [255].

Lorenzo et al. studied the effect of the chain topology (or chain architecture, linear versus miktoarm stars) on the crystallization of PCL-*b*-PS copolymers [117,118]. For that purpose, 4-miktoarm star block (PCL2)-*b*-(PS2) copolymers were studied and the results were compared with linear PCL-*b*-PS copolymers. According to the SAXS results, the copolymers are segregated in the melt. The morphology of the copolymers was investigated by TEM observing that miktoarms and linear copolymers of similar composition have different morphology.

The inverse of the half-crystallization time as a function of PCL composition is shown in Figure 19A for the different copolymers. Reducing the content of PCL in the copolymer causes a reduction in the crystallization temperatures needed to crystallize the copolymer. In other words, decreasing PCL content higher supercoolings are needed for crystallization. If the miktoarm star copolymer and the linear one are compared, higher supercoolings are needed to crystallize the miktoarm stars due to the higher confinement of star copolymers in comparison with analogous linear ones. The differences become more significant when reducing the PCL content, i.e., increasing the confinement effect. The difference between the two types of copolymers in the supercooling is as high as 35 ºC for the copolymer with the lowest PCL content, which reflects the higher confinement degree in the miktoarm star copolymer in comparison with the linear copolymer.

In Figure 19B, the Avrami index as a function of PCL content is shown. For each composition, several data points are plotted that were obtained at different crystallization temperatures. For copolymers rich in PCL there is an increase in Avrami index with crystallization temperature. Considering that the growth dimensionality is constant, this result can be explained by a change in nucleation mechanism, from instantaneous to sporadic. For copolymers with low PCL content, this effect is not very significant.

Reducing the PCL content in the copolymer, Figure 19B shows a decrease in the Avrami index for both, miktoarm star and linear copolymers, as a result of the increase in the degree of confinement. If both types of copolymers are compared, it can be observed that the miktoarm stars have lower Avrami index than the linear

copolymers, this results from the different morphology of the copolymers, caused by the chain architecture influence, which in turns increases the confinement degree for the miktoarm star copolymers. Furthermore, when similar morphologies are compared (having different composition) the miktoarm star copolymers show lower Avrami index than the linear ones, because the confinement is stronger in star copolymers. In the case of the miktoarm star copolymer with the lowest PCL content, Avrami indexes that could be approximated to one (i.e., 1.2-1.4) are obtained, which could indicate a surface or homogeneous nucleation.

The energy barrier associated with the overall crystallization is proportional to the K_g^τ term in the Lauritzen and Hoffman equation, which considers both nucleation and crystal growth as:

$$\frac{1}{\tau_{50\%}}(T) = G_0^\tau exp\left(-\frac{U^*}{R(T_C - T_\infty)}\right) exp\left(-\frac{K_g^\tau}{T\Delta T f}\right) \quad (9)$$

being $\frac{1}{\tau_{50\%}}$ the inverse of the half-crystallization time, G_0^τ the growth rate, U^* the activation energy for chain diffusion. R is the gas constant, T_c the isothermal crystallization temperature, T_∞ the temperature where chain mobility ceases, ΔT the supercooling, f a temperature correction term and K_g^τ the energy barrier associated with the overall crystallization.

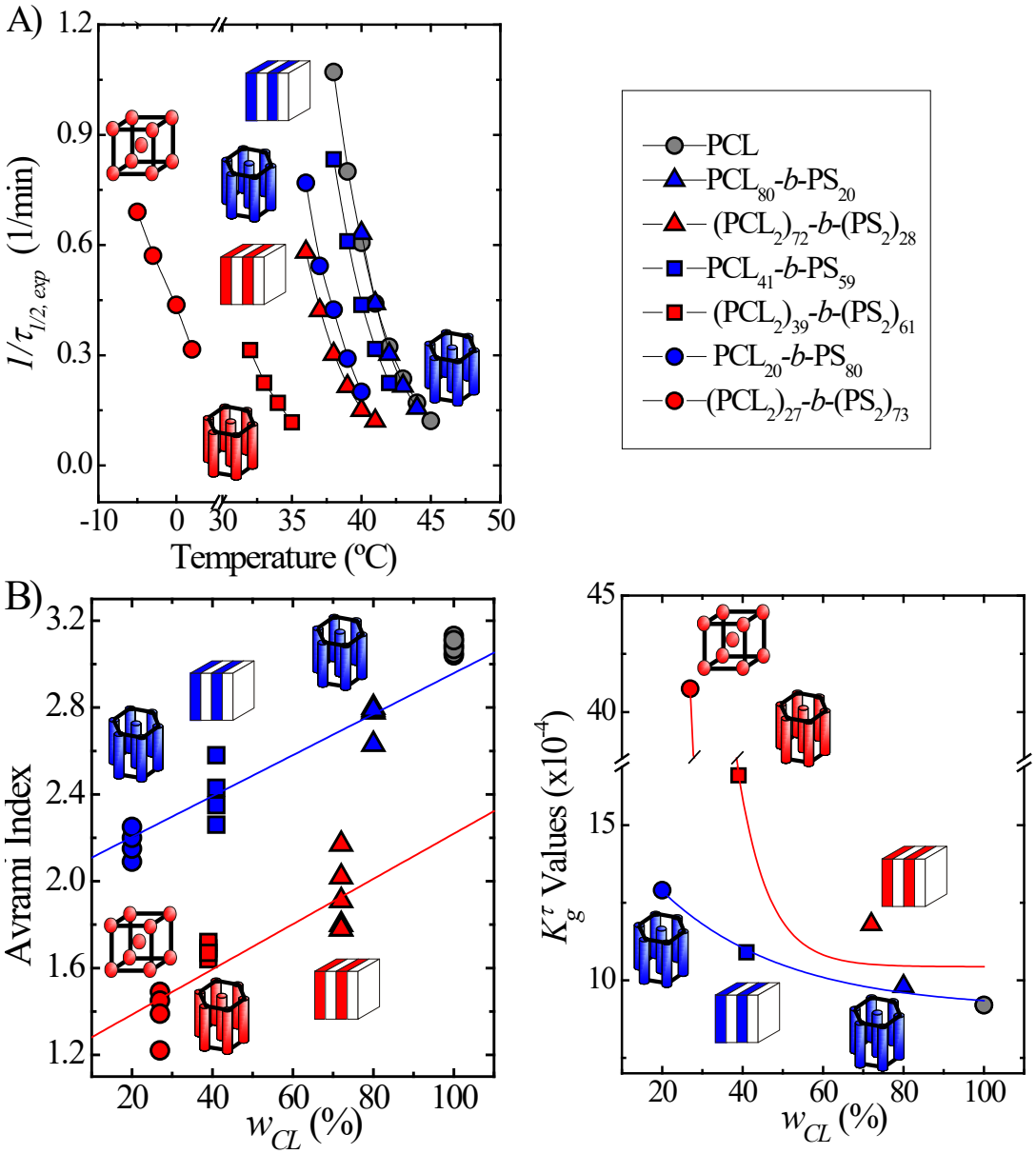

Figure 19. (A) The inverse of the half-crystallization time as a function of crystallization temperature, the lines correspond to Lauritzen Hoffman fittings. (B) Avrami index of linear and miktoarm star copolymers as a function of PCL content. (C) K_g^τ values as a function of PCL content for the different copolymers studied. [118], Copyright 2009. Adapted with permission from American Chemical Society.

Figure 19 shows how the K_g^τ values depend on the composition. It can be seen that the miktoarm star copolymers display higher K_g^τ values than the linear copolymers. This indicates that the energy barrier for overall crystallization (including nucleation and growth) is higher for the miktoarm star copolymers, confirming that there is a higher degree of confinement in miktoarm copolymers that hinders the

nucleation and growth process in comparison with linear copolymers. If the effect of PCL content is analysed for both linear and miktoarm star copolymers, it can be observed the K_g^τ values increase with the reduction of the PCL content in the copolymers, because the confinement increases.

2.3. Polymers infiltrated in AAO templates

Since the successful preparation of well-ordered Anodic Aluminum Oxide Templates (AAO) by Masuda and Fukuda [260], there has been growing interest in the crystallization of polymers inside the pores [97,261-264].

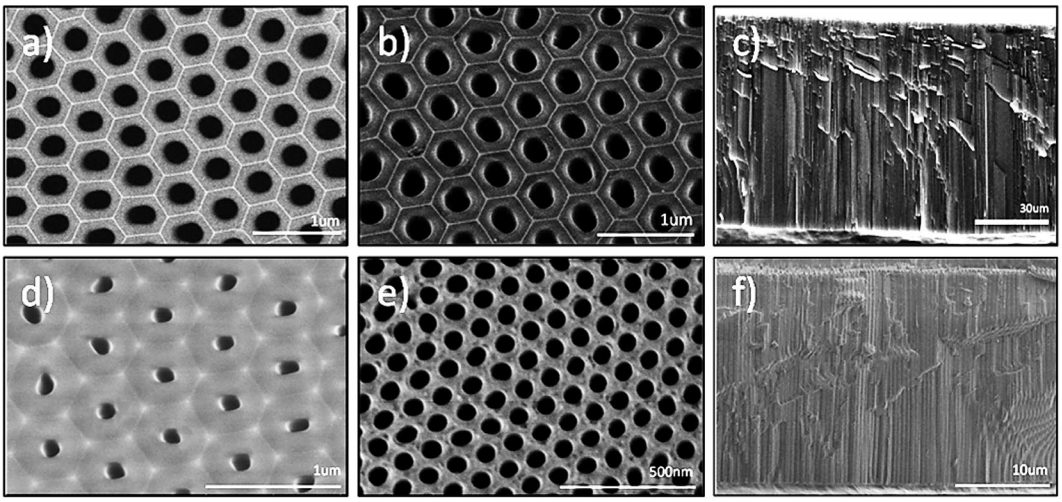

Figure 20. SEM micrographs of AAO templates with different pore diameters (nm) and lengths (μm): (A) 250 nm/80 μm (top view), (B) 350 nm/80 μm (top view), (C) 250 nm/80 μm (lateral view), (D) 140 nm/25 μm (top view), (E) 60 nm/25 μm (top view), and (F) 140 nm/25 μm (lateral view) [265]. [265], Copyright 2016. Reproduced with permission from American Chemical Society.

Geometrically, the AAO pores are similar to the cylinder phase of block copolymers but they are more physically isolated and there is no chemical bond at the interface. The diameter of the AAO pore is between 15 and ~ 400 nm and the length is tens to 100 μm. The typical surface morphology of the AAO is shown in Figure 20 displaying its uniform, hexagonally packed pores.

Fractionated crystallization was reported in various polymers infiltrated into AAO templates, including polyethylene (PE) [266], syndiotactic polystyrene (sPS) [267], isotactic polypropylene (iPP) [268, 269], polybutene-1 (PB-1) [270], poly(ε-caprolactone) (PCL) [265,271], poly(ethylene oxide) (PEO) [272,273],

Poly(vinylidene fluoride) (PVDF) [274], and copolymer such as PEO-*b*-PCL [275] and P(BS-*ran*-CL) [276].

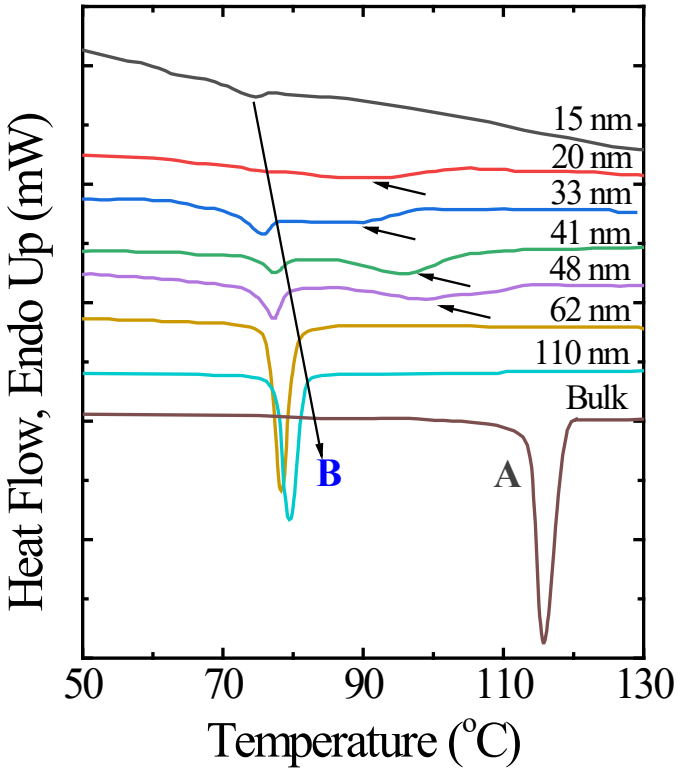

Figure 21. DSC cooling curves of monodisperse linear PE in the AAO with the diameters of 15-110 nm and in bulk. The cooling rate was 10 ºC/min [266]. [266], Copyright 2007. Adapted with permission from American Physical Society.

Woo et al. [266] studied the crystallization of a monodispersed PE within AAO templates. The DSC cooling curves are plotted in Figure 21. The bulk PE crystallized at 116 ºC (peak A). Within 110 nm templates, the T_c dropped to 80 ºC (peak B). With decreasing pore diameter, the T_c slightly decreased. Another broad peak appeared at ~80-110 ºC for 48 nm AAO. This higher T_c shifted towards lower temperatures with decreasing AAO diameter. This observation was interpreted by a transition from bulk heterogeneous to homogeneous nucleation for the 110 nm and 62 nm samples. Surprisingly, it was proposed that the nucleation mechanism changed back to heterogeneous nucleation for samples with smaller pores. No further interpretation was given on where the heterogeneities originated.

Fractionated crystallization of iPP was reported by Duran et al. [268]. The DSC cooling curves are plotted in Figure 22. The bulk iPP crystallized at 108.8 ºC

(peak A). For infiltrated iPP within 380 nm AAO, the major peak shifted to a slightly lower temperature (103.1 ºC, peak B) and a small peak appeared at 73.1 ºC (peak C). For the samples with 60 nm and 35 nm, three peaks are visible. Two of them located at temperatures near the bulk T_c. The highest T_c was interpreted as due to the residual iPP on the surface. The middle peak was proposed to be initiated by heterogeneous nucleation. The lowest T_c (peak D) was explained by crystallization from homogeneous nuclei. Reid et al. observed two exothermic peaks in infiltrated iPP only for 40 nm AAO [269].

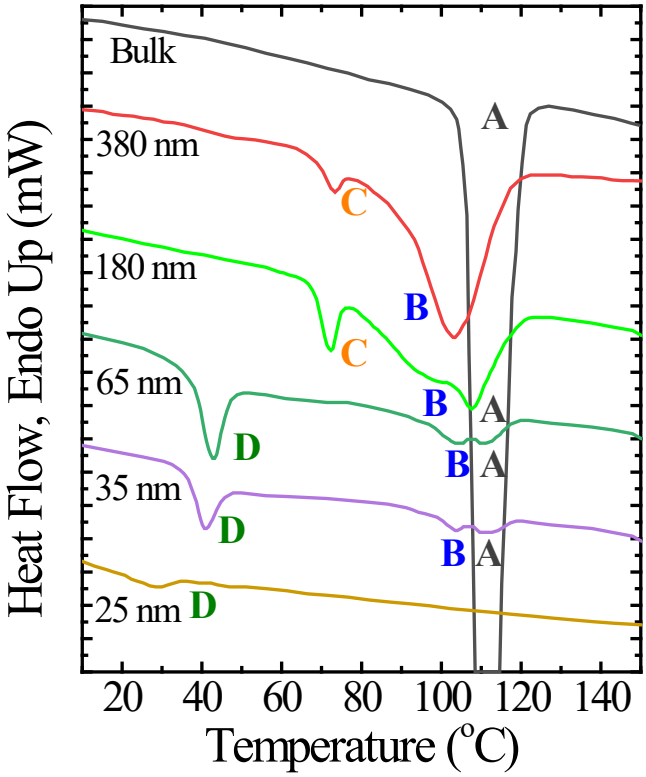

Figure 22. DSC cooling curves of bulk and infiltrated iPP within AAO with different pore sizes. The cooling rate was 10ºC/min [268]. [268], Copyright 2011. Adapted with permission from American Chemical Society.

Typical fractionated crystallization behavior of PCL was reported by Suzuki and coworkers, where a surface cleaning step was mentioned [271]. As shown in Figure 23, the bulk PCL shows a single T_c at 32 ºC (peak A). Two or three exothermic peaks (Peak B, C and D) were observed for the infiltrated PCL samples. Similarly, the lowest exothermic peak (peak E) was assigned to homogeneous nucleation. The other

peaks were interpreted as originating from “heterogeneous nucleation” of a different kind with respect to that of the bulk crystallization, because the number of pores is several orders of magnitude larger than the density of heterogeneities in the sample. It was hypothesized that the unusual heterogeneous nucleation was initiated from the pore walls.

The majority of studies have shown that the PEO exhibits a single exothermic peak during cooling when confined within AAO [218,277-280]. However, fractionated crystallization of PEO inside AAO was also reported occasionally. Suzuki et al. [272] observed a cooling rate dependent fractionated crystallization behavior for PEO inside 200 nm pores. Fast cooling suppressed the exothermic peaks at high temperatures. Liu et al. observed three exothermic peaks of PEO inside 23 nm AAO [273].

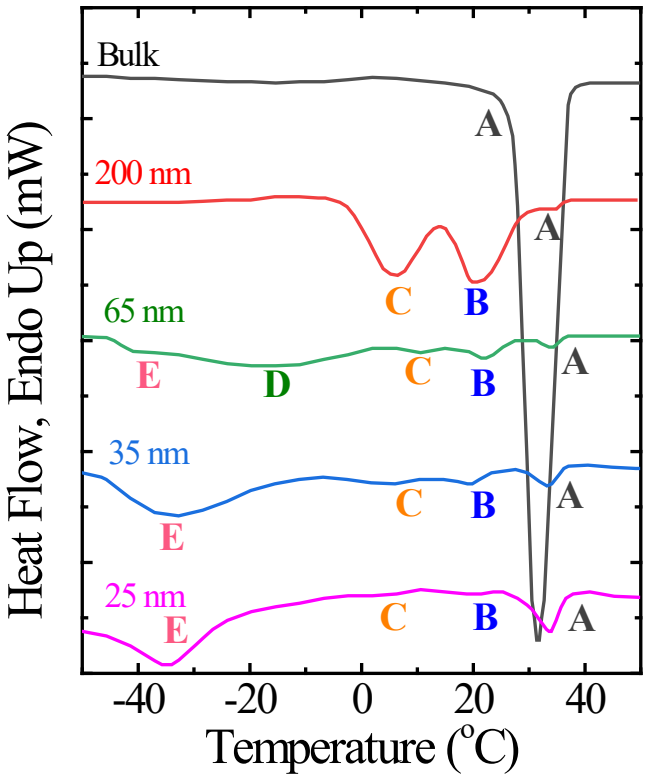

Figure 23. DSC cooling curves of bulk and infiltrated PCL within AAO with pore diameters ranging from 200 nm to 25 nm [271]. [271], Copyright 2013. Adapted with permission from The Royal Society of Chemistry.

The sample information, AAO parameters, and T_c for the polymers with fractionated crystallization are summarized in Table 4. The key question to understand the phenomenon is the origin of the high-temperature exothermic peaks.

Three possible origins can be envisaged: (1) nucleation due to the heterogeneities in the bulk polymer; (2) nucleation on the AAO walls; (3) percolation from possible surface layers. The first possible origin will be discussed in the next section in detail. Since the density of the heterogeneities of the bulk polymer is several orders of magnitude smaller than the density of AAO pores, statistically the heterogeneities in the bulk sample are negligible for the crystallization of polymers inside the pores. Nucleation by the AAO wall cannot explain the fact that in many cases only one exothermic peak is observable for the smallest AAO pores which have the largest surface/volume ratio. The influence of surface layer on the fractionated crystallization behavior was studied first by Michell et al. [91], where the remaining interconnecting surface PEO layer caused an extra exothermic peak at high temperatures (33 ºC). Similar observations were obtained by Suzuki et al. [281]: the surface layer makes fractionated crystallization more obvious.

Table 4. Summary of the crystallization conditions of polymers within AAO showing fractionated crystallization behavior.

Polymer	M_w[a] (Kg/mol)	Pore diameter (nm)	T_c (ºC)	ref.
PE	32.1 PDI[b]:1.11	Bulk	116	[266]
		110	80	
		62	78	
		48	99 / 77	
		41	96 / 77	
		33	89 / 76	
		20	89	
		15	75	
sPS	260 PDI:2.0	Bulk	239.7	[267]
		32	218.5 / 158.4	
iPP	108 PDI:3.32	Bulk	108.8	[268]
		380	103.1 / 73.1	
		180	108.5 / 99 / 72.4	
		65	111 / 104 / 43	
		35	111 / 104 / 41	
		25	28.9	
iPP	241	Bulk	120.4	[269]
		200	110.5	
		40	120 / 44.3	

		15	41.7	
PCL	8.9 PDI:1.16	Bulk	32	[271]
		200	21 / 6	
		65	34 / 22 / 10.4 / -17	
		35	20 / 6 / -34	
		25	34 / -35	
PCL	43 PDI:1.38	Bulk	19.4	[265]
		60	31.9 / -17.1	
PEO	1.33 PDI:1.24	Bulk	25.8	[272]
		200	5.3 / -29	
PEO	3.54 PDI:1.04	Bulk	32.4	[273]
		89	5 / -17	
		23	35 / 17.8 / -18.7	
PVDF	530	Bulk	135	[274]
		200	131 / 70	
		100	75	
		60	65	
		30	55	

a: weight-average molecular weight.

b: polydispersity index = M_w/M_n.

The question remains regarding the link between the surface layer and fractionated crystallization features, as a surface cleaning step was carried out in many of the studies. Shi et al. [282] reexamined the crystallization of PCL and iPP inside AAO with a particular focus on the surface cleaning procedure, including blade scratching, mechanical polishing, and solvent cleaning. With proper cleaning measures, all the infiltrated PCL and iPP samples exhibited a single exothermic peak during cooling (Figure 24). By controlling the surface cleaning procedure, and producing a "partial cleaning", similar fractionated crystallization behavior of the same polymer in the previous studies [265,268,269,271] can be reproduced. This proved that the surface residue is the reason for the observed fractionated crystallization behavior in infiltrated iPP and PCL. The importance of clean surface was emphasized because the presence of surface layer may influence many aspects of crystallization including the nucleation, crystallization kinetics, and crystal orientation. The influence of surface layer on crystal orientation has been discussed by Steinhart et al. [283]

As discussed in the previous sections, the crystallization kinetics of polymers within droplets or phase-separated domains of block copolymers generally exhibits a "first-order" kinetics or "nucleation-dominated" kinetics, manifesting itself by an Avrami index (n) of 1. The reason is that, in small volumes, compared to the time needed for nucleation, the time needed to fill the space is negligible. The isothermal crystallization kinetics of polymers within AAO has been investigated in PE [266,284], iPP [268,269], PEO [91,277,280], sPP [285], and PVDF [286]. The results are summarized in Table 5. The general observation is a reduction in the Avrami index. The n values of PE dropped from 2.4 (bulk) to 1.5 ~ 1.9 upon confinement in AAO with a diameter ranging from 15 to 100 nm. Similarly, n dropped from 3 ~ 4 for bulk iPP to 1.75 ~ 2.5 for confined iPP [268]. Those n values are still meaningfully higher than 1. Since $n = n_n + n_{gd}$, the $n \approx 2$ was interpreted by sporadic nucleation and 1-dimensional crystal growth along the AAO nanocylinders. [268,284] The n values of sPP exhibited a continuous change from 3 to 0.7 depending on the degree of supercooling, whereas confinement showed a minor effect. [285] An abnormal observation was reported in PVDF where the n values were essentially the same for bulk PVDF and infiltrated sample in 400 nm AAO [286]. Among all the studies, first-order kinetics is only reported in PEO/AAO so far [91,277,280].

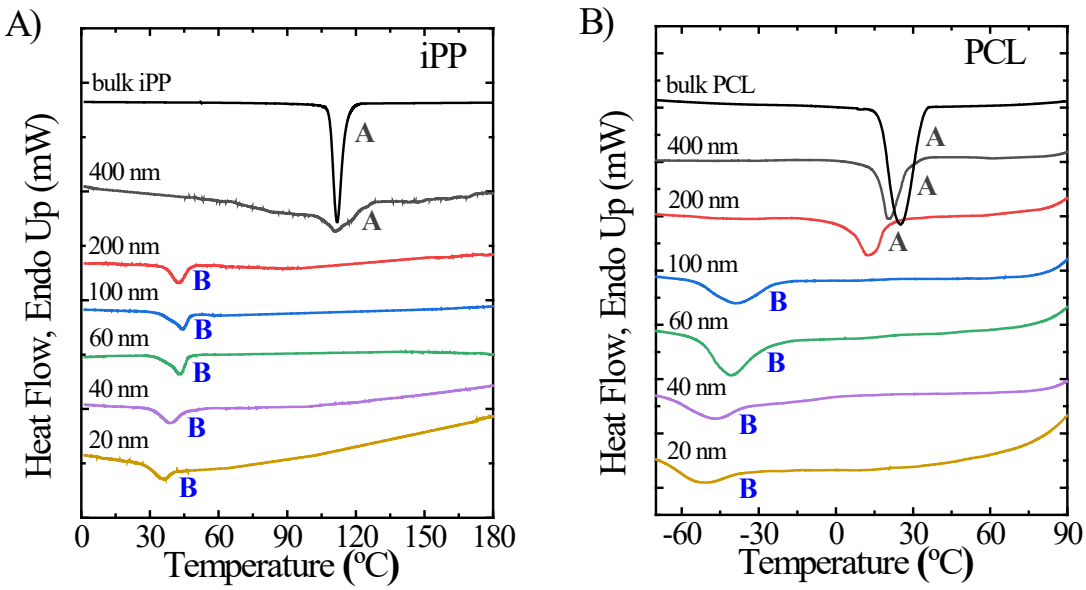

Figure 24. DSC cooling curves of bulk and infiltrated iPP (A) and PCL (B) within AAO with pore diameters ranging from 20 nm to 400 nm [282]. [282], Copyright 2017. Adapted with permission from American Chemical Society.

Table 5. Summary of the crystallization kinetics of polymers confined with AAO pores.

Polymer	M_w (Kg/mol)	Pore diameter (nm)	T_{iso} (ºC)[a]	Avrami index	T_m^o (ºC)[b]	Fractioned crystallization[c]	ref.
PE	32.1 PDI:1.11	bulk	114 ~ 122	2.4 ± 0.2	146.5	-	[266]
		15 ~ 110	75 ~ 99	1.6 ~ 1.9		yes	
iPP	108 PDI:3.32	bulk	115 ~ 125	3 ~ 4	186	-	[268]
		25 ~ 380	102 ~ 118	1.75 ~ 2.5		yes	
	241	bulk	132	2.2		-	[269]
		40, 200	132	1.5 ~ 1.6		yes	
sPP	174 PDI:2.3	Bulk	80~100	1.5 ~ 3.2	168.7	-	[285]
		300	70 ~100	0.8 ~ 2.2		no	
		110	55 ~ 90	0.7 ~ 1.4		yes	
PVDF	110 PDI:2.8	bulk	144 ~ 154	2.61 ~ 2.92	-	-	[286]
		400	143 ~ 151	2.48 ~ 3.07		no	
PEO	100	bulk	41 ~ 46	1.6 ~ 2.1	75 [287]	-	[277]
		400	-4 ~ 4	1.1 ~ 1.2		no	
	33 PDI:3	bulk	50.5 ~ 54	2.0-2.2		-	[91]
		35, 60	-8 ~ 1.0	0.7 ~1.4		no	
	10.5 PDI: 1.05	100	-12 ~ -4	0.5 ~ 1		no	[280]

a: T_{iso}: isothermal crystallization temperature.

b: equilibrium melting temperature.

c: This means whether the sample show fractionated crystallization during non-isothermal condition.

To better understand the results, the n values of different polymers are plotted as a function of supercooling (ΔT) in Figure 25. It is clear that infiltrated PE and iPP lay in the region of $n \sim 2$, while PEO is located in the $n \sim 1$ region. Interestingly, it occurs that fractionated crystallization is observed in PE and iPP and not in PEO. Another clear observation is that the ΔT of bulk PE, iPP, and sPP is very close to their infiltrated samples. However, a temperature gap of ~ 70 ºC exists for PEO. The issue of surface layer might be once again invoked to explain the results. Intuitively, if there is a surface layer that crystallizes at low supercoolings, the kinetics will be very different from that of the sample that has to nucleate inside the pores. For example, the n_n may change from 1 to 0 because the nucleation is instantaneous in the surface

layer. The growth dimension may change from 1 to 2 if we consider that surface spreading of the crystals is the rate-limiting step for crystallization.

One question arises when examining the different n values: is the 1-dimensional geometry compatible with the first-order kinetics? Or under what condition the growth dimension becomes important? First-order kinetics implies that the time needed for growth is negligible as compared to the nucleation. Hence, if the nucleation rate increases or the growth rate decreases, the n_{gd} has to be considered. Su et al. [280] applied a simple numerical model and showed clearly a transition from $n = 1$ to $n = 2$ when the growth rate inside the pore decreased. The n values of sPP show this trend, however more experimental evidence is still needed.

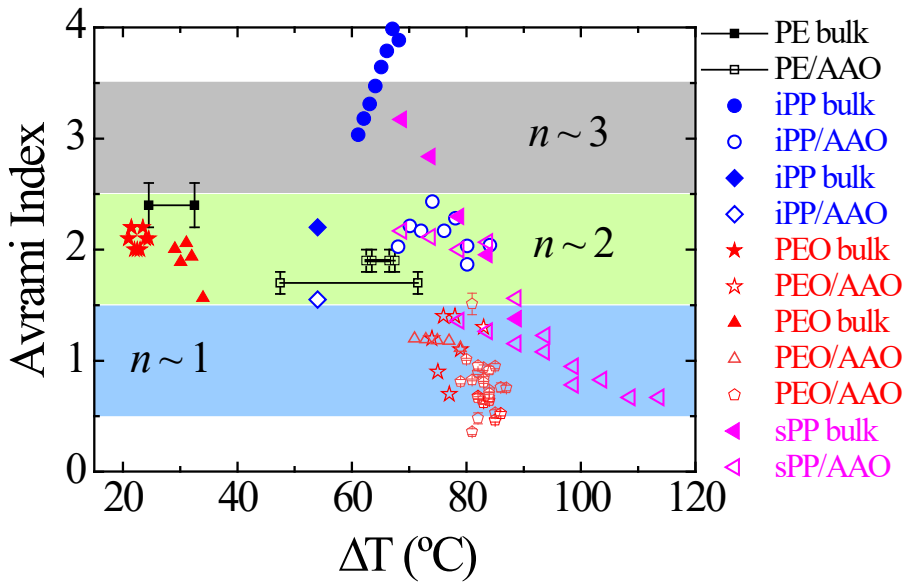

Figure 25. Avrami index of polymer within AAO. The bulk polymer is plotted as filled symbols and the infiltrated sample is plotted as hollow symbols. The data were taken from ref. [266] for PE, ref. [268] (blue circle) and [269] (blue diamond) for iPP, ref. [91] (red star), [277] (red up triangle) and [280](red pentagon) for PEO, ref. [285] (pink left triangle) for sPP.

2.4. Nanocomposites

It is well known that the addition of nanofillers endows polymer materials with superior properties and makes them attractive for industrial applications. The interfacial and spatial effects introduced by nanofillers are believed to be the main reasons for the reinforcement mechanism of the polymer nanocomposites (PNCs). The interfacial and spatial confinement effects originate from the polymer-

nanoparticle interaction and the restricted space between/among nanoparticles, respectively. Meanwhile, the crystallization behavior of the polymer matrix is significantly influenced by the presence of nanofillers.

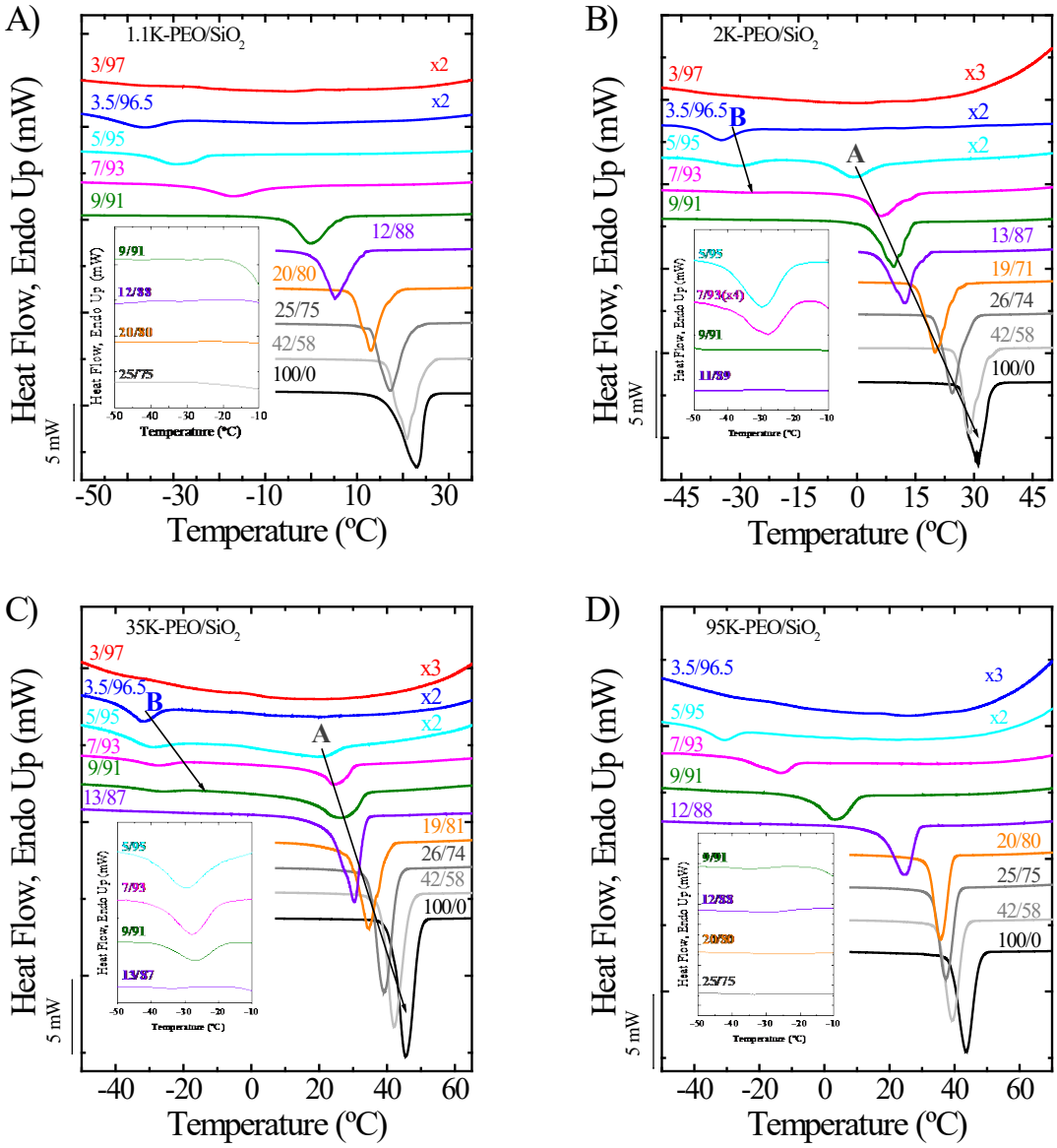

Figure 26. DSC cooling scans of 1.1K-PEO/SiO_2 (A), 2K-PEO/SiO_2 (B), 35K-PEO/SiO_2 (C), and 95K-PEO/SiO_2 (D) composites with various φ_{SiO2}. For clarity, the heat flow of PEO/SiO_2 composite with φ_{SiO2}>95 wt % was multiplied by a factor. [309], Copyright 2017. Adapted with permission from John Wiley & Sons Inc.

For the PNCs with low nanofiller contents, generally, the nanofillers may act as a nucleating agent, whereas they may exert confinement on crystallization at high contents. The crystallization behavior including nucleation mechanism, T_c, T_m,

crystallinity (X_c), crystal orientation and crystallization rate are significantly altered by these two effects, determining the ultimate properties of PNCs. Therefore, the crystallization of polymers confined by nanofillers has become a hot research topic for both scientific and industrial communities in the last two decades [288-307].

Interestingly, fractionated crystallization behavior has been observed in PEO/silica (SiO_2) [308-310] and PE/SiO_2 [311] at very high loadings of SiO_2. Unlike the dispersed system in the above sections (droplets, block copolymers, templates), the fractionated crystallization of nanocomposites is more complicated due to the strong impact of the interfacial effect, nanoparticle size and the molecular weight of polymer matrix.

Zhao et al. systematically investigated the effect of SiO_2 nanoparticles on the crystallization behavior of PEO nanocomposites considering the size and concentration of SiO_2 as well as the molecular weight (M_n) of PEO in the composites [308,309]. First, the PEO/SiO_2 nanocomposites with silica size of 110 nm and PEO of different M_n were investigated. Only when the M_n of PEO ranges from 1100 g/mol to 35000 g/mol, do the nanocomposites at silica content (φ_{SiO2}) higher than 91 wt % exhibit fractionated crystallization with two crystallization exotherms upon cooling from the melt (Figure 26). The high crystallization peak (peak A) at 0 –50 °C is assigned to the crystallization of bulk PEO., And the low crystallization peak (peak B) at –20 to –30 °C is attributed to the crystallization of loosely bound PEO chains (loops and tails) on SiO_2 surface. The large supercooling (ΔT~70 °C) necessary for the crystallization of bound PEO chains is caused by their very restricted mobility at the interface [308]. At a constant φ_{SiO2}, the percentage of crystallization enthalpies of peak B shows an increasing trend with the increase of M_n as shown in Figure 27A, indicating the fraction of loops and tails increases with M_n. Interestingly, the data shown in Figure 27B implies that $T_C{}^B$ is virtually independent of M_n. Moreover, $T_C{}^B$ is quite close to the glass transition temperature (T_g) of PEO under confinement (–50 ~ –30 °C) [308,312]. Ding et al. also reported a very weak low-temperature crystallization peak (-30 °C) which appeared at a low percentage of PEO, resulting from the PEO chains interacting with the silica surface [310]. Similar low crystallization temperatures were also found in PEO confined within block copolymers or AAO templates (see previous sections) [128,218,277-280].

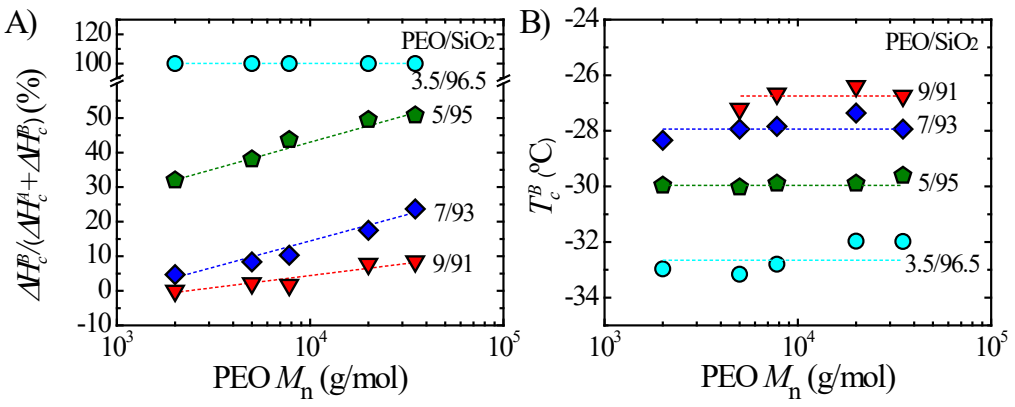

Figure 27. (A) The proportion of the peak B area against PEO M_n (The proportion of the peak B area is estimated by dividing the crystallization enthalpies under *LCP* ($\Delta H_C{}^B$) by the total crystallization enthalpies under both the peak B and peak A ($\Delta H_C{}^B$ + $\Delta H_C{}^A$). (B) Variation of the crystallization temperature of *LCP* ($T_C{}^B$) with φ_{SiO2} and M_n of PEO. The dashed line is a guide for the eye. [309], Copyright 2017. Adapted with permission from John Wiley & Sons Inc.

Focusing on the PEO with a fixed molecular weight (M_n = 20000 g/mol) and SiO_2 with different sizes (75, 130, 290 and 520 nm), the fractionated crystallization occurs with φ_{SiO2} in the range of 85–97 wt %. As shown in Figure 28, the $T_C{}^B$ of the PEO decreases and the proportion of the peak B area increases gradually with increasing φ_{SiO2}, implying an enhanced confinement effect on PEO crystallization. Furthermore, the smaller nanoparticles with larger specific surface areas can also exert stronger suppression on the crystallization behavior of PEO, and thus the $T_C{}^B$ of PEO decreases at the same φ_{SiO2}. The effect of nanoparticle size on the crystallization of PEO/SiO_2 nanocomposites has also been discussed by Ding et al. [310] and Papananou et al. [304]. It is also found that the degree of suppression of PEO crystallization increases with increasing φ_{SiO2} and decreasing SiO_2 size.

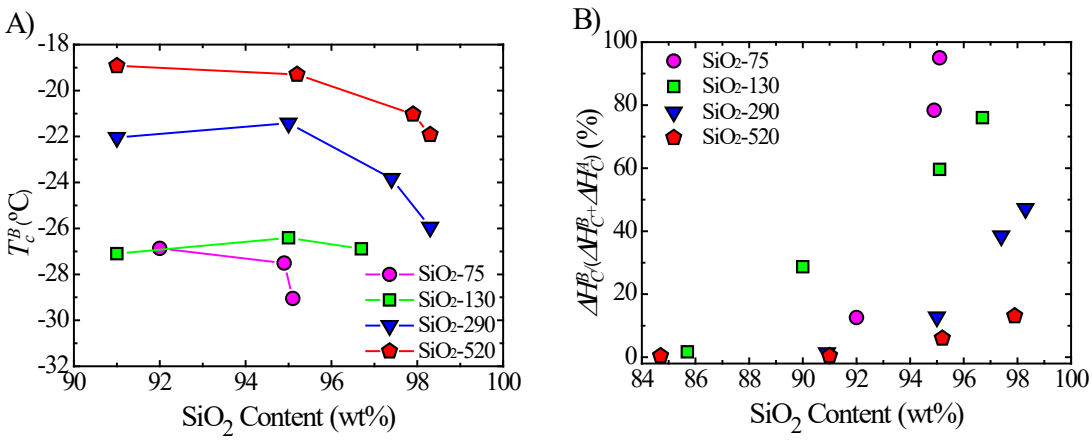

Figure 28. (A) Variation of the low crystallization temperature (T_C^B) with the SiO_2 sizes and ratios. (B) The proportions of the peak B area against the SiO_2 content. The proportion of the peak B area can be estimated by dividing the crystallization enthalpies under the peak B ((ΔH_C^B) by the total crystallization enthalpies under both of the peak B and peak A ($\Delta H_C^B + \Delta H_C^A$). [308], Copyright 2016. Adapted with permission from John Wiley & Sons Inc.

The high loading of nanofiller could affect the non-isothermal crystallization kinetics in PEO/SiO_2 [309] and HDPE/carbon nanotube (CNT) [87] nanocomposites, in which the fractionated crystallization was not found in the latter case. A decrease of X_c with φ_{filler} is observed and X_c reaches 10 % or even zero when the content of CNT or SiO_2 is higher than 10 % or 95 %, respectively, as shown in Figure 29A. A similar case was shown by Chrissopoulou et al. [304,313]. The X_c is nearly constant for PEO/SiO_2 and PEO/layered sodium montmorillonite (Na^+-MMT) nanocomposites with low filler content and it begins to decrease above a certain concentration (10-30 vol% SiO_2 depending on the size of nanoparticles or 10 vol% Na^+-MMT). The formation of a "filler network" at higher filler loading significantly suppresses the crystallization of the polymer.

The isothermal crystallization kinetics was analyzed by the Avrami equation in PEO/SiO_2 and HDPE/CNT composites. The Avrami index or exponent n exhibits a decreasing trend from 3 to 1 with increasing filler content as shown in Figure 29B. It is known that n strongly depends on both the mechanism of nucleation and crystal growth. For the unbound polymer (peak A), the value of n is always larger than 1, indicating heterogeneous nucleation of spherulitic structures. A value around 2 in fibrous nanocomposites corresponds to the development of a transcrystalline layer on the nanofiber surfaces and has been both predicted by modeling or computer simulations, as well as measured experimentally for different nanocomposites [314].

In the case of the loosely bound polymer (peak B), a percolated network is expected and the interaction of PEO with the SiO_2 surface creates stronger confinement effect, which possibly gives rise to sporadic nucleation (n_n = 1) controlled crystallization mechanism. As previously discussed, such low n values with a first-order kinetics, other than in PEO/SiO_2 and HDPE/CNT, were also observed in systems such as polymer droplets [315], AAO templates [277], and spherical microdomains of block copolymers [128].

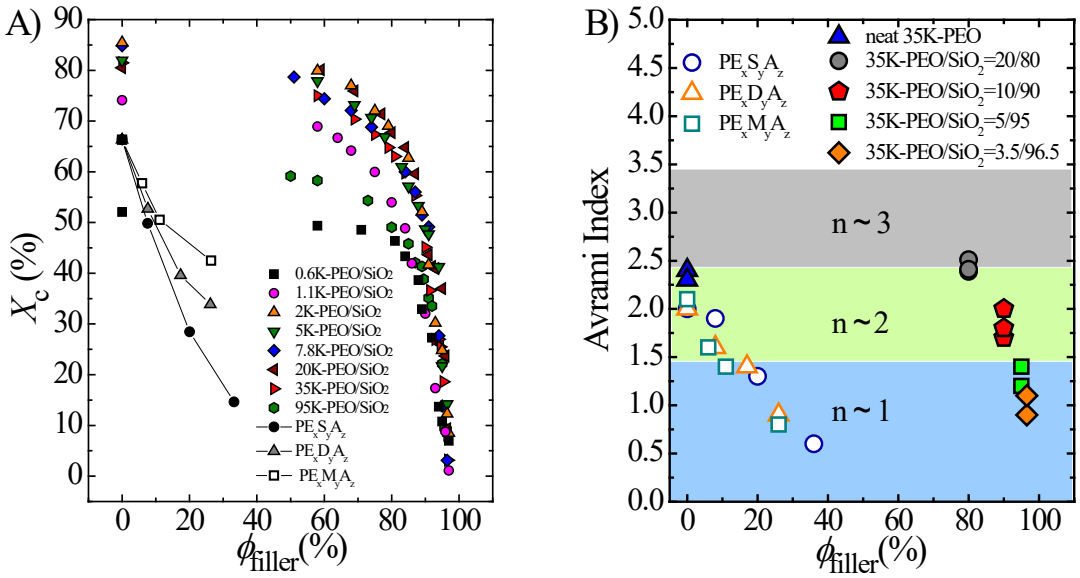

Figure 29. (A) The crystallinity (X_c) and (B) Avrami index (n) as a function of filler content in the nanocomposites of PEO/SiO_2 and HDPE/carbon nanotube. [87], Copyright 2011. Adapted with permission from Elsevier Science Ltd.

In the fractionated crystallization DSC cooling scans, peak B is characterized by $T_c \approx -30$ °C (i.e., close to the T_g of PEO) and the Avrami index values of 1 or even 0.5, indicating that restricted PEO chains are being nucleated homogeneously. However, peak A with lower supercooling is due to heterogeneous nucleation. Dalnoki-Veress et al. have pointed out that homogeneous nucleation mechanism does not depend on the molecular weight or chain length and the formation of a nucleus is only influenced by its immediate surroundings [316,317]. This probably accounts for the independence of T_C^B on M_n (Figure 26B).

3. Understanding of fractionated crystallization

3.1. Lack of sufficiently active heterogeneities

The fractionated crystallization phenomenon has been explained based on the absence of sufficiently active heterogeneities in every MD [39,85,91,97]. Fractionated crystallization is observed when the number of MDs is of the same order of magnitude or slightly larger than the number of heterogeneities present in the bulk polymer. When the number of MDs is exceedingly high, i.e., several orders of magnitude higher than the number of heterogeneities in the bulk polymer, the polymer chains inside the MDs usually nucleate at the surface of the MDs (surface nucleation) or inside their volume (i.e., homogeneous nucleation). This means that blends with micron size droplets usually display fractionated crystallization (with several exotherms) while in block copolymer with nanospheres of the crystallizable phase, the polymer tends to crystallize in a single exotherm at very high supercoolings, either by surface or homogeneous nucleation.

Fractionated crystallization has been observed when a polymeric material has been divided into a large number of MDs. Some of the MDs will have the most active heterogeneities (like the bulk polymer), other populations of MDs could have less active heterogeneities which need higher undercooling for crystallization, and finally some MDs will be clean (without heterogeneities), in which case the crystallization occurs via surface or homogeneous nucleation (see section 2.1, Figure 1) [39,85,91,97].

One strategy to prove that fractionated crystallization (with several crystallization exotherms) arises from the lack of active heterogeneities in every MD, is to inject heterogeneities, and this can be done by self-nucleation [17, 20] or by adding nucleating agents [18, 46, 48].

The self-nucleation procedure [318-321] is a thermal protocol designed to produce an increase in nucleation density coming from the sample own self-nuclei. The first step is to prepare a sample with a standard crystalline history. This is done by cooling the sample from a relaxed isotropic melt (after having erased all thermal history) at a constant rate in a DSC (i.e., 10 or 20 ºC/min) down to a temperature below the crystallization temperature range at that specific cooling rate. The peak crystallization temperature during this cooling from an isotropic melt is the standard T_c value.

Once a polymer with a standard thermal history is obtained, the sample is heated to a temperature denoted T_s, i.e., self-nucleation temperature, at which the sample is kept usually for 5 minutes. Depending on the value of this T_s temperature, different behaviours are observed by analysing the cooling scan from T_s and the subsequent heating.

If T_s temperature is high enough to erase crystalline memory, an isotropic melt will be obtained, and the sample will be in the *melting Domain* or *Domain I*. In this case the crystallization temperature upon cooling from any temperature in *Domain I* will be the same as the standard crystallization temperature. The crystallization temperature will in this case be determined by the pre-existing temperature resistant heterogeneities present in the bulk polymer under examination.

When the T_s value is sufficient to melt most crystals but low enough to leave "self-nuclei" (without causing any annealing), then the sample is in *Domain II*. This can be detected by the increase in the crystallization temperature in comparison with the standard crystallization temperature. The nature of the self-seeds is controversial [321-337]. Our group has proposed a division of *Domain II* into two sub-*Domains* [333]. In sub-*Domain IIb*, the polymer is not completely molten, as T_s is insufficient to melt all crystals and small crystal fragments remain, this is the so-called self-seeding sub-*Domain* or *Domain IIb*. Self-seeds or crystal fragments can act as epitaxially ideal nucleating agents for the polymer under consideration. The second sub-*Domain*, *Domain IIa* (or *melt memory Domain*) is located at higher T_s values, when all polymer crystals melt but some crystalline memory remains and still the crystallization temperature upon cooling from *Domain IIa* is higher than the standard crystallization temperature due to the increase in nucleation density caused by the created self-nuclei in *Domain IIa*. The nature of self-nuclei in *Domain IIa* is not known. It has been postulated that they can be regions in the melt where partial orientation of the chains remain, thanks to the survival of inter-segmental interactions that were present in the crystalline state [321,322, 333-337].

Finally, when the T_s temperature is too low to melt a substantial amount of the crystal population in the sample, annealing of the unmolten crystals occurs, which is reflected by the appearance of a second melting endotherm that corresponds to annealed crystals in the subsequent heating of the material. In this case, the sample is in *Domain III* or the *self-nucleation and annealing Domain*.

In order to inject self-nuclei to all the MDs of a sample, the material must be heated to a T_s temperature corresponding to *Domain II*, to produce the self-nuclei that will nucleate and accelerate the overall crystallization process upon recrystallization [320]. With the aim of injecting the maximum number of nuclei the ideal T_s temperature is used, this is the lowest temperature within *Domain II*. Performing self-nucleation at the ideal T_s guarantees the creation of the maximum number of self-nuclei without annealing of any unmolten crystal fragments (i.e., self-seeds).

As far as the authors are aware, Morales et al. were the first to employ self-nucleation as a way to inject nuclei in a blend system where fractionated crystallization occurs [17]. They studied linear low density polyethylene (LLDPE)/iPP blends, at compositions in which iPP droplets where dispersed in the LLDPE matrix. Their iPP homopolymer crystallized at 108.0 ºC whereas LLDPE crystallized at 101.4 ºC. However, when LLDPE 80/iPP 20 blend is cooled down from the isotropic melt (see Figure 30) a crystallization peak appeared at 102.1 ºC and a shoulder is observed at 86.0 ºC. Although only one crystallization peak is observed, during the subsequent heating two melting peaks are obtained, corresponding as expected to the two phases in the blend, iPP and LLDPE, indicating that both components were able to crystallize in the previous scan. Since iPP droplets crystallized at lower temperatures than in bulk, at 102.1 and 86.0 ºC, a fractionated crystallization must have occurred. Additionally, as the crystallization of iPP and LLDPE occurs at the same temperature, there is considerable overlap of their crystallization ranges, or the so-called coincident crystallization.

Considering that in the case of this blend, there are 10^{11} iPP droplets/cm^3 whereas in bulk iPP there are 10^6 heterogeneities/cm^3, fractionated crystallization could arise from the lack of heterogeneities. In order to prove this concept, Morales et al. applied a self-nucleation procedure to inject self-nuclei in every iPP droplet. Since the melting peaks of iPP and LLDPE lay at different temperatures, it is possible to apply self-nucleation to the iPP phase while LLDPE remains in the molten state. The sample was heated to a temperature corresponding to the ideal Ts temperature within *Domain II* of iPP, at this temperature iPP is self-nucleated, which results in an increase of crystallization temperature of iPP and thus, in a separation of the crystallization process of iPP and LLDPE. As can be seen in Figure 30, the LLDPE 80/iPP 20 sample that was heated to T_s=162 ºC, shows two crystallization peaks, at about 135 ºC the one corresponding to self-nucleated iPP and the second peak at 110

ºC that corresponds to LLDPE. The T_c of self-nucleated iPP in the blend is very similar to the one obtained with self-nucleated neat iPP. These results corroborate that the fractionated crystallization, which in this case turns into coincident crystallization, is a consequence of the lack of heterogeneities.

Fractionated crystallization is also observed in iPP/PS blends. Arnal et al. observed four different crystallization peaks in a PS 80/iPP 20 blend, in which iPP is dispersed as droplets in a PS matrix [20]. In this case, there are 10^{11} iPP droplets/cm^3 and only 10^7 heterogeneities/cm^3. According to Arnal et al. the formation of 4 crystallization peaks is related to the number and types of heterogeneities. Bulk iPP crystallized at about 110 ºC nucleated by the presence of type A heterogeneities, which are the most active ones. However, since in the blend there are more iPP droplets than heterogeneities some of the droplets will contain type A heterogeneities, while other droplets will contain less active heterogeneities such as type B or type C, which need higher supercoolings to crystallize, and finally some droplets will be statistically clean or free of heterogeneities. The clean droplets can undergo either surface or homogeneous nucleation. The exotherm labelled D in Figure 30 peaks at approximately 40 ºC, a temperature relatively close to the T_g of iPP (T_g=0 ºC), so it may be interpreted as homogeneous nucleation. A similar crystallization temperature has been reported by Duran et al. [268] for iPP in AAO templates proposing that this crystallization process is initiated by homogeneous nucleation.

In order to prove that the fractionated crystallization of iPP droplets observed in Figure 30 is due to the lack of the most active heterogeneities (i.e., type A) in every MD, Arnal et al. applied a self-nucleation procedure to inject self-nuclei in each iPP droplet. Employing the ideal T_s, they observed that the blend crystallizes at about 138 ºC, observing only one crystallization peak; this temperature is similar to the T_c of bulk self-nucleated iPP. Therefore, when enough nuclei are injected in the system, fractionated crystallization disappears, as the number of nuclei injected is enough to nucleate each iPP droplet dispersed in PS.

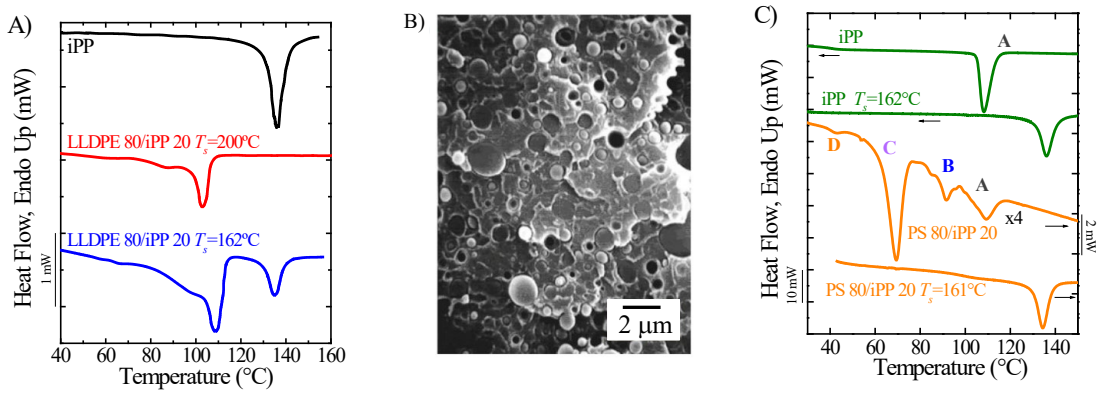

Figure 30. (A) DSC Cooling scan for self-nucleated iPP and self-nucleated and completely molten LLDPE 80/iPP 20 blend. (B) SEM image of PS 80/iPP 20 blend. (C) DSC cooling scan of iPP and PS 80/iPP 20 cooling from an isotropic melt and after self-nucleation at ideal T_s [17], Copyright 1995. Adapted with permission from Springer Nature Switzerland AG. [20], Copyright 1998. Adapted with permission from John Wiley & Sons Inc.

The self-nucleation procedure has been applied to block copolymers [99,108,114,131,224,225,236]. When the confinement degree is very high, *Domain II* disappears, which indicates that under confinement there are difficulties to inject nuclei. This is the case of the PE block in poly(styrene-*b*-ethylene-*b*-caprolactone) triblock copolymers (SEC) [236]. In Figure 31, the results corresponding to $S_{35}E_{15}C_{50}$ copolymer are shown. The DSC cooling scans from several T_s temperatures and the subsequent heating scans can be observed in Figure 31A and 31B.

From the DSC cooling scans (Figure 31A), a slight shift of the main crystallization peak (labelled "a" in Figure 31A) to lower temperatures is observed for T_s temperatures lower than 90 ºC, and at much lower T_s values, a second exotherm appears at higher temperatures which is labelled "b". In the DSC heating scans of Figure 31B, the appearance of a second melting peak at 89 ºC (highlighted with an arrow) indicates annealing of the unmolten crystals, however an increase of the "a" crystallization temperature was not observed at this T_s, thus solely annealing of the crystals occurs without self-nucleation at 89 ºC. If the T_s temperature is reduced even further, a second crystallization temperature (peak labelled "b") is observed for T_s=87.5 ºC. This exotherm appears at higher temperatures, so it is the result of self-nucleation. This behavior is completely different from that of neat PE, which shows the classical self-nucleation behavior: an increase of T_c when T_s is lowered, and at even lower T_s temperatures the appearance of a second melting peak which corresponds to the melting of annealed crystals. The crystallization temperatures of

the block copolymer for different T_s values as well as the location in comparison with the melting endotherm are shown in Figures 31C and 31D.

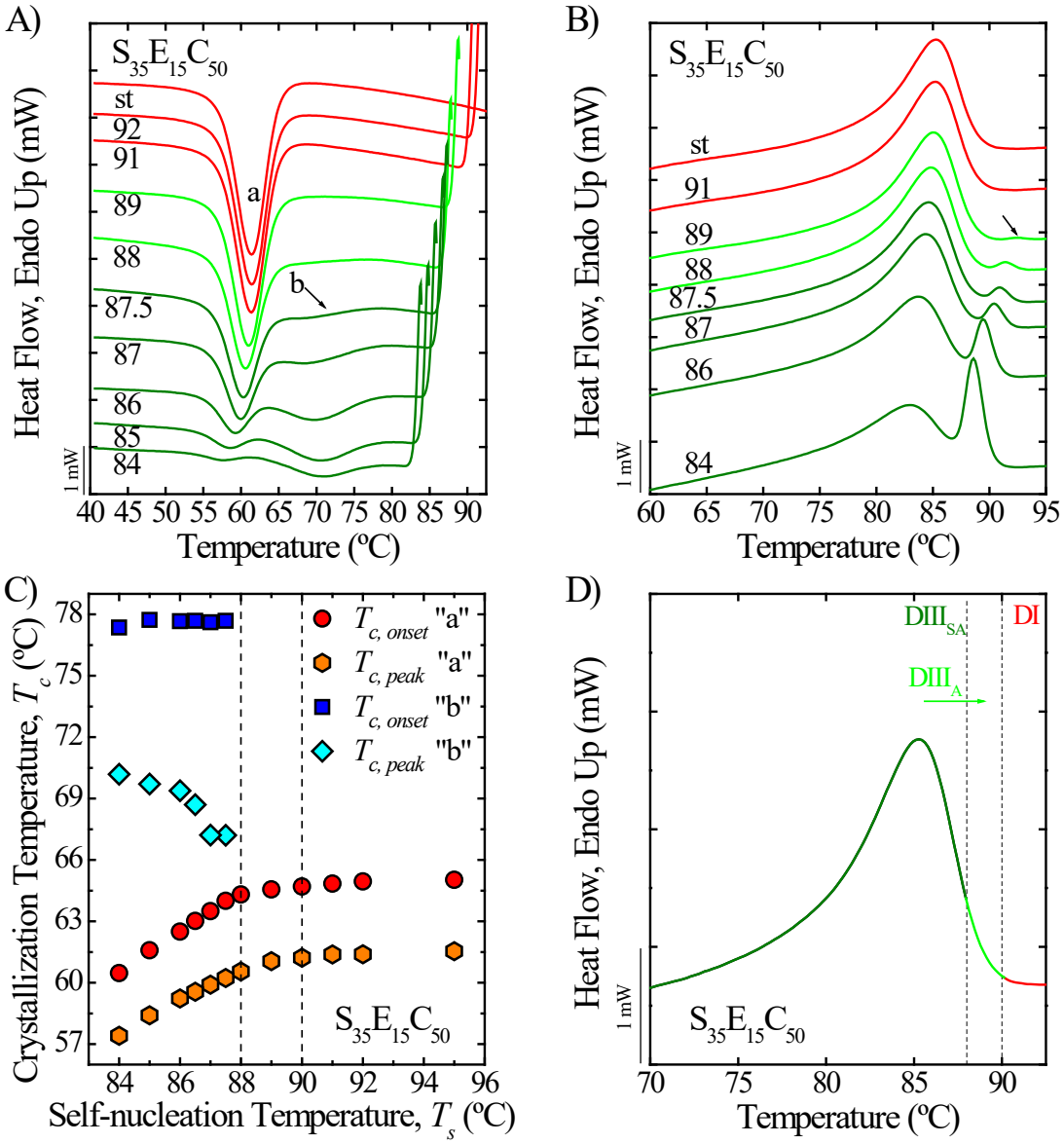

Figure 31. Self-nucleation behavior of the PE block within $S_{35}E_{15}C_{50}$ copolymer. (A) DSC cooling and (B) heating scans, (C) crystallization temperature as a function of T_s and (D) transition temperature between domains on top of the standard melting endotherm. [236], Copyright 2000. Adapted with permission from John Wiley & Sons Inc.

In summary, the neat PE precursor (hydrogenated 1,4 polybutadiene) of the $S_{35}E_{15}C_{50}$ terpolymer shows the three classical self-nucleation *Domains*: *DI, DII* and *DIII*. However, analogous PE chains (with identical molecular weight and short chain branching content generated by the residual 1,2 PB content) but confined within the triblock terpolymer $S_{35}E_{15}C_{50}$ (and with its two chain ends tethered to PS and PCL)

show a peculiar self-nucleation behavior with the following Domains: *DI, DIII$_A$* and *DIII$_{SA}$*. *Domain II* is absent as self-nucleation is never observed without annealing. This motivated the authors to denote new *Domains* as *Domain III$_A$*, which is a *Domain* where annealing is observed without self-nucleation; and *Domain III$_{SA}$*, which is identical to the usual *Domain III*, i.e., a self-nucleation and annealing *Domain*.

The authors conclude that the "a" crystallization peak could correspond to PE chains that are close to the interface, and therefore are highly restricted or confined, and also to PE chains that are in the middle of the PE block, which are less restricted. Reducing the T_s temperature to 87.5 ºC, the chains that are in the middle of PE block are able to self-nucleate, since they are not so confined as the chains near the interface, generating the "b" exotherm.

According to Balsamo et al. [236], confinement hinders the self-nucleation process of polymer chains. In this kind of system, in order to be able to inject nuclei, annealed crystals that are large enough have to be generated to observe self-nucleation of the less confined chains.

In order to analyze the effect of PE content in triblock terpolymers, on self-nucleation behavior, hence on the confinement degree, in Figure 32, the highest T_s temperature at which self-nucleation occurs minus the highest temperature at which annealing occurs is shown as a function of PE content in the copolymer. Reducing the PE content, i.e., going in the plot from the right to the left, a reduction of this temperature interval is observed due to the increase in chain confinement. According to Balsamo et al., the metastability of the crystals can also affect the results by increasing the temperature at which annealing appears, since the crystal thickness depends on the undercooling and on the PE block content [236].

It should be considered that $S_{27}E_{37}C_{36}$, which has the highest PE content of the copolymers studied, shows the classical SN behavior with a *Domain II* temperature range of 2.5 ºC. In the case of $S_{57}E_{27}C_{16}$, there is a direct transition from *Domain I* to *Domain III$_{SA}$*, in which self-nucleation and annealing occur, thus the $T_{SN} - T_{annealing}$ is equal to 0. However, in the case of the copolymers with 15% of PE, a negative value of $T_{SN} - T_{annealing}$ is obtained since in both cases, a reduction in T_s temperature causes the material to go from *Domain I* to *Domain III$_A$* in which only annealing occurs, and then to *Domain III$_{SA}$*.

In order to prove that confinement hinders self-nucleation, Balsamo et al. studied a cross-linked low density polyethylene, obtaining similar results to those with the block copolymer that contains 15% of PE [236]. In this case the confinement results from the covalent links between chains.

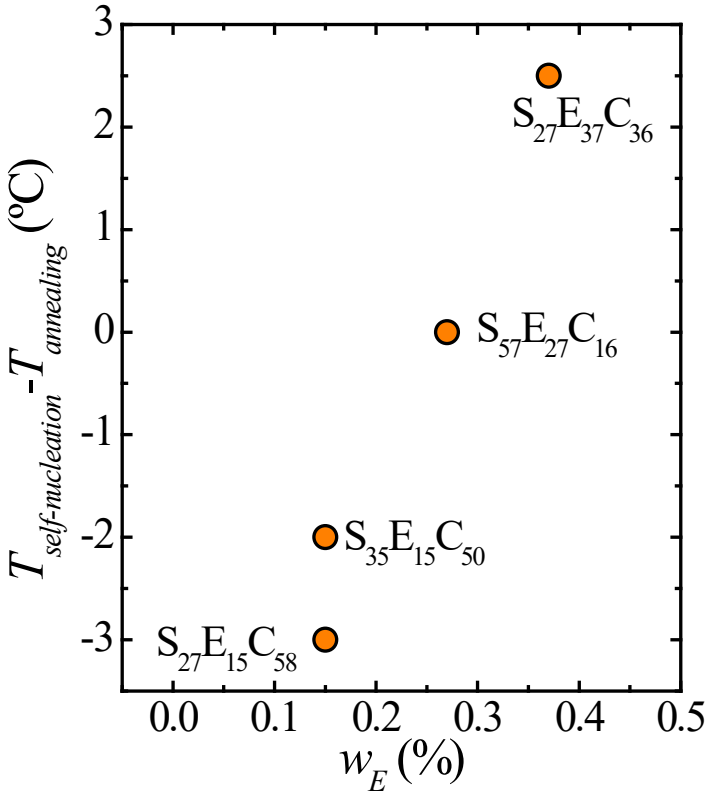

Figure 32. Highest T_s temperature at which self-nucleation occurs minus highest T_s temperature at which annealing occurs for the different SEC copolymers. Data taken from ref. [236].

The origin of fractionated crystallization is ascribed to the lack of efficient nuclei, and this hypothesis can also be verified by the addition of nucleating agents. [8,13,32,46,48,49] This strategy has been used with iPP and different PE matrices by Manaure et al. [18]. Figure 33 shows the DSC cooling scans of very low density polyethylene, VLDPE, iPP and some of their blends with a nucleating agent. In this case, sorbitol was added to the blend and to iPP, as it is a well-known nucleating agent for iPP. Neat iPP crystallizes at about 130 ºC showing a narrow peak, whereas VLDPE shows a peak at about 95 ºC and a broad shoulder. This broad shoulder could be due to the presence of short chain branches (SCB) that are heterogeneously distributed along the chain; during crystallization SCB provoke chain segregation. In the case of the unmixed blend (i.e., a superposition of the calorimetric behaviour of

neat iPP and neat VLDPE), the separate crystallization of iPP and VLDPE is clearly observed, as expected. However, when iPP and VLDPE are melt mixed, the crystallization peak corresponding to iPP cannot be observed at the same supercooling as in neat iPP. A peak is observed at higher temperatures than the T_c of VLDPE, this peak corresponds to a fraction of iPP and to VDLPE, which is nucleated by iPP. The peak at lower temperatures corresponds to other iPP fractions as well as VLDPE fractions. Since iPP in the blend crystallizes at lower temperatures than in bulk, fractionated crystallization occurs. According to Manure et al., in this blend there are 10^{12} iPP droplets/cm^3 whereas only 10^6 heterogeneities/cm^3 are observed for bulk iPP [18]. Therefore, this large difference in the number of iPP droplets and number of heterogeneities results in fractionated crystallization since the majority of the iPP droplets do not contain the most active heterogeneities. However, when sorbitol is added a crystallization peak at about 130 ºC appears, at a similar temperature to neat iPP/sorbitol blend, this indicates that with the addition of the nucleating agent, iPP is able to crystallize at higher temperatures since every iPP droplet has active heterogeneities. A broad peak is also observed which corresponds to VLDPE. Therefore, sorbitol is able to separate the crystallization process of iPP and VLDPE by injecting nuclei in iPP droplets.

Manaure et al. performed rheological measurements to detect the crystallization process [18]. They carried out small amplitude oscillatory shear experiments in the linear viscoelastic regime. When the material is cooled from the melt, there is a gradual increase in the storage modulus of the melt, until the material starts to crystallize and then a sudden increase of the modulus is observed. When there are crystal fragments dispersed in the melt, the materials behave as a filled polymer. iPP/sorbitol crystallizes at the highest temperature (see Figure 33), followed by iPP, due to the presence of the nucleating agent that accelerates the crystallization. The crystallization process is marked by a sudden increase of the storage modulus. In the case of the blend, a progressive and unique increase can be observed at lower temperatures since in this case the crystallization of iPP and VLDPE are overlapped, as has been observed by DSC, obtaining a very similar result to neat VLDPE. However, in the case of the blend containing sorbitol, two increases in the storage modulus are observed: one at about 130 ºC that corresponds to the crystallization of iPP and the other at about 110 ºC that corresponds to the crystallization of VDLPE.

This agrees with DSC results concluding that when sorbitol is added the crystallization process of iPP and VLDPE is separated by the nuclei injection.

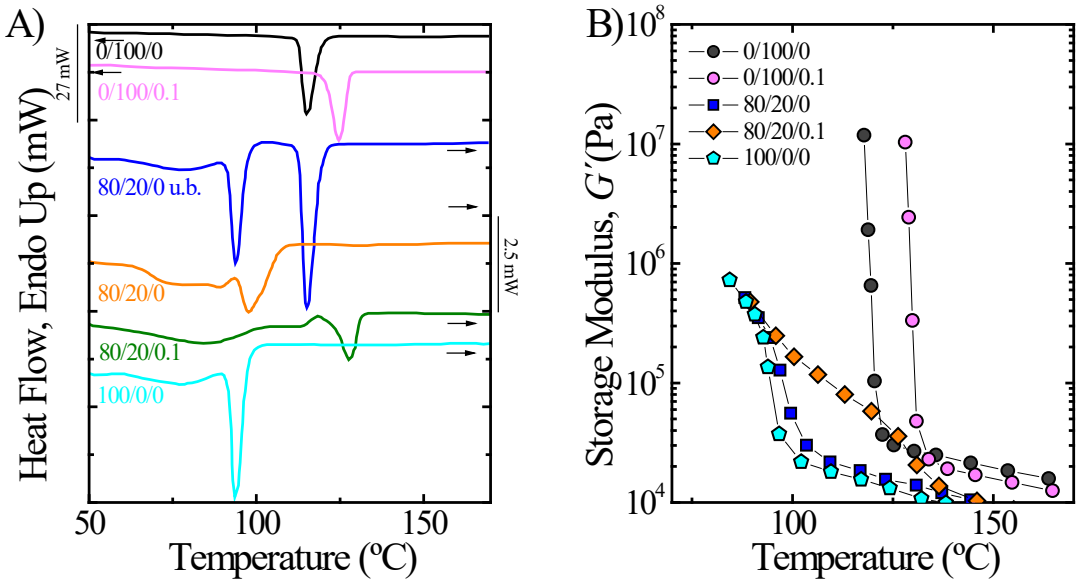

Figure 33. (A) DSC cooling scans of iPP/VLDPE/sorbitol system and (B) storage modulus as a function of temperature for the same system. [18], Copyright 1997. Adapted with permission from John Wiley & Sons Inc.

Fractionated crystallization has been also investigated in PA6/PS blends by Mathot et al. [32,338]. With the addition of talc, the exothermic enthalpy of the higher crystallization peak increased at the expense of that of the lower crystallization peak.

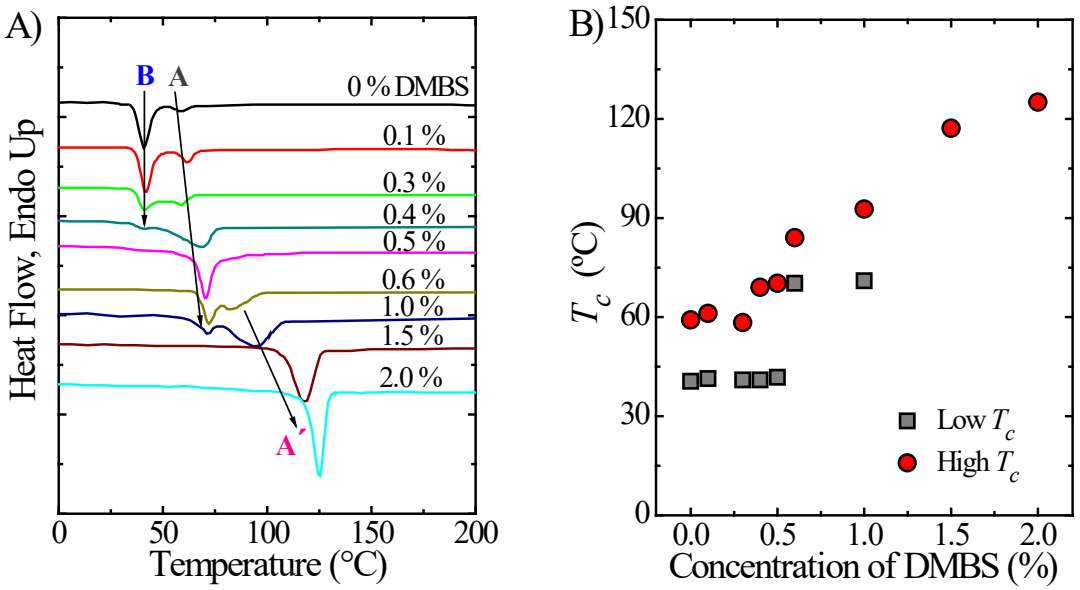

Figure 34. (A) DSC cooling scans of iPP micro-droplets obtained from thermal breakup of 12 nm iPP nanolayers with indicated concentration of DMBS; (B) crystallization peaks summarized from (A). [46], Copyright 2007. Adapted with permission from John Wiley & Sons Inc.

In iPP nanolayers, after the thermal breakup and formation of droplets, the crystallization of iPP shifted to much larger undercoolings at around 40 °C (homogeneous nucleation) and 60 °C, as shown in Figure 34A (see also section 2.2). Jin et al. [46] added different concentrations of the soluble nucleating agent 1,3:2,4-bis(3,4-dimethyl-benzylidene sorbitol) (DMBS) up to 2.0 wt % to the multilayer films. The DSC cooling curves of iPP droplets containing DMBS are shown in Figure 34A while the corresponding crystallization peaks are summarized in Figure 34B. It can be seen that with increasing the concentration of DMBS from 0 to 0.5 %, the enthalpy of homogeneous nucleation exotherm centered at 40 °C decreased, while on the opposite the enthalpy of 60 °C peak increased due to the presence of the nucleant in the iPP droplets. Moreover, with further increase of DMBS concentration, a new crystallization peak appeared and shifted to higher temperatures with the concentration of nucleating agent. This behavior is attributed to an increased number of DMBS particles in each droplet, which augments the possibility of nucleation.

The effect of a different kind of α form crystal nucleating agent (organic dicarboxylic acid salt), and a β form crystal nucleating agent (quinacridone quinone), as well as various additives and matrix substrates on the fractionated crystallization of iPP droplets, were also investigated by Baer et al. [8,46,49] In previous works by Galeski et al., the addition of PP nucleating agents to one of the components of immiscible blends was also used in order to investigate interphase migration of impurities. [339-342]

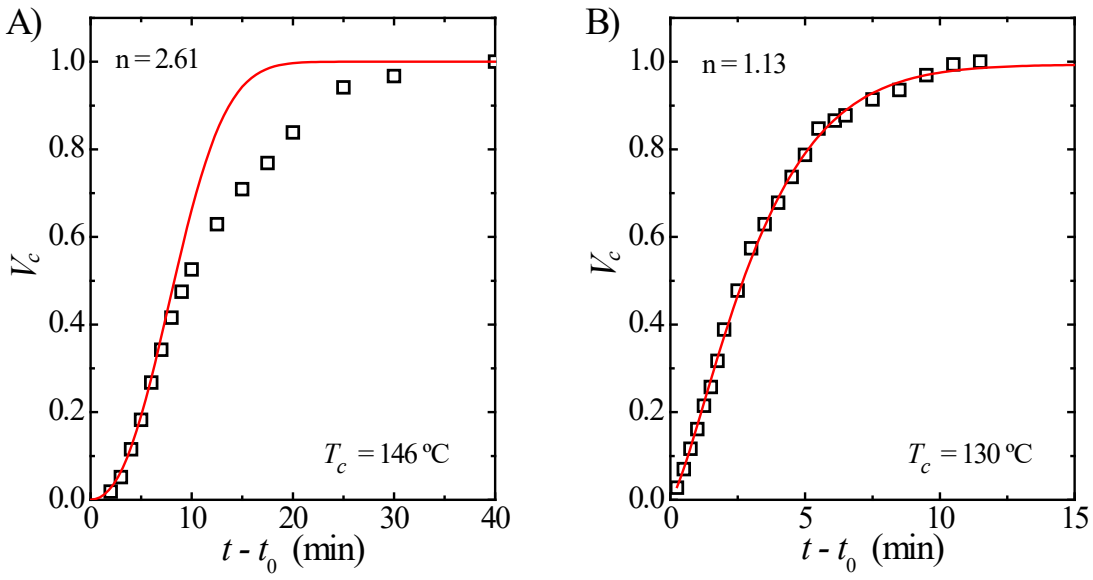

Figure 35. Evolution of the crystalline volume fraction as a function of time for iPP droplets (A) self-nucleated at T_s=160 °C and (B) with NA-11 (0.25 wt %) The crystallization temperatures are indicated in the Figures [7]. [7], Copyright 2020. Adapted with permission from American Chemical Society.

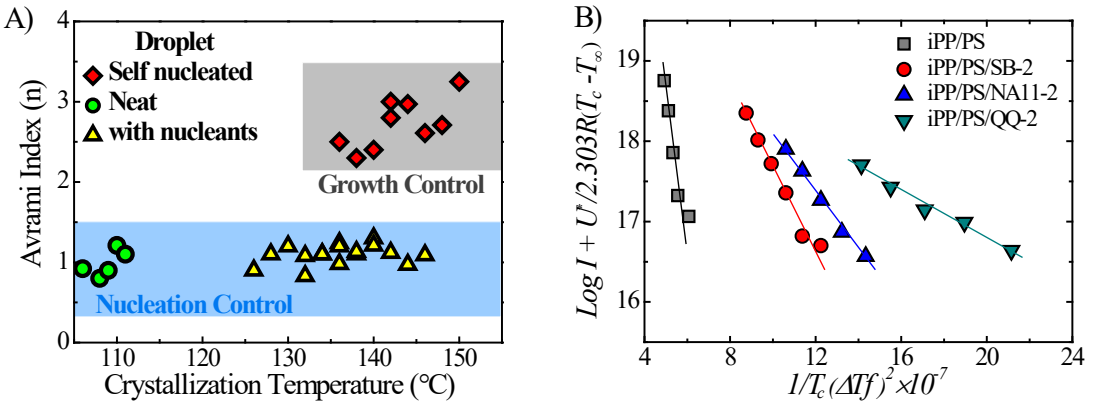

Figure 36 (A) Avrami index of various iPP micro-droplets (self-nucleated, neat, and containing different NAs); (B) nucleation rates as a function of crystallization temperatures, according to classical heterogeneous nucleation theory, for iPP droplets containing different heterogeneities [7]. [7], Copyright 2020. Adapted with permission from American Chemical Society.

Wang et al. [7] conducted further investigations of the crystallization kinetics of iPP droplets dispersed in PS matrix containing self-nuclei or nucleating agents (NAs), in order to quantitively evaluate the nucleation efficiency of different heterogeneities responsible for the multiple fractionated crystallization peaks. As two representative examples, the volume fraction of crystallized iPP droplets containing self-nuclei and the nucleating agent NA-11 and were recorded as a function of crystallization time, and analyzed on the basis of the Avrami equation in Figure 35A and 35B. Crystallization of iPP micro-droplets containing 0.25 wt % NA-11 showed a

first-order kinetics with Avrami index around 1.0, suggesting that heterogeneous nucleation was the rate-determining step for the entire crystallization process. However, ideally self-nucleated iPP droplets showed a sigmoidal crystallization curve with Avrami index around 3.0, indicating that the nucleation process is very fast (due to the presence of self-nuclei), hence it does not contribute to the kinetics, while crystal growth dominates the entire crystallization process.

The Avrami index for all the iPP droplets (neat, containing different nucleating agents, and self-nucleated) are summarized in Figure 36A. All the iPP droplets nucleated on known or unknown heterogeneities (e.g., NAs, PS surface or type B heterogeneities) exclusively showed a nucleation controlled first-order kinetics, which can be further analyzed based on the classical heterogeneous nucleation model [343] to derive the interfacial free energy difference, $\Delta\sigma$, between the heterogeneities and the crystallizing polymer. Accordingly, the slope of the lines reported in Figure 36B is directly proportional to $\Delta\sigma$. It can be seen that, among all the α form crystal nucleating agents, NA-11 is the most efficient one to nucleate iPP, exhibiting the lowest $\Delta\sigma$. It is worth to note that the concentration of NAs was demonstrated to have no effect on the derived intrinsic nucleation efficiency. The same method was also successfully applied to investigate the nucleation efficiency of β-crystal nucleating agent, like quinacridone quinone (QQ) (see Figure 36B).

Impurities are able to act as heterogeneous nuclei, as has been proved by Müller et al. [129]. This was observed for a polyethylene-*block*-poly(ethylene-*alt*-propylene)-block-polyethylene oxide block copolymer which was prepared hydrogenating the polybutylene-*block*- poly(ethylene-alt-propylene)-*block*-polyethylene oxide terpolymer. For that purpose, a Wilkinson catalyst was used. In order to elucidate if the presence of this catalyst affects the crystallization process, the block copolymer was purified to remove the catalyst, and the thermal properties of both unpurified and purified samples were analysed.

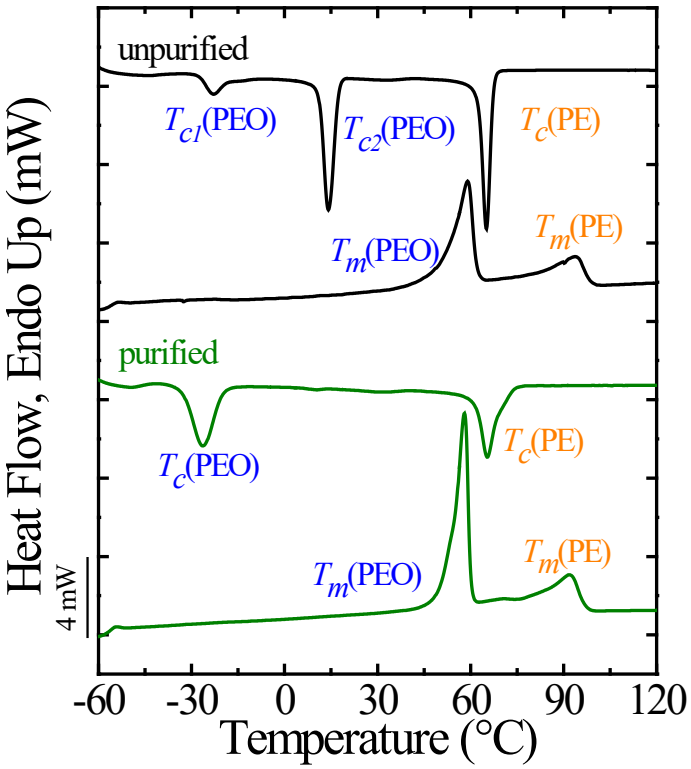

Figure 37. Cooling and heating scans of PE-PEP-PEO copolymer unpurified (black) and purified (green). [129], Copyright 2002. Adapted with permission from American Chemical Society.

In Figure 37, the unpurified sample can be observed in black. At about 60 ºC the crystallization of PE block occurs, and at lower temperatures, at 20 and -27 ºC, the crystallization of PEO block. The crystallization of PEO at 20 ºC is caused by heterogeneous nucleation and the peak at -27 ºC could be caused by less active heterogeneities or by surface nucleation. When the purified sample is analysed, it can be observed (green curve in Figure 37), that the peak at about 20 ºC disappears. In this case PEO crystallizes at -27 ºC and at -47 ºC. The peak at -27 ºC could be caused by weak heterogeneities or surface nucleation whereas the peak at -47 ºC results from the crystallization of a certain MD population that is homogeneously nucleated. This result indicates that the crystallization peak at 20 ºC of the unpurified sample was caused by Wilkinson catalyst, since it disappears in the case of the purified sample [129]. Thus, Wilkinson catalyst acts as heterogeneous nucleating agent.

3.2. Interface/Surface and Volume effects: Surface versus Homogeneous Nucleation

The unequivocal attribution of a given fractionated crystallization peak to homogeneous nucleation, rather than to surface-induced nucleation, is extremely challenging. Typically, in order to demonstrate the occurrence of homogeneous nucleation, the overall crystallization rate constant in isothermal experiments is plotted as a function of domain volume [316]. In fact, the probability of a homogeneous nucleus to be formed upon spontaneous aggregation of chain segments is proportional to the volume of undercooled polymer. On the other hand, a dependence on the system area is found for the case of surface-induced nucleation. Unfortunately, for the above discussed polymeric systems, isothermal crystallization experiments are just a minority [280], while there is an abundance of literature regarding non-isothermal crystallization.

In particular, many experimental data are available for two particular polymers discussed in the previous sections, i.e., iPP and PEO. For these polymers non-isothermal crystallization temperature data are typically measured spanning a variety of systems, from immiscible blends to AAO templates and block copolymers. Given the above, and following the suggestion of Müller et al. [39], we present a comprehensive collection of the measured T_C for the different systems, plotted against the average volume of the isolated micro- or nano-domains in the different systems.

Figure 38 gathers a selection of the reported crystallization temperatures of iPP for a wide range of domain sizes, spanning about 7-8 orders of magnitude. The values selected from the literature are those most probably ascribed to homogeneous nucleation, i.e., typically the lowest T_C if a series of fractionated crystallization peaks are present. Although a substantial overlap in the size range characteristic of each system exists, the largest domain sizes are those obtained for relatively coarse droplets in immiscible blends. In the intermediate size range, we find iPP infiltrated in AAO templates, while nanodroplets in emulsions and from nanolayer breakup extend the domain size range down to 10^5-10^6 nm^3.

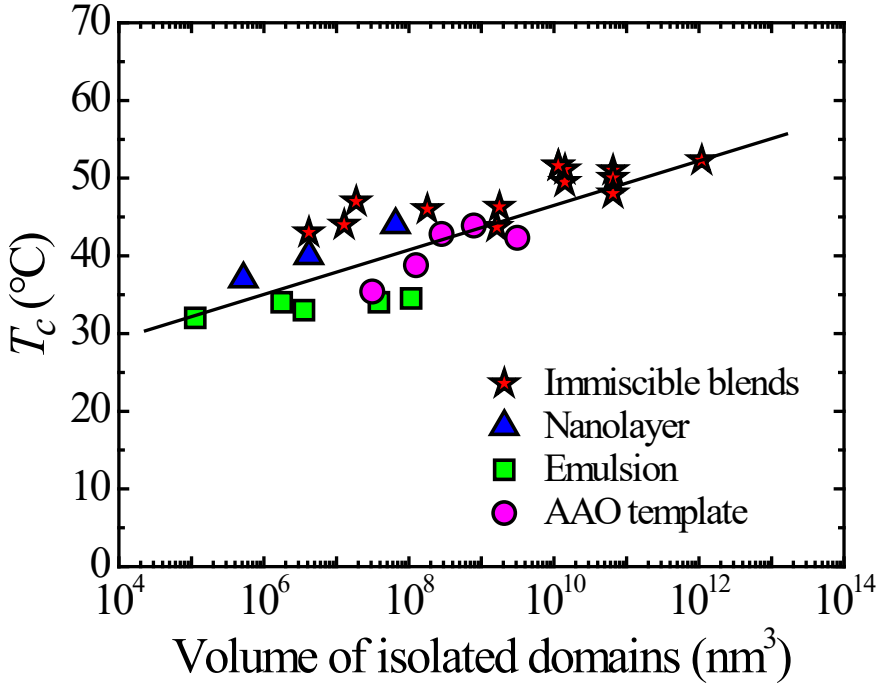

Figure 38. Collection of non-isothermal crystallization temperatures of iPP as a function of the volume of isolated polymer domains in different systems (immiscible blends, droplets form nanolayer breakup, nanoemulsions and AAO templates). The selected temperature are ascribed to the homogeneous nucleation mechanism. Immiscible blends (red stars [11,12,20,23,24]), nanolayer (blue triangles [8,46,47]), nanoemulsions (green squares [36]), AAO template (pink spheres [282]).

We note that, notwithstanding the large variation in isolated domain size, the corresponding non-isothermal crystallization temperature of iPP varies in quite a narrow range, between approximately 55 and 35 °C. Despite the scattering of the data, due to the collection of many different polymer grades and conditions, a clear linear relationship between the logarithm of domain volume and the crystallization temperature can be established. Such empirical relationship is described by the following equation:

$$T_c = 18.0 + 2.98 \log(v_d) \qquad (10)$$

This implies that, since the overall crystallization rate of clean and isolated micro- or nano-domains is controlled by nucleation, a homogeneous nucleation mechanism, whose rate is proportional to the volume of the crystallizing phase, is most likely active in the reported cases. Interestingly, the ultimately reached T_C is still somewhat 40 °C above the glass transition temperature of iPP, contrary to what occurs for other

examples of homogeneously crystallizing polymers, such as the case of PEO that will be discussed next.

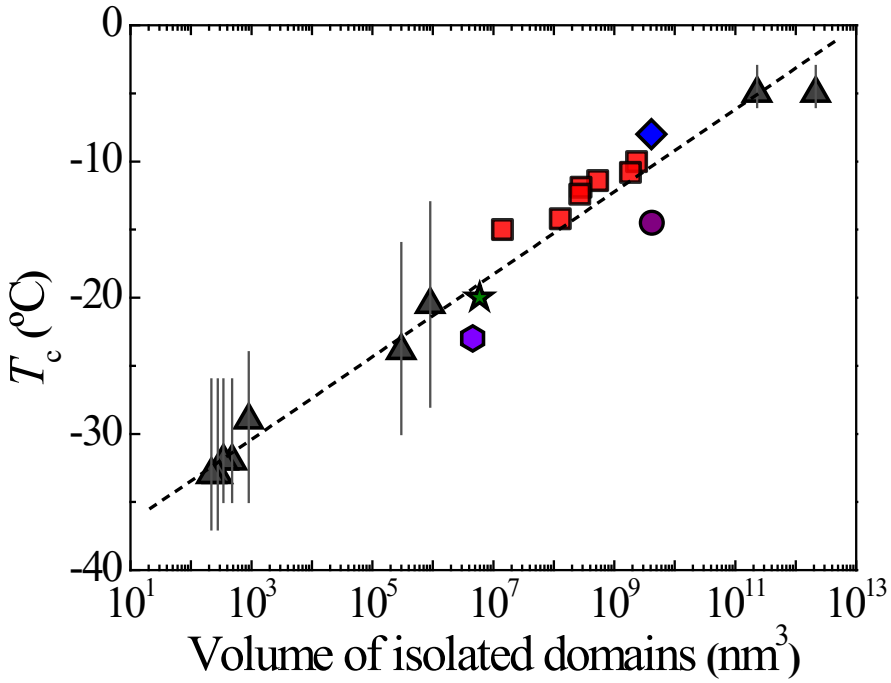

Figure 39. Collection of non-isothermal crystallization temperatures of PEO as a function of the volume of isolated polymer domains in different systems. The vertical bars indicate T_c ranges reported for isothermal crystallization temperatures, while the data points are values for non-isothermal experiments. AAO system (red squares [280], blue diamonds [277]), electrospun nanofibers (green stars [63], violet pentagons [64]), and immiscible blends (purple spheres [30]).

Müller et al. have summarized the nonisothermal crystallization data of PEO for homogeneous nucleation covering a broad range of domain sizes from varied systems, including droplets, miniemulsions, and nanodroplets obtained within block copolymers [39]. The following correlation relationship between the peak crystallization temperature during a DSC cooling scan (T_c, in ºC) and the volume of PEO phase (v_d, in nm^3) was obtained:

$$T_c = -41.8 + 2.89\log(v_d) \qquad (11)$$

Figure 39 shows an updated plot of T_c as a function of domain volume including the data points summarized by Müller et al. (grey up triangle). The gap in the range of 10^7 to 10^{10} nm^3 is filled with data points taken from the AAO system (red square [280], blue diamond [277]), electrospun nanofibers (green star [63], violet pentagon

[64]), and immiscible blends (purple sphere [30]). Although many values of T_c have been reported for infiltrated PEO within AAO in the literature, we only used those with clearly reported filled volumes/depths, since the pores can be partially filled or form nanotubes. The modified correlation relationship between T_c (ºC) and v_d (nm^3) is:

$$T_c = -39.5 + 3.03\log(v_d) \quad (12)$$

While homogeneous nucleation can be somehow recognized, although with the aid of empirical correlations, surface nucleation is more subtle and difficult to distinguish. A trivial case for immiscible polymer blends is related to the double-crystalline system PA-6/iPP, in which the polyamide matrix crystallizes before the dispersed phase (iPP droplets), causing an upward shift of the T_C of the minor component with respect to that of the bulk material [16].

Nucleation at the interface can also be hypothesized in the case of amorphous matrices in immiscible blends and nanodroplets generated by nanolayer breakup. For example, Tol et al. compared the crystallization of PA-6 droplets of different average diameters in matrices of PS/SMA or PPE/PS/SMA. [34] The fractionated crystallization temperature of the compatibilized PS matrix was systematically above that of the PPE/PS/SMA in the entire range of droplet size. Given the similar interfacial tension and identical morphology, the difference was attributed to surface nucleation, although vitrification of the matrix could also play a role in inducing crystallization. Nanodroplets of iPP dispersed in either PS, PMMA and PC matrices were obtained by breakup of nanolayers produced via co-extrusion. [8] While both iPP sub-micron droplets crystallized exclusively via homogeneous nucleation at about 40 °C when in contact with PS or PMMA, fractionated crystallization was observed in the case of PC matrix. In this case, the majority of droplets crystallized at around 85 °C, with a small fraction of droplets crystallizing at the homogeneous crystallization temperature. The authors ascribed the effect to surface-induced nucleation. Although the interpretation of the above results for immiscible blends seems the most plausible, the possibility of impurities or nuclei migration from the matrix to the dispersed phase cannot be totally excluded.

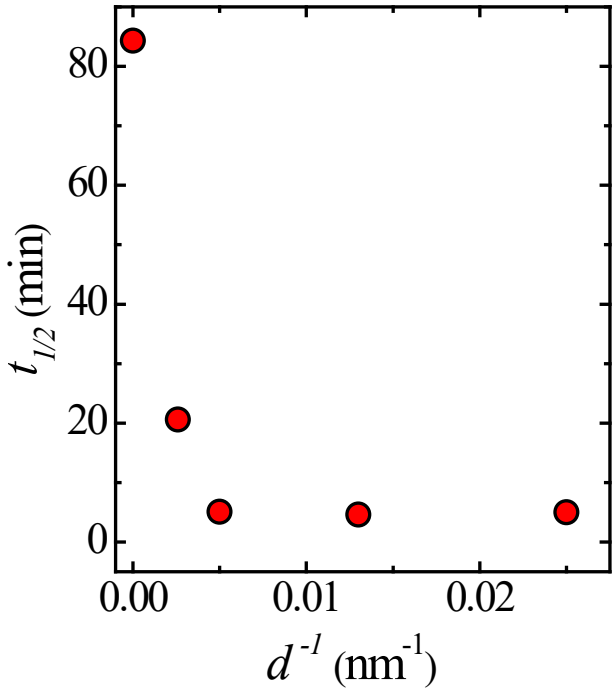

Figure 40. Crystallization half-time as a function of AAO pore diameter of bulk and infiltrated PLLA in AAO templates at 75 °C. [345], Copyright 2015. Adapted with permission from American Chemical Society.

As for polymer crystallization within AAO templates, a possible nucleation effect of the AAO wall has been frequently proposed to explain the relatively high T_c as compared to the T_g, such as in PE [218], PBS [344], PVDF [274], etc. Clear evidence of the AAO surface effects on crystallization was reported in poly(L-lactic acid) (PLLA). Guan et al. [345] found that the rate of cold crystallization from the glassy state was enhanced in AAO with respect to the bulk, as shown in Figure 40. A further study revealed that there was a highly mobile layer in the interface of AAO/PLLA which was used to explain the higher nucleation rates. The mobility of the interfacial layer depended strongly on the adsorption effect during annealing which in turn affected the crystallization rate [346].

4. Conclusions and Perspective

Fractionated crystallization is encountered when a bulk polymer is subdivided into MDs that are small enough to exhibit a number density of the same order of

magnitude as that of active heterogeneities present in the bulk material (i.e., type A heterogeneities). In a typical case, one exotherm will appear at the same undercooling as that of the bulk polymer produced by the crystallization of a population of MDs that contain type A heterogeneities. Then at increasing undercoolings, new exotherms can appear depending on the content of other types of heterogeneities that are present in specific MD populations (e.g., type B and type C in decreasing activity order or increasing interfacial free energy difference). Finally, at even higher undercooling, the clean MDs population (i.e. heterogeneity-free MDs) can crystallize either by surface nucleation or homogeneous nucleation inside the volume of the MDs. The homogeneous nucleation temperature occurs at the maximum possible undercooling and is a function of the volume of the microdomains. Hence, for very fine MDs (i.e., nano-spheres), homogeneous nucleation occurs at temperatures very close to the glass transition. Fractionated crystallization is thus easily observable in the dispersed component of immiscible blends and in some miscible double crystalline systems.

When the number density of MDs is several orders of magnitude (i.e., 6-10) higher than the number density of type A heterogeneities available in the bulk polymer, only clean MDs are formed on average. Hence, fractionated crystallization disappears and is replaced by a single exotherm located at very large undercoolings due to crystallization initiated by surface or homogeneous nucleation. This is the usual case in block copolymers MDs (cylinders or spheres) or in polymers infiltrated within nanoporous AAO templates. In this last case, fractionated crystallization has been often reported for infiltrated polymers. However, it has been demonstrated that when the surface of the infiltrated template is properly cleaned (i.e., any residual polymer that can percolate nanopores is removed) and the size of the nanopores is small enough, only surface or homogenous nucleation can be observed and thus a single crystallization exotherm at high undercoolings is found.

In the case of nanocomposites, as nanofiller content increases, the material is usually first nucleated and then at a certain concentration confinement takes over, and fractionated crystallization can be observed up to the point where at very large loads (or interactions between filler and matrix), surface or homogeneous nucleation can be observed.

When a crystallizable polymer goes from being a bulk, continuous or percolated phase (or MD) to a dispersed, highly confined phase (or MD), the crystallization gradually changes: from a single exotherm at very low undercoolings

(due to heterogeneous nucleation caused by type A heterogeneities), to fractionated crystallization with several exotherms to finally a single crystallization exotherm located at maximum supercooling (due to surface or homogeneous nucleation)

The above rationalization has been made possible thanks to the demonstration that fractionated crystallization is due to the lack of type A heterogeneities in every single MD. This demonstration has been achieved by either injecting nuclei (adding nucleating agents) or self-nuclei (self-nucleating the MDs) to all MDs.

Another consequence of confinement is that, as a result of the small size of the MDs, growth can occur very fast, as long as a nucleation site is provided to the MD. The slow or rate determining step for an ensemble of clean isolated MDs is usually the nucleation step. This means that the overall crystallization kinetics (which is a function of both nucleation and growth) typically goes from a sigmoidal higher order kinetics (3 or 4 for spherulitic forming polymers that nucleate instantaneously or sporadically) for the bulk material, to a first order kinetics (or lower depending on the nucleation rate) for the case where the same material is dispersed as small clean MDs. However, a first-order overall crystallization kinetics is not necessarily a sign of surface or homogeneous nucleation, as it can be present in MDs dispersions where only weak nucleating agents are injected, for example, and still the kinetics could be dominated by nucleation.

Fractionated crystallization or exclusive crystallization al large undercooling due to surface/homogeneous nucleation can have extreme consequences for the crystallinity and crystallization kinetics of confined polymers. In extreme cases (like PCL and PEO) the material can remain amorphous upon cooling to room temperature, as they usually crystallize above room temperature when they are heterogeneously nucleated, and well below room temperature (at temperatures lower than -30 ºC) when they are surface/homogeneously nucleated. Even when the material can crystallize upon cooling from the melt to room temperature (like in the case of PE or PP), the non-isothermal and isothermal crystallization rate decreases as the volume of the MDs decreases, reducing the final crystallinity of the MDs. Although fractionated crystallization is of importance for our fundamental understanding of polymer nucleation, this reduced crystallinity can also have large consequences on the mechanical and barrier properties of such materials. In the case of nanocomposites where the matrix is under confinement by the nanofiller, the crystallinity can drop to undetectable levels, once again impacting the mechanical and barrier properties of the

PNCs. More work is needed on the relationship between fractionated crystallization and final properties and applications. In principle, functional materials based with thermal responsivity could be prepared by taking advantage of the widely different crystallization ranges, depending on the fractionated crystallization details of the multiphasic material under consideration (i.e., blends, block copolymers, nanostructured fibers, hybrid materials). For example, the fractionated crystallization of PEO domains below room temperature in an i-PP/PEO blend has been exploited to create rewritable thermosensitive plastic films [347]. In fact, quenched films can exist either in a transparent or opaque state which is switched by cooling below the PEO domains crystallization temperature or above their melting temperature. The film can thus be written with a hot pen by melting the PEO droplets at around 60 °C. Furthermore, by adjusting the number and/or types of heterogeneities, the temperature-dependent crystallinity of the polymer can be delicately "programmed", which can be for instance used for creating shape-memory immiscible polymer blends with multiple tunable fixing or recovery temperatures [348,349].

ACKNOWLEDGMENTS

We acknowledge the financial support from the National Key R&D Program of China (2017YFE0117800) and the National Natural Science Foundation of China (21873109 and 21922308). We would like to thank the financial support provided by the BIODEST project; this project has received funding from the European Union's Horizon 2020 research and innovation program under the Marie Skłodowska-Curie grant agreement No. 778092. This work has also received funding from MINECO, project: MAT2017-83014-C2-1-P and from the Basque Government through grant IT1309-19. G.L. is grateful to the Youth Innovation Promotion Association of the Chinese Academy of Sciences (Y201908). L.S. acknowledges the postdoctoral grant from Basque Government.

References

1. Cormia R, Price F, Turnbull D. Kinetics of crystal nucleation in polyethylene. J Chem Phys 1982;37:1333-1340.
2. Vonnegut B. Variation with temperature of the nucleation rate of supercooled liquid tin and water drops. J Colloid Sci 1948;3:563-569.
3. Burns JR, Turnbull D. Kinetics of crystal nucleation in molten isotactic polypropylene. J Appl Phys 1966;37:4021-4026.

4. Koutsky J, Walton A, Baer E. Nucleation of polymer droplets. J Appl Phys 1967;38:1832-1839.
5. Pound GM, Mer VKL. Kinetics of crystalline nucleus formation in supercooled liquid Tin[1, 2]. J Am Chem Soc 1952;74:2323-2332.
6. Frensch H, Jungnickel, BJ. Some novel crystallization kinetic peculiarities in finely dispersing polymer blends. Colloid Polym Sci 1989;267:16-27.
7. Wang B, Utzeri R, Castellano M, Stagnaro P, Müller AJ, Cavallo D. Heterogeneous Nucleation and Self-Nucleation of Isotactic Polypropylene Microdroplets in Immiscible Blends: From Nucleation to Growth-Dominated Crystallization. Macromolecules 2020;53,5980-5991. https://doi.org/10.1021/acs.macromol.0c01167
8. Langhe DS, Hiltner A, Baer E. Effect of additives, catalyst residues, and confining substrates on the fractionated crystallization of polypropylene droplets. J Appl Polym Sci 2012;125:2110-2120. https://doi.org/10.1002/app.36300
9. Wang C, Liu FH, Huang WH. Electrospun-fiber induced transcrystallization of isotactic polypropylene matrix. Polymer 2011;52:1326-1336. https://doi.org/10.1016/j.polymer.2011.01.036
10. Groeninckx G, Harrats C, Vanneste M, Everaert V. Crystallization, micro-and nano-structure, and melting behavior of polymer blends. In: Utracki L, Wilkie C, editors. Polymer Blends Handbook, Dordrecht: Springer; 2014, p. 291-446. https://doi.org/10.1007/978-94-007-6064-6_5
11. Pukánszky B, Tüdös F, Kalló A, Bodor G. Multiple morphology in polypropylene/ethylene-propylene-diene terpolymer blends. Polymer 1989;30:1399-1406. https://doi.org/10.1016/0032-3861(89)90207-3
12. Ghijsels A, Groesbeek N, Yip C. Multiple crystallization behaviour of polypropylene/thermoplastic rubber blends and its use in assessing blend morphology. Polymer 1982;23:1913-1916. https://doi.org/10.1016/0032-3861(82)90217-8
13. Santana O, Müller A. Homogeneous nucleation of the dispersed crystallisable component of immiscible polymer blends. Polym Bull 1994;32:471-477. https://doi.org/10.1007/BF00587890
14. Bartczak Z, Galeski A. Homogeneous nucleation in polypropylene and its blends by small angle light scattering. Polymer 1990;31:2027-2038.
15. Long Y, Stachurski Z, Shanks R. Crystallization behaviour of isotactic polypropylene/linear low density polyethylene blends. Polym Int 1991;26:143-146. https://doi.org/10.1002/pi.4990260304
16. Ikkala O, Holsti-Miettinen R, Seppälä J. Effects of compatibilization on fractionated crystallization of PA6/PP blends. J Appl Polym Sci 1993;49:1165-1174. https://doi.org/10.1002/app.1993.070490705
17. Morales R, Arnal M., Müller A. The evaluation of the state of dispersion in immiscible blends where the minor phase exhibits fractionated crystallization. Polym Bull 1995;35:379-386. https://doi.org/10.1007/BF00963138
18. Manaure A, Morales R, Sánchez J, Müller AJ. Rheological and calorimetric evidences of the fractionated crystallization of iPP dispersed in ethylene/α-olefin copolymers. J Appl Polym Sci 1997;66:2481-2493. https://doi.org/10.1002/(SICI)1097-4628(19971226)66:13<2481::AID-APP11>3.0.CO;2-0
19. Manaure A, Müller AJ. Nucleation and crystallization of blends of poly (propylene) and ethylene/α-olefin copolymers. Macromol Chem Phys 2000;201:958-972. https://doi.org/10.1002/1521-3935(20000601)201:9<958::AID-MACP958>3.0.CO;2-0
20. Arnal ML, Matos ME, Morales RA, Santana OO, Müller AJ. Evaluation of the fractionated crystallization of dispersed polyolefins in a polystyrene matrix. Macromol Chem Phys 1998;199:2275-2288. https://doi.org/10.1002/(SICI)1521-3935(19981001)199:10<2275::AID-MACP2275>3.0.CO;2-%23
21. Tang T, Huang B. Fractionated crystallization in polyolefins–nylon 6 blends. J Appl Polym Sci 1994;53:355-360. https://doi.org/10.1002/app.1994.070530313
22. Li C, Tian G, Zhang Y, Zhang Y. Crystallization behavior of polypropylene/polycarbonate blends. Polym Test 2002;21:919-926. https://doi.org/10.1016/S0142-9418(02)00034-X
23. Balsamo V, Gouveia LM. Interplay of fractionated crystallization and morphology in polypropylene/poly (ϵ-caprolactone) blends. J Polym Sci Part B: Polym Phys 2007;45:1365-1379. https://doi.org/10.1002/polb.21137
24. Arnal ML, Müller AJ, Maiti P, Hikosaka M. Nucleation and crystallization of isotactic poly (propylene) droplets in an immiscible polystyrene matrix. Macromol Chem Phys 2000;201:2493-2504. https://doi.org/10.1002/1521-3935(20001101)201:17<2493::AID-MACP2493>3.0.CO;2-0
25. Baitoul M, Saint-Guirons H, Xans P, Monge P. Etude par analyze thermique differentielle de melanges diphasiques de polyethylene basse densite et de polystyrene atactique. Eur Polym J 1981;17:1281-1287. https://doi.org/10.1016/0014-3057(81)90092-6

26. Arnal ML, Müller AJ. Fractionated crystallisation of polyethylene and ethylene/α-olefin copolymers dispersed in immiscible polystyrene matrices. Macromol Chem Phys 1999;200:2559-2576. https://doi.org/10.1002/(SICI)1521-3935(19991101)200:11<2559::AID-MACP2559>3.0.CO;2-O
27. Dou R, Wang W, Zhou Y, Gong L, Yin B, Yang MB, Xie BH. Crystallisation behaviour of HDPE in PA6/EPDM-g-MA/HDPE ternary blend with different phase morphology. Plast, Rubber Compos 2016;45:207-215. https://doi.org/10.1080/14658011.2016.1165451
28. Mbarek S, Carrot C, Chalamet Y, Jaziri M, Elleuch B. Fractionated crystallization of high-density polyethylene as an evidence of dispersed phase morphology in PET/HDPE blends. Int J Mater Form 2008;1:635-638. https://link.springer.com/content/pdf/10.1007/s12289-008-0336-1.pdf
29. Wang Y, Gu K, Soman A, Gu T, Register RA, Loo Y-L, Priestley RD. Circumventing macroscopic phase separation in immiscible polymer mixtures by bottom-up deposition. Macromolecules 2020;53:5740-5746.
30. Tang T, Huang B. Compatibilization of polypropylene/poly (ethylene oxide) blends and crystallization behavior of the blends. J Polym Sci Part B: Polym Phys 1994;32:1991-1998. https://doi.org/10.1002/polb.1994.090321205
31. Qiu Z, Ikehara T, Nishi T. Miscibility and crystallization of poly (ethylene oxide) and poly (ε-caprolactone) blends. Polymer 2003;44:3101-3106. https://doi.org/10.1016/S0032-3861(03)00167-8
32. Tol R, Mathot V, Groeninckx G. Confined crystallization phenomena in immiscible polymer blends with dispersed micro-and nanometer sized PA6 droplets, part 2: reactively compatibilized PS/PA6 and (PPE/PS)/PA6 blends. Polymer 2005;46:383-396. https://doi.org/10.1016/j.polymer.2004.10.070
33. Córdova ME, Lorenzo AT, Müller AJ, Gani L., Tencé-Girault S, Leibler L. The Influence of Blend Morphology (Co-Continuous or Sub-Micrometer Droplets Dispersions) on the Nucleation and Crystallization Kinetics of Double Crystalline Polyethylene/Polyamide Blends Prepared by Reactive Extrusion. Macromol Chem Phys 2011;212:1335-1350. https://doi.org/10.1002/macp.201100039
34. Tol R, Mathot V, Groeninckx G. Confined crystallization phenomena in immiscible polymer blends with dispersed micro-and nanometer sized PA6 droplets, part 3: crystallization kinetics and crystallinity of micro-and nanometer sized PA6 droplets crystallizing at high supercoolings. Polymer 2005;46:2955-2965. https://doi.org/10.1016/j.polymer.2005.02.020
35. Sánchez MS, Mathot V, Poel GV, Groeninckx G, Bruls W. Crystallization of polyamide confined in sub-micrometer droplets dispersed in a molten polyethylene matrix. J Polym Sci Part B: Polym Phys 2006;44:815-825. https://doi.org/10.1002/polb.20738
36. Ibarretxe J, Groeninckx G, Bremer L, Mathot V. Quantitative evaluation of fractionated and homogeneous nucleation of polydisperse distributions of water-dispersed maleic anhydride-grafted-polypropylene micro-and nano-sized droplets. Polymer 2009;50:4584-4595. https://doi.org/10.1016/j.polymer.2009.06.067
37. Lorenzo AT, Arnal ML, Albuerne J, Müller AJ. DSC isothermal polymer crystallization kinetics measurements and the use of the Avrami equation to fit the data: Guidelines to avoid common problems. Polym Test 2007;26:222-231. https://doi.org/10.1016/j.polymertesting.2006.10.005
38. Balsamo V, Urdaneta N, Pérez L, Carrizales P, Abetz V, Müller AJ. Effect of the polyethylene confinement and topology on its crystallisation within semicrystalline ABC triblock copolymers. Eur Polym J 2004;40:1033-1049. https://doi.org/10.1016/j.eurpolymj.2004.01.009
39. Müller AJ, Balsamo V, Arnal ML. Nucleation and Crystallization in Diblock and Triblock Copolymers. Adv Polym Sci 2005;190:1-63. https://doi.org/10.1007/12_001
40. Müller, A. J.; Michell, R. M.; Lorenzo, A. T. Isothermal Crystallization Kinetics of Polymers. In: Guo Q, editor. Polymer Morphology: Principles, Characterization, and Processing, Hoboken: John Wiley & Sons Inc; 2016, p. 181-203. DOI: 10.1002/9781118892756.ch11
41. Langhe D, Ponting M. Manufacturing and novel applications of multilayer polymer films, Amsterdam: William Andrew; 2016. 231 pp.
42. Langhe D. Fractionated crystallization in polymer blends. In: Thomas S, Arif MP, Gowd EB, Kalarikkal N. Crystallization in multiphase polymer systems, Amsterdam: Elsevier; 2018, p. 239-267. https://doi.org/10.1016/B978-0-12-809453-2.00009-8
43. Carr JM, Langhe DS, Ponting MT, Hiltner A, Baer E. Confined crystallization in polymer nanolayered films: a review. J Mater Res 2012;27:1326-1350. DOI 10.1557/jmr.2012.17
44. Jin Y, Rogunova M, Hiltner A, Baer E, Nowacki R, Galeski A, Piorkowska E. Structure of polypropylene crystallized in confined nanolayers. J Polym Sci Part B: Polym Phys 2004;42:3380-3396. https://doi.org/10.1002/polb.20211
45. Jin Y, Hiltner A, Baer E, Masirek R, Piorkowska E, Galeski A. Formation and transformation of smectic polypropylene nanodroplets. J Polym Sci Part B: Polym Phys 2006;44:1795-1803. https://doi.org/10.1002/polb.20839

46. Jin Y, Hiltner A, Baer E. Effect of a sorbitol nucleating agent on fractionated crystallization of polypropylene droplets. J Polym Sci Part B: Polym Phys 2007;45:1788-1797. https://doi.org/10.1002/polb.21195
47. Langhe DS, Hiltner A, Baer E. Transformation of isotactic polypropylene droplets from the mesophase into the α-phase. J Polym Sci Part B: Polym Phys 2011;49:1672-1682. https://doi.org/10.1002/polb.22357
48. Jin Y, Hiltner A, Baer E. Effect of an organic dicarboxylic acid salt on fractionated crystallization of polypropylene droplets. J Appl Polym Sci 2007;105:3260-3273. https://doi.org/10.1002/app.26584
49. Langhe DS, Keum JK, Hiltner A, Baer E. Fractionated crystallization of α-and β-nucleated polypropylene droplets. J Polym Sci Part B: Polym Phys 2011;49:159-171. https://doi.org/10.1002/polb.22162
50. Bernal-Lara T, Liu R, Hiltner A, Baer E. Structure and thermal stability of polyethylene nanolayers. Polymer 2005;46:3043-3055. https://doi.org/10.1016/j.polymer.2005.01.055
51. Wang H, Keum JK, Hiltner A, Baer E, Freeman B, Rozanski A, Galeski A. Confined crystallization of polyethylene oxide in nanolayer assemblies. Science 2009;323:757-760. DOI: 10.1126/science.1164601
52. Lai CY, Hiltner A, Baer E, Korley LT. Deformation of confined poly (ethylene oxide) in multilayer films. ACS Appl. Mater. Interfaces 2012;4:2218-2227. https://doi.org/10.1021/am300240r
53. Wang H, Keum JK, Hiltner A, Baer E. Confined crystallization of PEO in nanolayered films impacting structure and oxygen permeability. Macromolecules 2009;42:7055-7066. https://doi.org/10.1021/ma901379f
54. Wang, H.; Keum, J. K.; Hiltner, A.; Baer, E. Crystallization kinetics of poly (ethylene oxide) in confined nanolayers. Macromolecules 2010;43:3359-3364.
55. Ponting M, Lin Y, Keum JK, Hiltner A, Baer E. Effect of substrate on the isothermal crystallization kinetics of confined poly (ε-caprolactone) nanolayers. Macromolecules 2010;43:8619-8627. https://doi.org/10.1021/ma101625h
56. Masirek R, Piorkowska E, Galeski A, Hiltner A, Baer E. High pressure crystallization of HDPE droplets. Macromolecules 2008;41:8086-8094. https://doi.org/10.1021/ma800933g
57. Liu RY, Jin Y, Hiltner A, Baer E. Probing nanoscale polymer interactions by forced-assembly. Macromol Rapid Commun 2003;24:943-948. https://doi.org/10.1002/marc.200300051
58. Ania F, Baltá-Calleja FJ, Flores A, Michler G, Scholtyssek S, Khariwala D, Hiltner A, Baer E, Rong L, Hsiao BS. Nanostructure and crystallization phenomena in multilayered films of alternating iPP and PA6 semicrystalline polymers. Eur Polym J 2012;48:86-96. https://doi.org/10.1016/j.eurpolymj.2011.10.003
59. Mackey M, Flandin L, Hiltner A, Baer E. Confined crystallization of PVDF and a PVDF-TFE copolymer in nanolayered films. J Polym Sci Part B: Polym Phys 2011;49:1750-1761. https://doi.org/10.1002/polb.22375
60. Zapala K, Piorkowska E, Hiltner A, Baer E. High-pressure crystallization of isotactic polypropylene droplets. Colloid Polym Sci 2012;290:1599-1607.
61. Wang H, Keum JK, Hiltner A, Baer E. Impact of nanoscale confinement on crystal orientation of poly (ethylene oxide). Macromol Rapid Commun 2010;31:356-361. https://doi.org/10.1002/marc.200900653
62. Zhong G, Zhu L, Fong H. Nanodroplet formations in electrospun fibers of immiscible polymer blends and their effects on fractionated crystallization. In: Wang Z, editors. Nanodroplets, New York: Springer; 2013, p. 25-50. https://doi.org/10.1007/978-1-4614-9472-0_2
63. Zhong G, Wang K, Zhang L, Li ZM, Fong H, Zhu L. Nanodroplet formation and exclusive homogenously nucleated crystallization in confined electrospun immiscible polymer blend fibers of polystyrene and poly (ethylene oxide). Polymer 2011;52:5397-5402. https://doi.org/10.1016/j.polymer.2011.09.045
64. Samanta P, Thangapandian V, Singh S, Srivastava R, Nandan B, Liu CL, Chen HL. Crystallization behaviour of poly (ethylene oxide) under confinement in the electrospun nanofibers of polystyrene/poly (ethylene oxide) blends. Soft Matter 2016;12:5110-5120. DOI: 10.1039/C6SM00648E
65. Samanta P, Srivastava R, Nandan B, Chen HL. Crystallization behavior of crystalline/crystalline polymer blends under confinement in electrospun nanofibers of polystyrene/poly (ethylene oxide)/poly (ε-caprolactone) ternary mixtures. Soft Matter 2017;13:1569-1582. DOI 10.1039/C6SM02748B
66. Zhong G, Zhang L, Su R, Wang K, Fong H, Zhu L. Understanding polymorphism formation in electrospun fibers of immiscible poly (vinylidene fluoride) blends. Polymer 2011;52:2228-2237. https://doi.org/10.1016/j.polymer.2011.03.024

67. Zhong G, Su R, Zhang L, Wang K, Li Z, Fong H, Zhu L. Evolution of nanodroplets and fractionated crystallization in thermally annealed electrospun blend fibers of poly (vinylidene fluoride) and polysulfone. Polymer 2012;53:4472-4480. https://doi.org/10.1016/j.polymer.2012.08.014
68. Ye HM, Song YY, Meng X, Zhou Q. Fractionated crystallization, polymorphism and crystal transformation of poly (butylene adipate) confined in electrospun immiscible blend fibers with polystyrene. RSC Adv 2016;6:55961-55969. DOI: 10.1039/C6RA09117B
69. He Y, Zhu B, Kai W, Inoue Y. Effects of crystallization condition of poly (butylene succinate) component on the crystallization of poly (ethylene oxide) component in their miscible blends. Macromolecules 2004;37:8050-8056. https://doi.org/10.1021/ma049482f
70. He Y, Zhu B, Kai W, Inoue Y. Nanoscale-confined and fractional crystallization of poly (ethylene oxide) in the interlamellar region of poly (butylene succinate). Macromolecules 2004;37:3337-3345. https://doi.org/10.1021/ma035886g
71. He Z, Liang Y, Han CC. Confined nucleation and growth of poly (ethylene oxide) on the different crystalline morphology of poly (butylene succinate) from a miscible blend. Macromolecules 2013;46:8264-8274. https://doi.org/10.1021/ma4015214
72. Pan P, Zhao L, Yang J, Inoue Y. Fractional crystallization and phase segregation in binary miscible poly (butylene succinate)/poly (ethylene oxide) crystalline blends: Effect of crystallization temperature. Macromol Mater Eng 2013;298:201-209. https://doi.org/10.1002/mame.201200006
73. Qiu Z, Ikehara T, Nishi T. Miscibility and crystallization in crystalline/crystalline blends of poly (butylene succinate)/poly (ethylene oxide). Polymer 2003;44:2799-2806. https://doi.org/10.1016/S0032-3861(03)00149-6
74. Yang J, Pan P, Hua L, Feng X, Yue J, Ge Y, Inoue Y. Effects of crystallization temperature of poly (vinylidene fluoride) on crystal modification and phase transition of poly (butylene adipate) in their blends: A novel approach for polymorphic control. J Phys Chem B 2012;116:1265-1272. https://doi.org/10.1021/jp209626x
75. Yang J, Pan P, Hua L, Zhu B, Dong T, Inoue Y. Polymorphic crystallization and phase transition of poly (butylene adipate) in its miscible crystalline/crystalline blend with poly (vinylidene fluoride). Macromolecules 2010;43:8610-8618. https://doi.org/10.1021/ma1015566
76. Yang J, Pan P, Hua L, Xie Y, Dong T, Zhu B, Inoue Y, Feng X. Fractionated crystallization, polymorphic crystalline structure, and spherulite morphology of poly (butylene adipate) in its miscible blend with poly (butylene succinate). Polymer 2011;52:3460-3468. https://doi.org/10.1016/j.polymer.2011.05.041
77. Avella M, Martuscelli E, Greco P. Crystallization behaviour of poly (ethylene oxide) from poly (3-hydroxybutyrate)/poly (ethylene oxide) blends: phase structuring, morphology and thermal behaviour. Polymer 1991;32:1647-1653. https://doi.org/10.1016/0032-3861(91)90401-4
78. Pan P, Zhao L, Zhu B, He Y, Inoue Y. Fractionated crystallization and self-nucleation behavior of poly (ethylene oxide) in its miscible blends with poly (3-hydroxybutyrate). J Appl Polym Sci 2010;117:3013-3022. https://doi.org/10.1002/app.32255
79. Zhao L, Kai W, He Y, Zhu B, Inoue Y. Effect of aging on fractional crystallization of poly (ethylene oxide) component in poly (ethylene oxide)/poly (3-hydroxybutyrate) blends. J Polym Sci Part B: Polym Phys 2005;43:2665-2676. https://doi.org/10.1002/polb.20552
80. Avella M, Martuscelli E, Raimo M. The fractionated crystallization phenomenon in poly (3-hydroxybutyrate)/poly (ethylene oxide) blends. Polymer 1993;34:3234-3240. https://doi.org/10.1016/0032-3861(93)90396-R
81. Weng M, Qiu Z. Unusual fractional crystallization behavior of novel crystalline/crystalline polymer blends of poly (ethylene suberate) and poly (ethylene oxide) with similar melting points. Macromolecules 2014;47:8351-8358. https://doi.org/10.1021/ma502019x
82. Wang T, Li H, Wang F, Yan S, Schultz J M. Confined growth of poly (butylene succinate) in its miscible blends with poly (vinylidene fluoride): morphology and growth kinetics. J Phys Chem B 2011;115:7814-7822. https://doi.org/10.1021/jp203680e
83. Hamley IW. Crystallization in Block Copolymers. Adv Polym Sci 1999;148:113-137.
84. Loo YL, Register RA. Crystallization within block copolymer mesophases. In: Hamley IW, editor. Developments in block copolymer science and Technology, Chichester: John Wiley & Sons, Ltd.; 2004, p. 213-243.
85. Müller AJ, Balsamo V, Arnal ML. Crystallization in block copolymers with more than one crystallizable block. In: Reiter G, Strobl GR, editors. Lecture Notes in Physics: Progress in Understanding of Polymer Crystallization, Berlin: Springer; 2007:229-259.
86. Castillo RV, Müller AJ. Crystallization and morphology of biodegradable or biostable single and double crystalline block copolymers. Prog Polym Sci 2009;34:516-560. https://doi.org/10.1016/j.progpolymsci.2009.03.002

87. Müller AJ, Arnal ML, Trujillo M, Lorenzo AT. Super-nucleation in nanocomposites and confinement effects on the crystallizable components within block copolymers, miktoarm star copolymers and nanocomposites. Eur Polym J 2011;47:614-629. https://doi.org/10.1016/j.eurpolymj.2010.09.027
88. Nandan B, Hsu JY, Chen HL. Crystallization Behavior of Crystalline - Amorphous Diblock Copolymers Consisting of a Rubbery Amorphous Block. J Macromol Sci Part C Polym Rev 2006;46:143-172. https://doi.org/10.1080/15321790600646802
89. He WN, Xu JT. Crystallization assisted self-assembly of semicrystalline block copolymers. Prog Polym Sci 2012;37:1350-1400. https://doi.org/10.1016/j.progpolymsci.2012.05.002
90. Takeshita H, Shiomi T, Takenaka K, Arai F. Crystallization and higher-order structure of multicomponent polymeric systems. Polymer 2013;54:4776-4789. https://doi.org/10.1016/j.polymer.2013.06.031
91. Michell RM, Blaszczyk-Lezak I, Mijangos C, Müller AJ. Confinement effects on polymer crystallization: From droplets to alumina nanopores. Polymer 2013;54:4059-4077. https://doi.org/10.1016/j.polymer.2013.05.029
92. Van Horn RM, Steffen MR, O'Connor D. Recent progress in block copolymer crystallization. Polym Crystallization 2018;1/1-46. https://doi.org/10.1002/pcr2.10039
93. Palacios JK, Mugica A, Zubitur M, Müller AJ. Crystallization and Morphology of Block Copolymers and Terpolymers With More Than One Crystallizable Block. In: Thomas S, Arif MP, Gowd EB, Kalarikkal N. Crystallization in multiphase polymer systems, Amsterdam: Elsevier; 2018, p. 123-180. https://doi.org/10.1016/B978-0-12-809453-2.00006-2
94. Nakagawa S, Marubayashi H, Nojima S. Crystallization of polymer chains confined in nanodomains. Eur Polym J 2015;70:262-275. https://doi.org/10.1016/j.eurpolymj.2015.07.018
95. Volynskii AL, Yarysheva AY, Rukhlya EG, Yarysheva LM, Bakeev NF. Effect of spatial restrictions at the nanometer scale on structuring in glassy and crystalline polymers. Polym Sci, Ser A 2015;57:515-551. https://doi.org/10.1134/S0965545X15050168
96. Zha L, Hu W. Molecular simulations of confined crystallization in the microdomains of diblock copolymers. Prog Polym Sci 2016;54-55:232-258. https://doi.org/10.1016/j.progpolymsci.2015.10.010
97. Michell RM, Müller AJ. Confined crystallization of polymeric materials. Prog Polym Sci 2016;54-55:183-213. https://doi.org/10.1016/j.progpolymsci.2015.10.007
98. Huang CL, Jiao L, Zhang JJ, Zeng JB, Yang KK, Wang YZ. Poly(butylene succinate)-poly(ethylene glycol) multiblock copolymer: Synthesis, structure, properties and shape memory performance. Polym Chem 2012;4:800-808. DOI: 10.1039/C2PY00603K
99. Huang CL, Jiao L, Zeng JB, Zhang JJ, Yang KK, Wang YZ. Fractional crystallization and homogeneous nucleation of confined PEG microdomains in PBS-PEG multiblock copolymers. J Phys Chem B 2013;117:10665-76. https://doi.org/10.1021/jp4059966
100. Zeng JB, Zhu QY, Lu X, He YS, Wang YZ. From miscible to partially miscible biodegradable double crystalline poly(ethylene succinate)-b-poly(butylene succinate) multiblock copolymers. Polym Chem 2012;3:399-408. DOI: 10.1039/C1PY00456E
101. Lin MC, Chen HL, Lin WF, Huang PS, Tsai JC. Crystallization of isotactic polypropylene under the spatial confinement templated by block copolymer microdomains. J Phys Chem B 2012;116:12357-12371. https://doi.org/10.1021/jp306410j
102. Quiram DJ, Register RA, Marchand GR, Ryan AJ. Dynamics of Structure Formation and Crystallization in Asymmetric Diblock Copolymers. Macromolecules 1997;30:8338-8343. https://doi.org/10.1021/ma9708050
103. Quiram DJ, Register RA, Marchand GR. Crystallization of asymmetric diblock copolymers from microphase-separated melts. Macromolecules 1997;30:4551-4558. https://doi.org/10.1021/ma961524f
104. Quiram DJ, Register RA, Marchand GR, Adamson DH. Chain orientation in block copolymers exhibiting cylindrically confined crystallization. Macromolecules 1998;31:4891-4898. https://doi.org/10.1021/ma971218h
105. Loo YL, Register RA, Ryan AJ, Dee GT. Polymer crystallization confined in one, two or three dimensions. Macromolecules 2001;34:8968-8977. https://doi.org/10.1021/ma011521p
106. Loo YL, Register RA, Ryan AJ. Modes of Crystallization in Block Copolymer Microdomains: Breakout, Templated, and Confined. Macromolecules 2002;35:2365-2374. https://doi.org/10.1021/ma011824j
107. Li S, Myers SB, Register RA. Solid-State Structure and Crystallization in Double-Crystalline Diblock Copolymers of Linear Polyethylene and Hydrogenated Polynorbornene. Macromolecules 2011;44:8835-8844. https://doi.org/10.1021/ma201951j

108. Lorenzo AT, Arnal ML, Müller AJ, Boschetti de Fierro A, Abetz V. Confinement effects on the crystallization and SSA thermal fractionation of the PE block within PE-b-PS diblock copolymers. Eur Polym J 2006;42:516-533. https://doi.org/10.1016/j.eurpolymj.2005.09.001
109. Lorenzo AT, Arnal ML, Müller AJ, Boschetti de Fierro A, Abetz V. Nucleation and isothermal crystallization of the polyethylene block within diblock copolymers containing polystyrene and poly(ethylene-alt-propylene). Macromolecules 2007;40:5023-5037. https://doi.org/10.1021/ma070252l
110. Müller C, Radano CP, Smith P, Stingelin-Stutzmann N. Crystalline–crystalline poly(3-hexylthiophene)–polyethylene diblock copolymers: Solidification from the melt. Polymer 2008;49:3973-3978. https://doi.org/10.1016/j.polymer.2008.07.006
111. Wang L, Xu JT, Ding PJ, Fan ZQ. Nucleation mechanism of PEO block in double-crystalline poly(ethylene-co-butene)-b-poly(ethylene oxide) block copolymers. Chin J Polym Sci 2006;24:473-482. https://doi.org/10.1142/S0256767906001540
112. Nojima S, Fukagawa Y, Ikeda H. Interactive Crystallization of a Strongly Segregated Double Crystalline Block Copolymer with Close Crystallizable Temperatures. Macromolecules 2009;42:9515-9522. https://doi.org/10.1021/ma901964a
113. Müller AJ, Castillo RV, Hillmyer MA. Nucleation and Crystallization of PLDA-b-PE and PLLA-b-PE Diblock Copolymers. Macromol Symp 2006;242:174-181. https://doi.org/10.1002/masy.200651025
114. Castillo RV, Müller AJ, Lin MC, Chen HL, Jeng US, Hillmyer MA. Confined crystallization and morphology of melt segregated PLLA-b-PE and PLDA-b-PE diblock copolymers. Macromolecules 2008;41:6154-6164. https://doi.org/10.1021/ma800859y
115. Higa T, Nagakura H, Sakurai T, Nojima S. Crystal orientation of poly(ε-caprolactone) blocks confined in crystallized polyethylene lamellar morphology of poly(ε-caprolactone)-block-polyethylene copolymers. Polymer 2010;51:5576-5584. https://doi.org/10.1016/j.polymer.2010.09.039
116. Nojima S, Ito K, Ikeda H. Composition dependence of crystallized lamellar morphology formed in crystalline–crystalline diblock copolymers. Polymer 2007;48:3607-3611. https://doi.org/10.1016/j.polymer.2007.04.053
117. Lorenzo AT, Müller AJ, Priftis D, Pitsikalis M, Hadjichristidis N. Synthesis and morphological characterization of miktoarm star copolymers (PCL)2(PS)2 of poly(ε-caprolactone) and polystyrene. J Polym Sci Part A: Polym Chem 2007;45:5387-5397. https://doi.org/10.1002/pola.22283
118. Lorenzo AT, Müller AJ, Lin MC, Chen HL, Jeng US, Priftis D, Pitsikalis M, Hadjichristidis N. Influence of Macromolecular Architecture on the Crystallization of (PCL2)-b-(PS2) 4-Miktoarm Star Block Copolymers in Comparison to Linear PCL-b-PS Diblock Copolymer Analogues. Macromolecules 2009;42:8353-8364. https://doi.org/10.1021/ma901289t
119. Montoya Rojo UM, Riccardi CC, Ninago MD, Ciolino AE, Villar MA, Ceolín M, Zucchi IA, Schroeder WF. Photopolymerization-assisted self-assembly as a strategy to obtain a dispersion of very high aspect ratio nanostructures in a polystyrene matrix. Eur Polym J 2019;112:704-713. https://doi.org/10.1016/j.eurpolymj.2018.10.037
120. Nojima S, Toei M, Hara S, Tanimoto S, Sasaki S. Size dependence of crystallization within spherical microdomain structures. Polymer 2002;43:4087-4090. https://doi.org/10.1016/S0032-3861(02)00217-3
121. Müller AJ, Albuerne J, Marquez L, Raquez JM, Degée P, Dubois P, Hobbs J, Hamley IW. Self-nucleation and crystallization kinetics of double crystalline poly(p-dioxanone)-b-poly(epsilon-caprolactone) diblock copolymers. Faraday Discuss 2005;128:231-252. DOI: 10.1039/B403085K
122. Albuerne J, Márquez L, Müller AJ, Raquez JM, Degée P, Dubois P, Castelletto V, Hamley IW. Nucleation and Crystallization in Double Crystalline Poly(p-dioxanone)-b-poly(ε-caprolactone) Diblock Copolymers. Macromolecules 2003;36:1633-1644. https://doi.org/10.1021/ma025766t
123. Jeon O, Lee SH, Kim SH, Lee YM, Kim YH. Synthesis and characterization of poly(L-lactide)-poly(e-caprolactone) multiblock copolymers. Macromolecules 2003;36:5585-5592. https://doi.org/10.1021/ma034006v
124. He C, Sun J, Ma J, Chen X, Jing X. Composition Dependence of the Crystallization Behavior and Morphology of the Poly(ethylene oxide)-poly(ε-caprolactone) Diblock Copolymer. Biomacromolecules 2006;7:3482-3489. https://doi.org/10.1021/bm060578m
125. Castillo RV, Müller AJ, Raquez JM, Dubois P. Crystallization Kinetics and Morphology of Biodegradable Double Crystalline PLLA-b-PCL Diblock Copolymers. Macromolecules 2010;43:4149-4160. https://doi.org/10.1021/ma100201g
126. Hamley IW, Castelletto V, Castillo RV, Müller AJ, Martin CM, Pollet E, Dubois P. Crystallization in Poly(L-lactide)-b-poly(e-caprolactone) double crystalline diblock copolymers: a study using X-ray scattering, differential scanning calorimetry, and polarized optical microscopy. Macromolecules 2005;38:463-472. https://doi.org/10.1021/ma0481499

127. Sun J, Hong Z, Yang L, Tang Z, Chen X, Jing X. Study on crystalline morphology of poly(l-lactide)-poly(ethylene glycol) diblock copolymer. Polymer 2004;45:5969-5977. https://doi.org/10.1016/j.polymer.2004.06.026
128. Castillo RV, Arnal ML, Müller AJ, Hamley IW, Castelletto V, Schmalz H, Abetz V. Fractionated crystallization and fractionated melting of confined PEO microdomains in PB-b-PEO and PE-b-PEO diblock copolymers. Macromolecules 2008;41:879-889. https://doi.org/10.1021/ma0718907
129. Müller AJ, Balsamo V, Arnal ML, Jakob T, Schmalz H, Abetz V. Homogeneous nucleation and fractionated crystallization in block copolymers. Macromolecules 2002;35:3048-3058. https://doi.org/10.1021/ma012026w
130. Schmalz H, Müller AJ, Abetz V. Crystallization in ABC triblock copolymers with two different crystalline end blocks: influence of confinement on self-nucleation behavior. Macromol Chem Phys 2003;204:111-124. https://doi.org/10.1002/macp.200290063
131. Schmalz H, Knoll A, Müller AJ, Abetz V. Synthesis and characterization of ABC triblock copolymers with two different crystalline end blocks: influence of confinement on crystallization behavior and morphology. Macromolecules 2002;35:10004-10013. https://doi.org/10.1021/ma020983f
132. Arnal ML, Balsamo V, López-Carrasquero F, Contreras J, Carrillo M, Schmalz H, Abetz V, Laredo E, Müller AJ. Synthesis and Characterization of Polystyrene-b-poly(ethylene oxide)-b-poly(ε-caprolactone) Block Copolymers. Macromolecules 2001;34:7973-79982. https://doi.org/10.1021/ma011058g
133. Balsamo V, Von Gyldenfeldt F, Stadler R. Thermal behavior and spherulitic superstructures of SBC triblock copolymers based on polystyrene (S), polybutadiene (B) and a crystallizable poly(ε-caprolactone) (C) block. Macromol Chem Phys 1996;197:3317-3341. https://doi.org/10.1002/macp.1996.021971021
134. Schmalz H, Abetz V, Lange R. Thermoplastic elastomers based on semicrystalline block copolymers. Compos Sci Technol 2003;63:1179-1186. https://doi.org/10.1016/S0266-3538(03)00039-3
135. Wang H, Chen X, Pan CY. Synthesis and crystallization behaviors of poly(styrene-b-isoprene-b-ε-caprolactone) triblock copolymers. Eur Polym J 2007;43:1905-1915. https://doi.org/10.1016/j.eurpolymj.2007.01.044
136. Yu X, Yang H, Wu S, Geng Y, Han Y. Microphase Separation and Crystallization of All-Conjugated Phenylene–Thiophene Diblock Copolymers. Macromolecules 2012;45:266-274. https://doi.org/10.1021/ma201024z
137. Jin J, Du J, Xia Q, Liang Y, Han CC. Effect of Mesophase Separation on the Crystallization Behavior of Olefin Block Copolymers. Macromolecules 2010;43:10554-10559. https://doi.org/10.1021/ma102075c
138. Voet VSD, van Ekenstein G, Meereboer NL, Hofman AH, Brinke GT, Loos K. Double-crystalline PLLA-b-PVDF-b-PLLA triblock copolymers: preparation and crystallization. Polym Chem 2014;5:2219-2230. DOI: 10.1039/C3PY01560B
139. Meereboer NL, Terzic I, Saidi S, Merino DH, Loos K. Nanoconfinement-Induced beta-Phase Formation Inside Poly(vinylidene fluoride)-Based Block Copolymers. ACS Macro Lett 2018;7:863-867. https://doi.org/10.1021/acsmacrolett.8b00418
140. Terzic I, Meereboer NL, Acuautla M, Portale G, Loos K. Electroactive materials with tunable response based on block copolymer self-assembly. Nat Commun 2019;10,601/1-10. https://doi.org/10.1038/s41467-019-08436-2
141. Terzic I, Meereboer NL, Acuautla M, Portale G, Loos K. Tailored Self-Assembled Ferroelectric Polymer Nanostructures with Tunable Response. Macromolecules 2019;52:354-364. https://doi.org/10.1021/acs.macromol.8b02131
142. Lin Y, Zhang S, Ye L, Gu Y, Wang Y, Ma L, Tang T. Morphology and linear rheology of comb-like copolymer melts with high grafting density: Ⅱ Heterografted PVSt-g-(PS/PE) comb-like copolymer with short backbone and mixed side chains. Polymer 2018;137:222-230. https://doi.org/10.1016/j.polymer.2018.01.023
143. Xu JT, Liang GD, Fan ZQ. Polarized optical microscopy study on the superstructures of oxyethylene/oxybutylene block copolymers. Polymer 2004;45:6675-6680. https://doi.org/10.1016/j.polymer.2004.07.071
144. Hempel E, Budde H, Höring S, Beiner M. Side chain crystallization in microphase-separated poly(styrene-block-octadecylmethacrylate) copolymers. Thermochim Acta 2005;432:254-261. https://doi.org/10.1016/j.tca.2005.01.037
145. Brown RA, Masters AJ, Price C, Yuan CF. Chain segregation in block copolymers. In: Aggarwal S, editor. Comprehensive Polymer Science- The synthesis, characterizations, reaction & applications of polymers, London: Pergamon Press plc.;1989:155-197.

146. Hadjichristidis N, Pispas S, Floudas G. Block copolymers: Synthetic strategies, physical properties and applications. Hoboken, NJ: Wiley-Interscience; 2003. 409 pp.
147. Abetz V. Block Copolymers. In Mark HF, editor. Encyclopedia of polymer science and engineering, New York: John Wiley & Sons, Inc.;2001:212 pp.
148. Abetz V. Assemblies in complex block copolymer systems. In Ciferri A, editor. Supramolecular Polymers, New York: Marcel Dekker Inc.; 2000;215-390.
149. Hamley IW. The physics of block copolymers. London: Oxford University Press; 1998. 424 pp.
150. Rangarajan P, Register RA, Fetters LJ. Morphology of semicrystalline block copolymers of ethylene-(ethylene-alt-propylene). Macromolecules 1993;26:4640-4645. https://doi.org/10.1021/ma00069a034
151. Rangarajan P, Register RA, Adamson DH, Fetters LJ, Bras W, Naylor S, Ryan AJ. Dynamics of structure formation in crystallizable block copolymers. Macromolecules 1995;28:1422-1428. https://doi.org/10.1021/ma00109a013
152. Ryan AJ, Hamley IW, Bras W, Bates FS. Structure Development in Semicrystalline Diblock Copolymers Crystallizing from the Ordered Melt. Macromolecules 1995;28:3860-3868. https://doi.org/10.1021/ma00115a016
153. Richardson PH, Richards RW, Blundell DJ, MacDonald WA, Mills P. Differential scanning calorimetry and optical microscopy investigations of the isothermal crystallization of a poly(ethylene oxide)-poly(methyl methacrylate) block copolymer. Polymer 1995;36:3059-3069. https://doi.org/10.1016/0032-3861(95)97866-E
154. D'Ambrosio RM, Michell RM, Mincheva R, Hernández R, Mijangos C, Dubois P, Müller AJ. Crystallization and Stereocomplexation of PLA-mb-PBS Multi-Block Copolymers. Polymers 2017;10:8/1-18. https://doi.org/10.3390/polym10010008
155. Ho RM, Hsieh PY, Tseng WH, Lin CC, Huang BH, Lotz B. Crystallization-induced orientation for microstructures of poly(L-lactide)-b-poly(e-caprolactone) diblock copolymers. Macromolecules 2003;36:9085-9092. https://doi.org/10.1021/ma0347868
156. Michell RM, Müller AJ, Deshayes G; Dubois P. Effect of sequence distribution on the isothermal crystallization kinetics and successive self-nucleation and annealing (SSA) behavior of poly(ε-caprolactone-co-ε-caprolactam) copolymers. Eur Polym J 2010;46:1334-1344. https://doi.org/10.1016/j.eurpolymj.2010.03.013
157. Takeshita H, Fukumoto K, Ohnishi T, Ohkubo T, Miya M, Takenaka K, Shiomi T. Formation of lamellar structure by competition in crystallization of both components for crystalline–crystalline block copolymers. Polymer 2006;47:8210-8218. https://doi.org/10.1016/j.polymer.2006.09.043
158. Yang J, Liang Y, Luo J, Zhao C, Han CC. Multilength Scale Studies of the Confined Crystallization in Poly(l-lactide)-block-Poly(ethylene glycol) Copolymer. Macromolecules 2012;45:4254-4261. https://doi.org/10.1021/ma202505f
159. Yang J, Zhao T, Cui J, Liu L, Zhou Y, Li G, Zhou E, Chen X. Nonisothermal crystallization behavior of the poly(ethylene glycol) block in poly(L-lactide)–poly(ethylene glycol) diblock copolymers: Effect of the poly(L-lactide) block length. J Polym Sci Part B: Polym Phys 2006;44:3215-3226. https://doi.org/10.1002/polb.20886
160. Douzinas KC, Cohen RE, Halasa AF. Evaluation of domain spacing scaling laws for semicrystalline diblock copolymers. Macromolecules 1991;24:4457-4459. https://doi.org/10.1021/ma00015a033
161. Hamley IW, Fairclough JPA, Terrill NJ, Ryan AJ, Lipic PM, Bates FS, Towns-Andrews E. Crystallization in oriented semycristalline diblock copolymers. Macromolecules 1996;29:8835-8843. https://doi.org/10.1021/ma960343a
162. Rangarajan P, Register RA, Fetters LJ, Bras W, Naylor S, Ryan AJ. Crystallization of a weakly segregated polyolefin diblock copolymer. Macromolecules 1995;28:4932-4938. https://doi.org/10.1021/ma00118a022
163. Nojima S, Kato K, Yamamoto S, Ashida T. Crystallization of block copolymers. 1. Small-angle x-ray scattering study of a e-caprolactone-butadiene diblock copolymer. Macromolecules 1992;25:2237-2242. https://doi.org/10.1021/ma00034a027
164. Rohadi A, Endo R, Tanimoto S, Sasaki S, Nojima S. Effects of molecular weight and crystallization temperature on the morphology formation in asymmetric diblock copolymers with a highly crystalline block. Polym J 2000;32:602-609. https://doi.org/10.1295/polymj.32.602
165. Rohadi A, Tanimoto S, Sasaki S, Nojima S. Morphological Difference between Solution-Cast and Melt-Quenched Crystalline-Amorphous Diblock Copolymers. Polym J 2000;32:859-865. https://doi.org/10.1295/polymj.32.859
166. Ryan AJ, Fairclough JPA, Hamley IW, Mai SM, Booth C. Chain folding in crystallizable block copolymers. Macromolecules 1997;30:1723-1727. https://doi.org/10.1021/ma960943+

167. Hamley IW, Parras P, Castelletto V, Castillo RV, Müller AJ, Pollet E, Dubois P, Martin CM. Melt Structure and its Transformation by Sequential Crystallization of the Two Blocks within Poly(L-lactide)-block-Poly(ε-caprolactone) Double Crystalline Diblock Copolymers. Macromol Chem Phys 2006;207:941-953. https://doi.org/10.1002/macp.200600085
168. Huang M, Dong X, Wang L, Zheng L, Liu G, Gao X, Li C, Müller AJ, Wang D. Reversible Lamellar Periodic Structures Induced by Sequential Crystallization/Melting in PBS-co-PCL Multiblock Copolymer. Macromolecules 2018;51:1100-1109. https://doi.org/10.1021/acs.macromol.7b01779
169. Laredo E, Prutsky N, Bello A, Grimau M, Castillo RV, Müller AJ, Dubois P. Miscibility in poly(L-lactide)-b-poly(epsilon-caprolactone) double crystalline diblock copolymers. Eur Phys J E Soft Matter Biol Phys 2007;23:295-303. https://doi.org/10.1140/epje/i2007-10191-6
170. Moon HC, Bae D, Kim JK. Self-Assembly of Poly(3-dodecylthiophene)-block-poly(methyl methacrylate) Copolymers Driven by Competition between Microphase Separation and Crystallization. Macromolecules 2012,45:5201-5207. https://doi.org/10.1021/ma300902n
171. Müller AJ, Albuerne J, Esteves LM, Marquez L, Raquez JM, Degée P, Dubois P, Collins S, Hamley IW. Confinement Effects on the Crystallization Kinetics and Self-Nucleation of Double Crystalline Poly(p-dioxanone)-b-poly(ε-caprolactone) Diblock Copolymers. Macromol Symp 2004;215:369-382. https://doi.org/10.1002/masy.200451128
172. Coote JP, Kim JS, Lee B, Han J, Kim BJ, Stein GE. Crystallization Modes of Poly(3-dodecylthiophene)-Based Block Copolymers Depend on Regioregularity and Morphology. Macromolecules 2018;51:9276-9283. https://doi.org/10.1021/acs.macromol.8b01985
173. Lin MC, Chen HL, Su WB, Su CJ, Jeng US, Tzeng FY, Wu JY, Tsai JC, Hashimoto T. Interactive Crystallization Kinetics in Double-Crystalline Block Copolymer. Macromolecules 2012;45:5114-5127. https://doi.org/10.1021/ma300711k
174. Burns AB, Register RA. Large, Reversible, and Coherent Domain Spacing Dilation Driven by Crystallization under Soft Lamellar Confinement. Macromolecules 2017;50:8106-8116. https://doi.org/10.1021/acs.macromol.7b01632
175. Chen D. Crystal behavior of semicrystalline polystyrene-block-poly(l-lactide) diblock copolymer in thin films with various structures. Polym Int 2013;62:1343-1350. https://doi.org/10.1002/pi.4426
176. Davidson EC, Segalman RA. Thermal Control of Confined Crystallization within P3EHT Block Copolymer Microdomains. Macromolecules 2017;50:8097-8105. https://doi.org/10.1021/acs.macromol.7b01616
177. Davidson EC, Segalman RA. Confined Crystallization within Cylindrical P3EHT Block Copolymer Microdomains. Macromolecules 2017;50:6128-6136. https://doi.org/10.1021/acs.macromol.7b01323
178. Hood MA, Wang B, Sands JM, La Scala JJ, Beyer FL, Li CY. Morphology control of segmented polyurethanes by crystallization of hard and soft segments. Polymer 2010;51:2191-2198. https://doi.org/10.1016/j.polymer.2010.03.027
179. Liang GD, Xu JT, Fan ZQ. Crystallization and melting behaviors of polystyrene-b-poly(ethylene-co-butene) block copolymers. Eur Polym J 2007;43:3153-3162. https://doi.org/10.1016/j.eurpolymj.2007.05.028
180. Lin MC, Wang YC, Chen HL, Müller AJ, Su CJ, Seng US. Critical analyzis of the crystal orientation behavior in polyethylene-based crystalline-amorphous diblock copolymer. J Phys Chem B 2011;115:2494-502. https://doi.org/10.1021/jp1103565
181. Müller AJ, Lorenzo AT, Castillo RV, Arnal ML, Boschetti de Fierro A, Abetz V. Crystallization Kinetics of Homogeneous and Melt Segregated PE Containing Diblock Copolymers. Macromol Symp 2006;245-246:154-160. https://doi.org/10.1002/masy.200651321
182. Vasilev C, Heinzelmann H, Reiter G. Controlled melting of individual, nano-meter-sized, polymer crystals confined in a block copolymer mesostructure. J Polym Sci Part B: Polym Phys 2004;42:1312-1320. https://doi.org/10.1002/polb.20002
183. Vasilev C, Reiter G, Pispas S, Hadjichristidis N. Crystallization of block copolymers in restricted cylindrical geometries. Polymer 2006;47:330-340. https://doi.org/10.1016/j.polymer.2005.11.040
184. Zhu L, Mimnaugh BR, Ge Q, Quirk RP, Cheng SZD, Thomas EL, Lotz B, Hsiao BS, Yeh F, Liu L. Hard and soft confinement effects on polymer crystallization in microphase separated cylinder-forming PEO-b-PS/PS blends. Polymer 2001;42:9121-9131. https://doi.org/10.1016/S0032-3861(01)00394-9
185. Floudas G, Tsitsilianis C. Crystallization Kinetics of Poly(ethylene oxide) in Poly(ethylene oxide)−Polystyrene−Poly(ethylene oxide) Triblock Copolymers. Macromolecules 1997,30:4381-4390. https://doi.org/10.1021/ma9616118

186. Gervais M, Gallot B. Use of freeze-fracture electron microscopy to study the refolding of crystallized chains in block copolymers. Polymer 1981;22:1129-1133. https://doi.org/10.1016/0032-3861(81)90304-9
187. Lotz B, Kovacs, AJ. Phase transitions in block-copolymers of polystyrene and poly(ethylene oxide). Polym Preprints (Am Chem Soc, Div Polym Chem), 1969;10: 820-825.
188. O´Malley JJ. Morphology of crystalline multiblock copolymers. J Polym Sci, Polym Symp 1977;60:151-160.
189. Zhu L, Chen Y, Zhang A, Calhoun BH, Chun M, Quirk RP, Cheng SZD, Hsiao BS, Yeh F, Hashimoto T. Phase structures and morphologies determined by competitions among self-organization, crystallization, and vitrification in a disordered poly(ethylene oxide)-b-polystyrene diblock copolymer. Phys Rev B 1999;60:10022/1-10. https://doi.org/10.1103/PhysRevB.60.10022
190. Zhu L, Cheng SZD, Calhoun BH, Ge Q, Quirk RP, Thomas EL, Hsiao BS, Yeh F, Lotz B. Phase structures and morphologies determined by self-organization, vitrification, and crystallization: confined crystallization in an ordered lamellar phase of PEO-b-PS diblock copolymer. Polymer 2001;42:5829-5839. https://doi.org/10.1016/S0032-3861(00)00902-2
191. Zhu L, Cheng SZD, Huang P, Ge Q, Quirk RP, Thomas EL, Lotz B, Hsiao BS, Yeh F, Liu L. Nanoconfined Polymer Crystallization in the Hexagonally Perforated Layers of a Self- Assembled PS-b- PEO Diblock Copolymer. Adv Mater 2002;14:31-34. https://doi.org/10.1002/1521-4095(20020104)14:1<31::AID-ADMA31>3.0.CO;2-3
192. Zhu L, Huang P, Chen WY, Ge Q, Quirk RP, Cheng SZD, Thomas EL, Lotz B, Hsiao BS, Yeh F, Liu L. Nanotailored Crystalline Morphology in Hexagonally Perforated Layers of a Self-Assembled PS-b-PEO Diblock Copolymer. Macromolecules 2002;35:3553-3562. https://doi.org/10.1021/ma012184n
193. Xu JT, Yuan JJ, Cheng SY. SAXS/WAXS/DSC studies on crystallization of a polystyrene-b-poly(ethylene oxide)-b-polystyrene triblock copolymer with lamellar morphology and low glass transition temperature. Eur Polym J 2003;39:2091-2098. https://doi.org/10.1016/S0014-3057(03)00155-1
194. Weimann PA, Hajduk DA, Chu C, Chaffin KA, Brodil JC, Bates FS. Crystallization of tethered polyethylene in confined geometries. J Polym Sci Part B: Polym Phys 1999;37:2053-2068. https://doi.org/10.1002/(SICI)1099-0488(19990815)37:16<2053::AID-POLB9>3.0.CO;2-L
195. Nakagawa S, Kadena K, Ishizone T, Nojima S, Shimizu T, Yamaguchi K, Nakahama S. Crystallization Behavior and Crystal Orientation of Poly(ε-caprolactone) Homopolymers Confined in Nanocylinders: Effects of Nanocylinder Dimension. Macromolecules 2012;45:1892-1900. https://doi.org/10.1021/ma202566f
196. Nakagawa S, Tanaka T, Ishizone T, Nojima S, Kakiuchi Y, Yamaguchi K, Nakahama S. Crystallization Behavior of Poly(ε-caprolactone) Chains Confined in Nanocylinders: Effects of Block Chains Tethered to Nanocylinder Interfaces. Macromolecules 2013;46:2199-2205. https://doi.org/10.1021/ma400071f
197. Kawazu K, Nakagawa S, Ishizone T, Nojima S, Arai D, Yamaguchi K, Nakahama S. Effects of Bulky End-Groups on the Crystallization Kinetics of Poly(ε-caprolactone) Homopolymers Confined in a Cylindrical Nanodomain. Macromolecules 2017;50:7202-7210. https://doi.org/10.1021/acs.macromol.7b01536
198. Nakagawa S, Yoneguchi Y, Ishizone T, Nojima S, Yamaguchi K, Nakahama S. Crystal orientation of poly(ε-caprolactone) chains confined in lamellar nanodomains: Effects of chain-ends tethering to nanodomain interfaces. Polymer 2017;112:116-124. https://doi.org/10.1016/j.polymer.2017.01.075
199. Yoneguchi Y, Kikuchi H, Nakagawa S, Marubayashi H, Ishizone T, Nojima S, Yamaguchi K. Combined effects of confinement size and chain-end tethering on the crystallization of poly(ε-caprolactone) chains in nanolamellae. Polymer 2019;160:73-81. https://doi.org/10.1016/j.polymer.2018.11.030
200. Ho RM, Lin FH, Tsai CC, Lin CC, Ko BT, Hsiao BS, Sics I. Crystallization-induced undulated morphology in polystyrene-b-poly(L-lactide) block copolymer. Macromolecules 2004;37:5985-5994. https://doi.org/10.1021/ma0492869
201. Huang L, Kiyofuji G, Matsumoto J, Fukagawa Y, Gong C, Nojima S. Isothermal crystallization of poly(β-propiolactone) blocks starting from lamellar microdomain structures of double crystalline poly(β-propiolactone)-block-polyethylene copolymers. Polymer 2012;53:5856-5863. https://doi.org/10.1016/j.polymer.2012.10.013
202. Kikuchi H, Watanabe T, Marubayashi H, Ishizone T, Nojima S, Yamaguchi K. Control of crystal orientation of spatially confined PCL homopolymers by cleaving chain-ends of PCL blocks tethered to

nanolamella interfaces. Polymer 2019;181:121786/1-10. https://doi.org/10.1016/j.polymer.2019.121786
203. Li MC, Chang GW, Lin T, Ho RM, Chuang WT, Kool S. Birefringence control of semicrystalline block copolymers by crystallization under confinement. Langmuir 2010;26:17640-8. https://doi.org/10.1021/la1034432
204. Loo YL, Register RA, Adamson DH, Polyethylene crystal orientation induced by block copolymer cylinders. Macromolecules 2000;33:8361-8366. https://doi.org/10.1021/ma000962q
205. Nojima S, Akutsu Y, Akaba M, Tanimoto S. Crystallization behavior of poly(ε-caprolactone) blocks starting from polyethylene lamellar morphology in poly(ε-caprolactone)-block-polyethylene copolymers. Polymer 2005;46:4060-4067. https://doi.org/10.1016/j.polymer.2005.02.075
206. Nojima S, Higaki Y, Ishige R Kabayama H, Ohta N, Masunaga H, Hirai T, Kojio K, Takahara A. Crystallization-induced structure fluctuation of crystallized microdomain structure composed of strongly segregated crystalline-crystalline diblock copolymers. Polymer 2016;102:256-265. https://doi.org/10.1016/j.polymer.2016.09.024
207. Nojima S, Higaki Y, Kaetsu K, Ishige R, Ohta N, Masunaga H, Hirai T, Kojio K, Takahara A. Effect of molecular mobility of pre-ordered phase on crystallization in microphase-separated lamellar morphology of strongly segregated crystalline-crystalline diblock copolymers. Polymer 2017;116:403-411. https://doi.org/10.1016/j.polymer.2017.02.086
208. Nojima S, Inokawa D, Kawamura T, Nitta K. Dynamic Mechanical Study of Block Copolymer Crystallization Confined within Spherical Nanodomains. Polym J 2008;40:986-991. https://doi.org/10.1295/polymj.PJ2008139
209. Nojima S, Kiji T, Ohguma Y, Characteristic melting behavior of double crystalline poly(ε-caprolactone)-block-polyethylene copolymers. Macromolecules 2007;40:7566-7572. https://doi.org/10.1021/ma0627830
210. Nojima S, Ohguma Y, Kadena K, Ishizone T, Iwasaki Y, Yamaguchi K. Crystal Orientation of Poly(ε-caprolactone) Homopolymers Confined in Cylindrical Nanodomains. Macromolecules 2010;43:3916-3923. https://doi.org/10.1021/ma100236u
211. Nojima S, Ohguma Y, Namiki S, Ishizone T, Yamaguchi K. Crystallization of homopolymers confined in spherical or cylindrical nanodomains. Macromolecules 2008;41:1915-1918. DOI 10.1021/ma7027903
212. Sakurai T, Nagakura H, Gondo S, Nojima S. Crystallization of poly(ε-caprolactone) blocks confined in crystallized lamellar morphology of poly(ε-caprolactone)-block-polyethylene copolymers: effects of polyethylene crystallinity and confinement size. Polym J 2012;45:436-443. https://doi.org/10.1038/pj.2012.164
213. Sakurai T, Nojima S. Significant increase in the melting temperature of poly(ε-caprolactone) blocks confined in the crystallized lamellar morphology of poly(ε-caprolactone)-block-polyethylene copolymers. Polym J 2011;43:370-377. https://doi.org/10.1038/pj.2011.4
214. Sun L, Liu Y, Zhu L, Hsiao BS, Avila-Orta CA. Self-assembly and crystallization behavior of a double-crystalline polyethylene-block-poly(ethylene oxide) diblock copolymer. Polymer 2004;45:8181-8193. https://doi.org/10.1016/j.polymer.2004.09.063
215. Sun L, Zhu L, Ge Q, Quirk RP, Xue C, Cheng SZD, Hsuai BS, Avila-Orta CA, Sics I, Cantino ME. Comparison of crystallization kinetics in various nanoconfined geometries. Polymer 2004;45:2931-2939. https://doi.org/10.1016/j.polymer.2004.02.068
216. Sun YS, Chung TM, Li YJ, Ho RM, Ko BT, Jeng US, Lotz B. Crystalline Polymers in nanoscale 1D spatial confinement. Macromolecules 2006;39:5782-5788. https://doi.org/10.1021/ma0608121
217. Boschetti-de-Fierro A, Lorenzo AT, Müller AJ, Schmalz H, Abetz V. Crystallization Kinetics of PEO and PE in Different Triblock Terpolymers: Effect of Microdomain Geometry and Confinement. Macromol Chem Phys 2008;209:476-487. https://doi.org/10.1002/macp.200700434
218. Michell RM, Lorenzo AT, Müller AJ, Lin MC, Chen HL, Blaszczyk-Lezak I, Martín J, Mijangos C. The Crystallization of Confined Polymers and Block Copolymers Infiltrated Within Alumina Nanotube Templates. Macromolecules 2012;45:1517-1528. https://doi.org/10.1021/ma202327f
219. Carvalho J, Dalnoki-Veress K, Surface nucleation in the crystallisation of polyethylene droplets. Eur Phys J E: Soft Matter Biol Phys 2011;34:6/1-6. https://doi.org/10.1140/epje/i2011-11006-y
220. Müller AJ, Arnal ML, Thermal fractionation of polymers. Prog Polym Sci 2005;30:559-603. https://doi.org/10.1016/j.progpolymsci.2005.03.001
221. Müller AJ, Hernández, ZH, Arnal ML, Sánchez JJ. Successive self-nucleation/annealing (SSA): A novel technique to study molecular segregation during crystallization. Polym Bull 1997;39:465-472. https://doi.org/10.1007/s002890050174

222. Arnal ML, Balsamo V, Ronca G, Sánchez A, Müller A, Cañizales E, Urbina de Navarro C. Applications of Successive Self-Nucleation and Annealing (SSA) to Polymer Characterization. J Therm Anal Calorim 2000;59:451-470. https://doi.org/10.1023/a:1010137408023
223. Müller AJ, Michell RM, Pérez RA, Lorenzo AT. Successive Self-nucleation and Annealing (SSA): Correct design of thermal protocol and applications. Eur Polym J 2015;65:132-154. https://doi.org/10.1016/j.eurpolymj.2015.01.015
224. Arnal ML, López-Carrasquero F, Laredo E, Müller AJ. Coincident or sequential crystallization of PCL and PEO blocks within polystyrene-b-poly(ethylene oxide)-b-poly(ε-caprolactone) linear triblock copolymers. Eur Polym J 2004;40:1461-1476. https://doi.org/10.1016/j.eurpolymj.2004.02.023
225. Müller AJ, Arnal ML, López-Carrasquero F. Nucleation and crystallization of PS-b-PEO-b-PCL triblock copolymers. Macromol Symp 2002;183:199-204. https://doi.org/10.1002/1521-3900(200207)183:1<199::AID-MASY199>3.0.CO;2-S
226. Chen S, Wang L, Confined crystallization kinetics and scale of semicrystalline block copolymer via non-isothermal method. J Therm Anal Calorim 2016;127:2341-2351. DOI 10.1007/s10973-016-5761-7
227. Ding S, Fang C, Wang X, Wang Z. Crystallization-driven microstructure changes during microphase separation for environment-friendly thermoplastic triblock copolymer elastomers. Polymer, 2020;186:121993/1-11. https://doi.org/10.1016/j.polymer.2019.121993
228. Feng CS, Chen Y, Shao J, Li G, Hou HQ. The Crystallization and Melting Behaviors of PDLA-b-PBS-b-PDLA Triblock Copolymers. Chin J Polym Sci 2019;38:298-310. https://doi.org/10.1007/s10118-020-2361-6
229. Gitsas A, Floudas G, Butt HJ, Pakula T, Matyjaszewski K. Effects of Nanoscale Confinement and Pressure on the Dynamics of pODMA-b-ptBA-b-pODMA Triblock Copolymers. Macromolecules 2010;43:2453-2462. https://doi.org/10.1021/ma902639g
230. Hu X, Xu JZ, Zhing GJ, Luo XL, Li ZM. Shear induced crystallization of poly(L-lactide) and poly(ethylene glycol) (PLLA-PEG-PLLA) copolymers with different block length. J Polym Res 2010;18:675-680. https://doi.org/10.1007/s10965-010-9463-8
231. Nagarajan S, Gowd EB. *Cold* Crystallization of PDMS and PLLA in Poly(l-lactide-b-dimethylsiloxane-b-l-lactide) Triblock Copolymer and Their Effect on Nanostructure Morphology. Macromolecules 2015;48:5367-5377. https://doi.org/10.1021/acs.macromol.5b01179
232. Qian J, Ding L, Zhu G, Wu X, Li W, Zhao C, Mu J. Synthesis and self-assembly of PMMA-b-(u)PE-b-PMMA copolymers: study the aggregate morphology in toluene vapor. J Polym Res 2019;26:148/1-10. https://doi.org/10.1007/s10965-019-1808-3
233. Petreska SG, Auschra C, Paulis M. Confinement driven crystallization of ABA crystalline-soft-crystalline block copolymers synthesized via RAFT mediated miniemulsion polymerization. Polymer 2018;158:327-337. https://doi.org/10.1016/j.polymer.2018.10.073
234. Terzic I, Meereboer NL, Loos K, CuAAC click chemistry: a versatile approach towards PVDF-based block copolymers. Polym Chem 2018;9:3714-3720. https://doi.org/10.1039/C8PY00742J
235. Yu PQ, Xie XM, Wang Z, Li HS, Bates FS. Control of the confined and unconfined crystallization in glassy-crystalline poly(vinylcyclohexane)-b-poly(ethylene)-b-poly-(vinylcyclohexane) triblock copolymer in solution. Polymer 2006;47:1460-1464. https://doi.org/10.1016/j.polymer.2005.12.059
236. Balsamo V, Paolini Y, Ronca G, Müller AJ. Crystallization of the polyethylene block in polystyrene-b-polyethylene-b-polycaprolactone triblock copolymers, 1 Self-nucleation behavior. Macromol Chem Phys 2000;201:2711-2720. https://doi.org/10.1002/1521-3935(20001201)201:18<2711::AID-MACP2711>3.0.CO;2-6
237. Beckingham BS, Register RA. Architecture-Induced Microphase Separation in Nonfrustrated A–B–C Triblock Copolymers. Macromolecules 2013;46:3486-3496. https://doi.org/10.1021/ma400397h
238. Ge H, Zhang F, Huang H, He T. Interplay between Stereocomplexation and Microphase Separation in PS-b-PLLA-b-PDLA Triblock Copolymers. Macromolecules 2019;52:1004-1012. https://doi.org/10.1021/acs.macromol.8b02627
239. Palacios JK,Tercjak A, Liu G, Wang D, Zhao J, Hadjichristidis N, Müller AJ. Trilayered Morphology of an ABC Triple Crystalline Triblock Terpolymer. Macromolecules 2017;50:7268-7281. https://doi.org/10.1021/acs.macromol.7b01576
240. Kim JK, Park DJ, Lee MS, Ihn KJ. Synthesis and crystallization behavior of poly(L-lactide)-block-poly(e-caprolactone) copolymer. Polymer 2001;42:7429-7441. https://doi.org/10.1016/S0032-3861(01)00217-8
241. Wang L, Feng C, Shao J, Li G, Hou H. The crystallization behavior of poly(ethylene glycol) and poly(l- lactide) block copolymer: Effects of block length of poly(ethylene glycol) and poly(l - lactide). Polym Crystallization 2019;2:e10071/1-9. https://doi.org/10.1002/pcr2.10071

242. Sun L, Shen LJ, Zhu MQ, Dong CM, Wei Y. Synthesis, self-assembly, drug-release behavior, and cytotoxicity of triblock and pentablock copolymers composed of poly(ε-caprolactone), poly(L-lactide), and poly(ethylene glycol). J Polym Sci Part A: Polym Chem 2010;48:4583-4593. https://doi.org/10.1002/pola.24255
243. Chiang YW, Hu YY, Li JN, Huang SH, Kuo SW. Trilayered Single Crystals with Epitaxial Growth in Poly(ethylene oxide)-block-poly(ε-caprolactone)-block-poly(l-lactide) Thin Films. Macromolecules 2015;48:8526-8533. https://doi.org/10.1021/acs.macromol.5b02042
244. Palacios JK, Zhao J, Hadjichristidis N, Müller AJ. How the Complex Interplay between Different Blocks Determines the Isothermal Crystallization Kinetics of Triple-Crystalline PEO-b-PCL-b-PLLA Triblock Terpolymers. Macromolecules 2017;50:9683-9695. https://doi.org/10.1021/acs.macromol.7b02148
245. Palacios JK, Mugica A, Zubitur M, Iturrospe A, Arbe A, Liu G, Wang D, Zhao J, Hadjichristidis N, Müller AJ. Sequential crystallization and morphology of triple crystalline biodegradable PEO-b-PCL-b-PLLA triblock terpolymers. RSC Adv 2016;6:4739-4750. DOI 10.1039/C5RA25812J.
246. Brogly M, Bistac S, Delaite C, Alzina C. Influence of semi‐crystalline poly(ε‐caprolactone) and non‐crystalline polylactide blocks on the thermal properties of polydimethylsiloxane‐based block copolymers. Polym Int 2020;69,1105-1112. https://doi.org/10.1002/pi.5964
247. Floudas G, Reiter G, Lambert O, Dumas P. Structure and Dynamics of Structure Formation in Model Triarm Star Block Copolymers of Polystyrene, Poly(ethylene oxide), and Poly(e-caprolactone). Macromolecules 1998;31:7279-7290. https://doi.org/10.1021/ma9806716
248. Müller AJ, Lorenzo AT, Hirao A. Crystallization behavior of polyethylene/polystyrene AmBn miktoarm star copolymers. Polym Adv Technol 2014;25:1257-1263. https://doi.org/10.1002/pat.3308
249. Xiang S, Zhou DD, Feng LD, Bian XC, Li G, Chen XS, Wang TC. Influence of Chain Architectures on Crystallization Behaviors of PLLA Block in PEG/PLLA Block Copolymers. Chin J Polym Sci 2018;37:258-267. https://doi.org/10.1007/s10118-019-2202-7
250. Guan F, Yang L, Wang J, Guan B, Han K, Wang Q, Zhu L. Confined Ferroelectric Properties in Poly(Vinylidene Fluoride-co-Chlorotrifluoroethylene)-graft-Polystyrene Graft Copolymers for Electric Energy Storage Applications. Adv Funct Mater 2011;21:3176-3188. https://doi.org/10.1002/adfm.201002015
251. Macko T, Schulze U, Brüll R, Albrecht A, Pasch H, Fónagy T, Häussler L, Iván B. Monitoring the Chemical Heterogeneity and the Crystallization Behavior of PP-g-PS Graft Copolymers Using SEC-FTIR and CRYSTAF. Macromol Chem Phys 2008;209:404-409. https://doi.org/10.1002/macp.200700398
252. Zhou C, Wei Z, Jin C, Wang Y, Yu Y, Leng X, Li Y. Fully biobased thermoplastic elastomers: Synthesis of highly branched linear comb poly(β-myrcene)-graft-poly(l-lactide) copolymers with tunable mechanical properties. Polymer 2018;138:57-64. https://doi.org/10.1016/j.polymer.2018.01.045
253. Cai J, Li C, Kong N, Lu Y, Lin G, Wang X, Yao Y, Manners I, Qiu H. Tailored multifunctional micellar brushes via crystallization-driven growth from a surface. Science 2019;366:1095-1098. DOI: 10.1126/science.aax9075
254. Kripotou S, Psylla C, Kyriakos K, Raftopoulos KN, Zhao J, Zhang G, Pispas S, Papadakis CM, Kyritsis A. Structure and Crystallization Behavior of Poly(ethylene oxide) (PEO) Chains in Core–Shell Brush Copolymers with Poly(propylene oxide)-block-poly(ethylene oxide) Side Chains. Macromolecules 2016;49:5963-5977. https://doi.org/10.1021/acs.macromol.6b00879
255. Xia N, Zhang G, Li T, Wang W, Zhu H, Chen Y, Deng G. Dynamically confined crystallization in a soft lamellar space constituted by alternating polymer co-brushes. Polymer 2011;52:4581-4589. https://doi.org/10.1016/j.polymer.2011.08.004
256. Johnson MA, Iyer J, Hammond PT, Microphase Segregation of PEO-PAMAM Linear-Dendritic Diblock Copolymers. Macromolecules 2004;37:2490-2501. https://doi.org/10.1021/ma030450m
257. Hofman AH, ten Brinke G, Loos K. Asymmetric supramolecular double-comb diblock copolymers: From plasticization, to confined crystallization, to breakout. Polymer 2017;121:312-319. https://doi.org/10.1016/j.polymer.2017.05.057
258. Elmahdy MM, Gournis D, Ladavos A, Spanos C, Floudas G. H-Shaped Copolymer of Polyethylene and Poly(ethylene oxide) under Severe Confinement: Phase State and Dynamics. Langmuir, 2020;36:4261-4271. https://doi.org/10.1021/acs.langmuir.0c00127
259. Pitet LM, Chamberlain BM, Hauser AW, Hillmyer MA. Dispersity and architecture driven self-assembly and confined crystallization of symmetric branched block copolymers. Polym. Chem. 2019;10:5385-5395. DOI 10.1039/C9PY01173K

260. Masuda H, Fukuda K. Ordered metal nanohole arrays made by a two-step replication of honeycomb structures of anodic alumina. Science 1995;268;1466-1468. DOI 10.1126/science.268.5216.1466
261. Michell RM, Blaszczyk-Lezak I, Mijangos C, Muller AJ. Confined Crystallization of Polymers within Anodic Aluminum Oxide Templates. J. Polym. Sci. Part B: Polym. Phys. 2014;52:1179-1194. DOI: 10.1002/polb.23553.
262. Samanta P, Liu CL, Nandan B, Chen HL. Crystallization of Polymers in Confined Space. In: Thomas S, Arif MP, Gowd EB, Kalarikkal N. Crystallization in multiphase polymer systems, Amsterdam: Elsevier; 2018,367-431. https://doi.org/10.1016/B978-0-12-809453-2.00013-X
263. Wu H, Higaki Y, Takahara A. Molecular self-assembly of one-dimensional polymer nanostructures in nanopores of anodic alumina oxide templates. Prog. Polym. Sci. 2018;77:95-117. https://doi.org/10.1016/j.progpolymsci.2017.10.004
264. Liu G, Shi G, Wang D. Research Progress on Polymer Crystallization Confined within Nano-porous AAO Templates. Acta Polym Sin 2020;51:501-516. DOI: 10.11777/j.issn1000-3304.2020.20003.
265. Sanz B, Blaszczyk-Lezak I, Mijangos C, Palacios JK, Müller AJ. New Double-Infiltration Methodology to Prepare PCL–PS Core–Shell Nanocylinders Inside Anodic Aluminum Oxide Templates. Langmuir 2016;32:7860-7865. DOI: 10.1021/acs.langmuir.6b01258.
266. Woo E, Huh J, Jeong YG, Shin K. From Homogeneous to Heterogeneous Nucleation of Chain Molecules under Nanoscopic Cylindrical Confinement. Phys Rev Lett 2007;98:136103/1-4. https://doi.org/10.1103/PhysRevLett.98.136103
267. Wu H, Wang W, Huang Y, Wang C, Su, Z. Polymorphic Behavior of Syndiotactic Polystyrene Crystallized in Cylindrical Nanopores. Macromolecules 2008;41:7755-7758. DOI: 10.1021/ma801498b.
268. Duran H, Steinhart M, Butt HJ, Floudas G. From Heterogeneous to Homogeneous Nucleation of Isotactic Poly(propylene) Confined to Nanoporous Alumina. Nano Lett. 2011;11:1671-1675. DOI: 10.1021/nl200153c.
269. Reid DK, Ehlinger BA, Shao L, Lutkenhaus JL. Crystallization and orientation of isotactic poly(propylene) in cylindrical nanopores. J. Polym. Sci. Part B: Polym. Phys. 2014;52:1412-1419. DOI: 10.1002/polb.23577.
270. Crystallization, Orientation, and Solid–Solid Crystal Transition of Polybutene-1 Confined within Nanoporous Alumina. Shi G, Wang Z, Wang M, Liu G, Cavallo D, Müller AJ, Wang D. Macromolecules 2020;53:6510-6518. https://doi.org/10.1021/acs.macromol.0c01384
271. Suzuki Y, Duran H, Akram W, Steinhart M, Floudas G, Butt HJ. Multiple nucleation events and local dynamics of poly(epsilon-caprolactone) (PCL) confined to nanoporous alumina. Soft Matter 2013;9:9189-9198. DOI: 10.1039/c3sm50907a.
272. Suzuki Y, Duran H, Steinhart M, Butt HJ, Floudas G. Homogeneous crystallization and local dynamics of poly(ethylene oxide) (PEO) confined to nanoporous alumina. Soft Matter 2013;9:2621-2628. DOI: 10.1039/c2sm27618f.
273. Liu CL, Chen HL. Crystal orientation of PEO confined within the nanorod templated by AAO nanochannels. Soft Matter 2018;14:5461-5468. DOI: 10.1039/C8SM00795K.
274. Dai X, Niu J, Ren Z, Sun X, Yan S. Effects of Nanoporous Anodic Alumina Oxide on the Crystallization and Melting Behavior of Poly(vinylidene fluoride). J. Polym. Sci. Part B: Polym. Phys 2016;120:843-850. DOI: 10.1021/acs.jpcb.5b11178.
275. Suzuki Y, Duran H, Steinhart M, Butt HJ, Floudas G. Suppression of Poly(ethylene oxide) Crystallization in Diblock Copolymers of Poly(ethylene oxide)-b-poly(epsilon-caprolactone) Confined to Nanoporous Alumina. Macromolecules 2014;47:1793-1800. DOI: 10.1021/ma4026477.
276. Effect of Nanoconfinement on the Isodimorphic Crystallization of Poly(butylene succinate-*ran*-caprolactone) Random Copolymers. Safari M, Leon Boigues L, Shi G, Maiz J, Liu G, Wang D, Mijangos C, Müller AJ. Macromolecules 2020;53,6486-6497. https://doi.org/10.1021/acs.macromol.0c01081
277. Maiz J, Martin J, Mijangos C. Confinement Effects on the Crystallization of Poly(ethylene oxide) Nanotubes. Langmuir 2012;28:12296-12303. DOI: 10.1021/la302675k.
278. Guan Y, Liu G, Gao P, Li L, Ding G, Wang D. Manipulating Crystal Orientation of Poly(ethylene oxide) by Nanopores. Acs Macro Lett. 2013;2:181-184. DOI: 10.1021/mz300592v.
279. Su C, Shi G, Li X, Zhang X, Müller AJ, Wang D, Liu G. Uniaxial and Mixed Orientations of Poly(ethylene oxide) in Nanoporous Alumina Studied by X-ray Pole Figure Analyzis. Macromolecules 2018;51:9484-9493. DOI: 10.1021/acs.macromol.8b01801.

280. Su C, Chen Y, Shi G, Li T, Liu G, Müller AJ, Wang D. Crystallization Kinetics of Poly(ethylene oxide) under Confinement in Nanoporous Alumina Studied by in Situ X-ray Scattering and Simulation. Langmuir 2019;35:11799-11808. DOI: 10.1021/acs.langmuir.9b01968.
281. Suzuki Y, Steinhart M, Kappl M, Butt HJ, Floudas G. Effects of polydispersity, additives, impurities and surfaces on the crystallization of poly(ethylene oxide)(PEO) confined to nanoporous alumina. Polymer 2016;99:273-280. DOI: https://doi.org/10.1016/j.polymer.2016.07.021.
282. Shi G, Liu G, Su C, Chen H, Chen Y, Su Y, Müller AJ, Wang D. Reexamining the Crystallization of Poly(ε-caprolactone) and Isotactic Polypropylene under Hard Confinement: Nucleation and Orientation. Macromolecules 2017;50:9015-9023. DOI: 10.1021/acs.macromol.7b02284.
283. Steinhart M, Goring P, Dernaika H, Prabhukaran M, Gosele U, Hempel E, Thurn-Albrecht T. Coherent kinetic control over crystal orientation in macroscopic ensembles of polymer nanorods and nanotubes. Phys Rev Lett 2006;97:027801/1-4. DOI: 10.1103/PhysRevLett.97.027801.
284. Shin K, Woo E, Jeong Y G, Kim C, Huh J, Kim KW. Crystalline Structures, Melting, and Crystallization of Linear Polyethylene in Cylindrical Nanopores. Macromolecules 2007;40:6617-6623. https://doi.org/10.1021/ma070994e
285. Li L, Liu J, Qin L, Zhang C, Sha Y, Jiang J, Wang X, Chen W, Xue G, Zhou D. Crystallization kinetics of syndiotactic polypropylene confined in nanoporous alumina. Polymer 2017;110:273-283. DOI: https://doi.org/10.1016/j.polymer.2016.12.081.
286. Shingne N, Geuss M, Thurn-Albrecht T, Schmidt HW, Mijangos C, Steinhart M, Martín J. Manipulating Semicrystalline Polymers in Confinement. J. Phys. Chem. B 2017;121:7723-7728. DOI: 10.1021/acs.jpcb.7b05424.
287. Hay JN. The equilibrium melting point of poly(ethylene oxide). Makromol Chem 1976;177:2559-2561. DOI: 10.1002/macp.1976.021770825.
288. Huang HD, Xu JZ, Fan Y, Xu L, Li ZM. Poly(L-lactic acid) Crystallization in a Confined Space Containing Graphene Oxide Nanosheets. J Phys Chem B 2013;117:10641-10651. DOI: 10.1021/jp4055796.
289. Chen JB, Xu JZ, Pang H, Zhong GJ, Xu L, Tang H, Tang J H, Li ZM. Crystallization of Isotactic Polypropylene inside Dense Networks of Carbon Nanofillers. J Appl Polym Sci 2014;131:39505/1-10. DOI: 10.1002/app.39505.
290. Kratochvil J, Rotrekl J, Kapralkova L, Hromadkova J, Kelnar I. Epoxy/poly(epsilon-caprolactone) nanocomposites: Effect of transformations of structure on crystallization. J Appl Polym Sci 2013;130:3197-3204. DOI: 10.1002/app.39536.
291. Yang H, Feng L, Wang C, Zhao W, Li X. Confinement effect of SiO_2 framework on phase change of PEG in shape-stabilized PEG/SiO_2 composites. Eur Polym J 2012;48:803-810. DOI: 10.1016/j.eurpolymj.2012.01.016.
292. Zhen WJ, Lu CH, Li CY, Liang M. Structure and properties of thermoplastic saponite/poly(vinyl alcohol) nanocomposites. Appl Clay Sci 2012;57:64-70. DOI: 10.1016/j.clay.2012.01.002.
293. Wang ZC, Fan X, Wang K, Deng H, Chen F, Fu Q, Na B. Ordered long-helical conformation of isotactic polypropylene obtained in constrained environment of nanoclay. Polym Adv Technol 2011;22:1375-1380. DOI: 10.1002/pat.1827.
294. Sencadas V, Martins P, Pitaes A, Benelmekki M, Ribelles JLG, Lanceros-Mendez S. Influence of Ferrite Nanoparticle Type and Content on the Crystallization Kinetics and Electroactive Phase Nucleation of Poly(vinylidene fluoride). Langmuir 2011;27:7241-7249. DOI: 10.1021/la2008864.
295. Pan FS, Jia HP, Cheng QL, Jiang ZY, Bio-inspired fabrication of composite membranes with ultrathin polymer-silica nanohybrid skin layer. J Membr Sci 2010;362:119-126. DOI: 10.1016/j.memsci.2010.06.027.
296. Zhang HZ, Wang XD. Self-assembly and confinement behaviors of poly(ethylene glycol) distearate within lamellar-mesostructured silica. J Non-Cryst Solids 2008;354:5068-5073. DOI: 10.1016/j.jnoncrysol.2008.07.022.
297. Yan SF, Yin JB, Yang JY, Chen XS. Structural characteristics and thermal properties of plasticized poly(L-lactide)-silica nanocomposites synthesized by sol-gel method. Mater Lett 2007;61:2683-2686. DOI: 10.1016/j.matlet.2006.10.023.
298. Famulari A, Arosio P, Filippi S, Marazzato C, Magagnini P, Minkova L, Meille SV. Clay-induced preferred orientation in polyethylene/compatibilized clay nanocomposites. J Macromol Sci Part B: Phys 2007;46:355-371. DOI: 10.1080/00222340601158225.
299. Yoshioka M, Takabe K, Sugiyama J, Nishio Y, Newly developed nanocomposites from cellulose acetate/layered silicate/poly(epsilon-caprolactone): synthesis and morphological characterization. J Wood Sci 2006;52:121-127. DOI: 10.1007/s10086-005-0742-7.

300. Xu JT, Zhao YQ, Wang Q, Fan ZQ. Isothermal crystallization of intercalated and exfoliated polyethylene/montmorillonite nanocomposites prepared by in situ polymerization. Polymer 2005;46:11978-11985. DOI: 10.1016/j.polymer.2005.10.004.
301. Xu JT, Wang Q, Fan ZQ. Non-isothermal crystallization kinetics of exfoliated and intercalated polyethylene/montmorillonite nanocomposites prepared by in situ polymerization. Eur Polym J 2005;41:3011-3017. DOI: 10.1016/j.eurpolymj.2005.04.042.
302. Gun'ko VM, Turov VV, Turova AA, Krupska TV, Pissis P, Leboda R, Skubiszewska-Zieba J. Interactions of poly(dimethylsiloxane) with nanosilica and silica gel upon cooling-heating. J Colloid Interface Sci 2014;426:48-55. DOI: 10.1016/j.jcis.2014.03.055.
303. Rissanou AN, Papananou H, Petrakis VS, Doxastakis M, Andrikopoulos KS, Voyiatzis GA, Chrissopoulou K, Harmandaris V, Anastasiadis SH. Structural and Conformational Properties of Poly(ethylene oxide)/Silica Nanocomposites: Effect of Confinement. Macromolecules 2017;50:6273-6284. DOI: 10.1021/acs.macromol.7b00811.
304. Papananou H, Perivolari E, Chrissopoulou K, Anastasiadis SH. Tuning polymer crystallinity via the appropriate selection of inorganic nanoadditives. Polymer 2018;157:111-121. DOI: 10.1016/j.polymer.2018.10.018.
305. Jabbarzadeh A. The Origins of Enhanced and Retarded Crystallization in Nanocomposite Polymers. Nanomaterials 2019;9:1472/1-13. DOI: 10.3390/nano9101472.
306. Jimenez AM, Krauskopf AA, Perez-Camargo RA, Zhao D, Pribyl J, Jestin J, Benicewicz BC, Muller AJ, Kumar SK. Effects of Hairy Nanoparticles on Polymer Crystallization Kinetics. Macromolecules 2019;52:9186-9198. DOI: 10.1021/acs.macromol.9b01380.
307. Jouibari IS, Haddadi-Asl V, Mirhosseini MM. Effect of nanofiller content and confined crystallization on the microphase separation kinetics of polyurethane nanocomposites. Polym Compos 2019;40:E422-E430. DOI: 10.1002/pc.24717.
308. Zhao WW, Su YL, Gao X, Xu JJ, Wang DJ. Interfacial effect on confined crystallization of poly(ethylene oxide)/silica composites. J Polym Sci Part B: Polym Phys 2016;54:414-423. DOI: 10.1002/polb.23915.
309. Zhao WW, Su YL, Muller AJ, Gao X, Wang DJ. Direct Relationship Between Interfacial Microstructure and Confined Crystallization in Poly(Ethylene Oxide)/Silica Composites: The Study of Polymer Molecular Weight Effects. J Polym Sci Part B: Polym Phys 2017;55:1608-1616. DOI: 10.1002/polb.24418.
310. Ding J, Maitra P, Wunder SL. Characterization of the interaction of poly(ethylene oxide) with nanosize fumed silica: Surface effects on crystallization. J Polym Sci Part B: Polym Phys 2003;4:1978-1993. DOI: 10.1002/polb.10549.
311. Zhao WW, Su YL, Gao X, Qian QY, Chen X, Wittenbrink R, Wang DJ. Confined Crystallization Behaviors in Polyethylene/Silica Nanocomposites: Synergetic Effects of Interfacial Interactions and Filler Network. J Polym Sci Part B: Polym Phys 2017;55:498-505. DOI: 10.1002/polb.24291.
312. Klonos P, Pissis P, Gun'ko VM, Kyritsis A, Guzenko NV, Pakhlov EM, Zarko VI, Janusz W, Skubiszewska-Zieba J, Leboda R. Interaction of poly(ethylene glycol) with fumed silica and alumina/silica/titania. Colloid Surf, A 2010;360:220-231. DOI: 10.1016/j.colsurfa.2010.03.002.
313. Chrissopoulou K, Andrikopoulos KS, Fotiadou S, Bollas S, Karageorgaki C, Christofilos D, Voyiatzis GA, Anastasiadis SH. Crystallinity and Chain Conformation in PEO/Layered Silicate Nanocomposites. Macromolecules 2011;44:9710-9722. DOI: 10.1021/ma201711r.
314. Galeski S, Piorkowska E, Rozanski A, Regnier G, Galeski A, Jurczuk K. Crystallization kinetics of polymer fibrous nanocomposites. Eur Polym J 2016;83:181-201.
315. Carvalho JL, Dalnoki-Veress K. Homogeneous Bulk, Surface, and Edge Nucleation in Crystalline Nanodroplets. Phys Rev Lett 2010;105:237801/1-4. DOI: 10.1103/PhysRevLett.105.237801.
316. Massa MV, Dalnoki-Veress K. Homogeneous crystallization of poly(ethylene oxide) confined to droplets: The dependence of the crystal nucleation rate on length scale and temperature. Phys Rev Lett 2004;92:255509/1-4. DOI: 10.1103/PhysRevLett.92.255509.
317. Massa MV, Carvalho JL, Dalnoki-Veress K. Confinement effects in polymer crystal nucleation from the bulk to few-chain systems. Phys Rev Lett 2006;97:247802/1-4. DOI: 10.1103/PhysRevLett.97.247802.
318. Blundell DJ, Keller A, Kovacs AJ. A new self-nucleation phenomenon and its application to the growing of polymer crystals from solution. J Polym Sci Part B: Polym Phys 1966;4:481-486. https://doi.org/10.1002/pol.1966.110040709
319. Fillon B, Wittmann JC, Lotz B, Thierry. Self-nucleation and recrystallization of isotactic polypropylene (α phase) investigated by differential scanning calorimetry. J Polym Sci Part B: Polym Phys 1993;31:1383-1393. https://doi.org/10.1002/polb.1993.090311013

320. Michell RM, Mugica A, Zubitur M, Müller AJ. Self-Nucleation of Crystalline Phases Within Homopolymers, Polymer Blends, Copolymers, and Nanocomposites. Adv Polym Sci 2015;276:215-256.
321. Sangroniz L, Cavallo D, Müller AJ, Self-Nucleation Effects on Polymer Crystallization. Macromolecules, 2020;53:4581-4604. https://doi.org/10.1021/acs.macromol.0c00223
322. Lorenzo AT, Arnal ML, Sánchez JJ, Müller AJ. Effect of annealing time on the self-nucleatio behavior of semicrystalline polymers. J Polym Sci Part B: Polym Phys, 2006;44:1738-1750. https://doi.org/10.1002/polb.20832
323. Muthukumar M. Communication: Theory of melt-memory in polymer crystallization. J Chem Phys 2016;45:031105/1-5.
324. Xu J, Ma Y, Hu W, Rehahn M, Reiter G. Cloning polymer single crystals through self-seeding. Nat Mater 2009;8:348-353. https://doi.org/10.1038/nmat2405
325. Reiter G. Some unique features of polymer crystallisation. Chem Soc Rev 2014;43:2055-2065. DOI 10.1039/C3CS60306G
326. Luo C, Sommer JU. Frozen topology: Entanglements control nucleation and crystallization in polymers. Phys Rev Lett 2014;112:195702/1-5. https://doi.org/10.1103/PhysRevLett.112.195702
327. Reid BO, Vadlamudi M, Mamun A, Janani H, Gao H, Hu W, Alamo RG. Strong memory effect of crystallization above the equilibrium melting point of random copolymers. Macromolecules 2013;46:6485-6497. https://doi.org/10.1021/ma400839d
328. Gao H, Vadlamudi M, Alamo RG, Hu W. Monte Carlo simulations of strong memory effect of crystallization in random copolymer. Macromolecules 2013;46:6498-6506. https://doi.org/10.1021/ma400842h
329. Häfele A, Heck B, Hippler T, Kawai T, Kohn P, Strobl G. Crystallization of poly(ethylene-co-octene): II Melt memory effects on first order kinetics. Eur Phys J E: Soft Matter Biol Phys 2005;16:217-224. https://doi.org/10.1140/epje/e2005-00023-0
330. Gurarslan A, Joijode AS, Tonelli AE, Polymers coalesced from their cyclodextrin inclusion complexes: What can they tell us about the morphology of melt‐crystallized polymers? J Polym Sci Part B: Polym Phys 2012;50:813-823. https://doi.org/10.1002/polb.23074
331. Tonelli AE. Enhancing the melt crystallization of polymers, especially slow crystallizing polymers like PLLA and PET. Polym Crystallization 2019;3:10095/1-10. https://doi.org/10.1002/pcr2.10095
332. Ziabicki A, Alfonso G. Memory effects in isothermal crystallization. I. Theory. Colloid Polym Sci 1994;272:1027-1042. https://doi.org/10.1007/BF00652372
333. Sangroniz L, Alamo RG, Cavallo D, Santamaria A, Müller AJ, Alegría A. Differences between isotropic and self-nucleated PCL melts detected by dielectric experiments. Macromolecules 2018;51:3663-3671. https://doi.org/10.1021/acs.macromol.8b00708
334. Sangroniz L, Cavallo D, Santamaria A, Müller AJ, Alamo RG. Thermorheologically complex self-seeded melts of propylene–ethylene copolymers. Macromolecules 2017;50:642-651. https://doi.org/10.1021/acs.macromol.6b02392
335. Sangroniz L, Barbieri F, Cavallo D, Santamaria A, Alamo RG, Müller AJ. Rheology of self-nucleated poly(ε-caprolactone) melts. Eur Polym J 2018;99:495-503. https://doi.org/10.1016/j.eurpolymj.2018.01.009
336. Sangroniz L, Sangroniz A, Meabe L, Basterretxea A, Sardon H, Cavallo D, Müller AJ. Chemical Structure Drives Memory Effects in the Crystallization of Homopolymers. Macromolecules 2020;53:4874-4881. https://doi.org/10.1021/acs.macromol.0c00751
337. Liu X, Wang Y, Wang Z, Cavallo D, Müller AJ, Zhu P, Zhao Y, Dong X, Wang D. The origin of memory effects in the crystallization of polyamides: Role of hydrogen bonding. Polymer 2020;188:122117/1-9. https://doi.org/10.1016/j.polymer.2019.122117
338. Tol R, Mathot V, Reynaers H, Goderis B, Groeninckx G. Confined crystallization phenomena in immiscible polymer blends with dispersed micro-and nanometer sized PA6 droplets part 4: polymorphous structure and (meta)-stability of PA6 crystals formed in different temperature regions. Polymer 2005;46:2966-2977. https://doi.org/10.1016/j.polymer.2005.02.021
339. Bartczak Z, Galeski A, Krasnikova NP. Primary nucleation and spherulite growth rate in isotactic polypropylene polystyrene blends. Polymer 1987;28:1627-1634.
340. Bartczak Z, Galeski A, Pracella M. Spherulite Nucleation in isotactic polypropylene with high density polyethylene. Polymer 1986;27:537-543.
341. Bartczak Z, Galeski A, Martuscelli E, Janik H. Primary nucleation behavior in isotactic polypropylene/ ethylene-propylene random copolymers blends. Polymer 1985;26:1843-1848.
342. Galeski A, Bartczak Z, Pracella M. Spherulite nucleation in polypropylene blends with low-density polyethylene. Polymer 1984;25:1323-1326.

343. Wunderlich B. Macromolecular Physics Vol. 2. New York: Academic Press; 1976. 437 pp.
344. Safari M, Maiz J, Shi G, Juanes D, Liu G, Wang D, Mijangos C, Alegría A, Müller AJ. How Confinement Affects the Nucleation, Crystallization, and Dielectric Relaxation of Poly(butylene succinate) and Poly(butylene adipate) Infiltrated within Nanoporous Alumina Templates. Langmuir 2019;35:15168-15179. DOI: 10.1021/acs.langmuir.9b02215.
345. Guan Y, Liu G, Ding G, Yang T, Müller AJ, Wang D. Enhanced Crystallization from the Glassy State of Poly(L-lactic acid) Confined in Anodic Alumina Oxide Nanopores. Macromolecules 2015;48:2526-2533. https://doi.org/10.1021/acs.macromol.5b00108
346. Shi G, Guan Y, Liu G, Müller AJ, Wang D. Segmental Dynamics Govern the Cold Crystallization of Poly(lactic acid) in Nanoporous Alumina. Macromolecules 2019;52:6904-6912. https://doi.org/10.1021/acs.macromol.9b00542
347. Kowaleski T, Ragosta G, Martuscelli E, Galeski A. Crystallization of Poly(ethylene oxide) in i-Polypropylene-Poly(ethylene oxide) Blends. J Appl Polym Sci 1997;66:2047-2057.
348. Meng Q, Hu J. A review of shape memmory polymer composites and blends. Composites: Part A 2009;40:1661-1672.
349. Kolesov I, Dolynchuk O, Radusch H-J. Shape-memory behavior of cross-linked semi-crystalline polymers and their blends. EXPRESS Polym Lett 2015;9:255-276.

Declaration of interests

X The authors declare that they have no known competing financial interests or personal relationships that could have appeared to influence the work reported in this paper.

☐The authors declare the following financial interests/personal relationships which may be considered as potential competing interests: